UNIVERSITY OF ICELAND

GRÓ · GTP Geothermal Training Programme

unesco Centre Under the auspices of UNESCO

M.S. thesis
in Geology

Prediction of Injection-Induced Cooling using Tracer Test Data in the Hellisheiði Geothermal Field, SW-Iceland

Comparison of Numerical and Analytical Modelling Approaches

Teka Nigussie Gebru

Supervisors:

Dr. Samuel Warren Scott,
Post-Doctoral Researcher, University of Iceland, Faculty of Earth Science, School of Engineering and Natural Sciences, Iceland

Dr. Gudni Axelsson,
Director, Geothermal Training Program (GRÓ GTP), Iceland

February, 2023

FACULTY OF EARTH SCIENCE

Prediction of Injection-Induced Cooling using Tracer Test Data in the Hellisheiði Geothermal Field, SW Iceland

Comparison of Numerical and Analytical Modelling Approaches

Teka Nigussie Gebru
M.S. thesis in Geology

Supervisors:

Dr. Samuel Warren Scott,
Post-Doctoral Researcher, University of Iceland, Faculty of Earth Science, School of Engineering and Natural Sciences, Iceland

Dr. Gudni Axelsson,
Director, Geothermal Training Program (GRÓ GTP), Iceland

Faculty of Earth Science
School of Engineering and Natural Sciences, University of Iceland
February, 2023

Prediction of Injection-Induced Cooling using Tracer Test Data in the Hellisheiði Geothermal Field, SW Iceland
Comparison of Numerical and Analytical Modelling Approaches

This thesis satisfies 60 credits towards an M.S.
in Geology in the Faculty of Earth Science,
University of Iceland, School of Engineering and Natural Sciences

Abstract

The Hellisheiði geothermal system is a fracture-controlled geothermal system located in the south part of the Hengill volcanic system in SW-Iceland. The bedrock mainly consists of a sequence of basaltic lavas, hyaloclastites and intrusions. Abundant extensional and transform faults reflect its location near a triple junction. The objective of this study is to construct a numerical reservoir model of the Hellisheiði geothermal system with a particular focus on reinjection-induced cooling in the Húsmúli subfield. A numerical model is calibrated using natural state temperature profiles, as well as recent tracer data collected in 2019, and is used to predict magnitude and timescale of cooling due to long term reinjection. Using the dual porosity approach, the model is able to achieve a fairly good match to field data for three monitoring wells (HE-31, HE-48, HE-48). The tracer flow in the numerical model constructed underscores the role of the NE oriented fault structures as the main conduits for tracer migration, and the role of transform structures as flow barriers. The model predict an annual temperature decrease of less than 1°C for wells HE-31 and HE-48. On the other hand, although very little tracer appeared in well HE-33 suggesting little risk of injection-induced cooling, the model suggests it may be affected by cooling due to cold water recharge from neighbouring formations. The cooling predictions are compared with those of a simple one-dimensional model (*TRINV* software). Despite its simple internal structure, *TRINV* provides greater tracer simulation accuracy. This study supports the importance of reinjection that not only provides pressure support but also helps to counteract colder marginal recharge from surrounding formations.

Dedication

This thesis is dedicated to my parents, siblings, relatives, and the people of Tigray, including those who have passed away due to the ongoing war in Ethiopia. They remain trapped and isolated for more than two years without access to telecommunication-, electricity-, bank-, health-, school-, food- and water-services and other basic services on top of the rampant sexual violence and extra-judicial killings inflicted on innocent civilians. Tigrayans living in other parts of Ethiopia have been exposed to excessive brutality including extra-judicial killing, detention, humiliation, and persecution for having originated in Tigray. Tigrayans living abroad, including myself, are devasted by hearing harrowing news and experiencing the agony of their people all the time, which has even caused many to develop mental disorders. It is indeed too hard to accept this kind of atrocity during the 21st century. This resilient and hard-working society is in my thoughts all the time.

Table of Contents

List of Figures

List of Tables

Abbreviations

1-D	1-Dimensional
2-D	2-Dimensional
3-D	3-Dimensional
EGS	Enhanced Geothermal System
ENE	East-northeast
EOS	Equation of State
EVZ	Eastern Volcanic Zone
EW	East-west
FVM	Finite Volume Method
GUI	Graphical User Interface
IAPWS-IF	Industrial Formulation for Thermodynamic Properties of Water and Steam
ISOR	Iceland GeoSurvey
MINC	Multiple Interacting Continua
ML	Local Magnitude
MT	Magnetotelluric
MWe	Megawatt Electric
MWth	Megawatt Thermal
NCG	Non-Condensable Gases
NDS	Naphthalenedisulfonic acid disodium salt
NE	Northeast
NNE	North-northeast
NW	Northwest
OR	Orkuveita Reykjavíkur
RPR	Reykjanes Peninsula Ridge
SISZ	South Iceland Seismic Zone
SW	Southwest
TEM	Transient Electromagnetic
TIM	Tim Isn't Mulgraph
TRINV	Tracer Inversion
UNU-GTP	United Nations University Geothermal Training Program
WNW	West-northwest
WVZ	Western Volcanic Zone

Acknowledgements

At most, my sincere gratitude belongs to the Government of Iceland through GRÓ GTP for awarding me full sponsorship for studying at the University of Iceland and Ethiopian Electric Power (EEP) for granting me to peruse my MSc study.

Indeed, I am appreciative of my supervisors: Samuel Scott and Gudni Axelsson. They have gone beyond to ensure my successful completion of this research work. My first advisor, Samuel Scott, has paid a tremendous effort in helping me organize theoretical and technical ideas. My second supervisor, Gudni Axelsson, provided great advice in proposing the title of this report and later his patience and guidance in revising all the document contents.

My special appreciation goes to Peter Franz and Jonathan Clearwater, directors of Flow State Solutions Ltd., a New Zealand based geothermal reservoir modelling company for providing full access to a commercial license for free all the time during my research work. Their initiative and genuine guidance concerning the working principles of the software was incredible. To be honest, this acknowledgement is too little for them. Let GOD pay them out for all their contribution in my research work.

My cordial acknowledgment belongs to Reykjavík Energy for the trust and for allowing me to work with their database and awesome people such as Thomas Ratouis and Pálmar Sigurðsson. Besides, the contribution of ISOR in providing technical expertise such as Kjartan Marteinsson and Gunnlaugur M. Einarsson was commendable.

I appreciate the GRÓ GTP staff Gudni Axelsson, Director of GRÓ GTP, Ingimar G. Haraldsson, Deputy Director, Vigdís Hardasdottír, Operations Manager, Málfrídur Ómarsdóttir, Project Manager, Lúdvík S. Georgsson, former director of GTP and finally Markús Wilde, former Service Manager, for their support during my study period.

Furthermore, my acknowledgment goes to Benedikt Steingrímsson for conducting a thesis review at the end. I would like to thank my GRÓ GTP and MSc fellows, especially, Jose Erick and Eyasu Solomon for their sincere contribution in figuring out scripting with python and QGIS maps, respectively.

I would like to pay sincere thanks to founder of ThinkGeoEnergy, a geothermal web-based digital magazine, Alexander Richter, for his amazing encouragement during my study.

Finally, my distinguished family and friends deserve special acknowledgment. Even though the project has come to an end now, their patience during my thesis work was enormous.

1 Introduction

1.1 Geothermal Reinjection

In the geothermal industry, the reinjection of produced fluids back into the subsurface was initially performed for the purpose of disposal of effluent liquid in a more environmentally friendly manner than discharging it on the surface, into rivers or the ocean (Stefánsson, 1997; Axelsson et al., 2005). However, it was later shown that geothermal reinjection (Figure 1. 1) improves heat recovery and increases the production capacity of geothermal fields by reducing reservoir pressure decline (Hardarson et al., 2010). The importance of reinjection is not restricted to the above-mentioned advantages, as it also serves a variety of purposes such as preventing surface subsidence caused by pressure decline due to production and providing extra recharge to supplement the natural recharge (Axelsson, 2012; 2022).

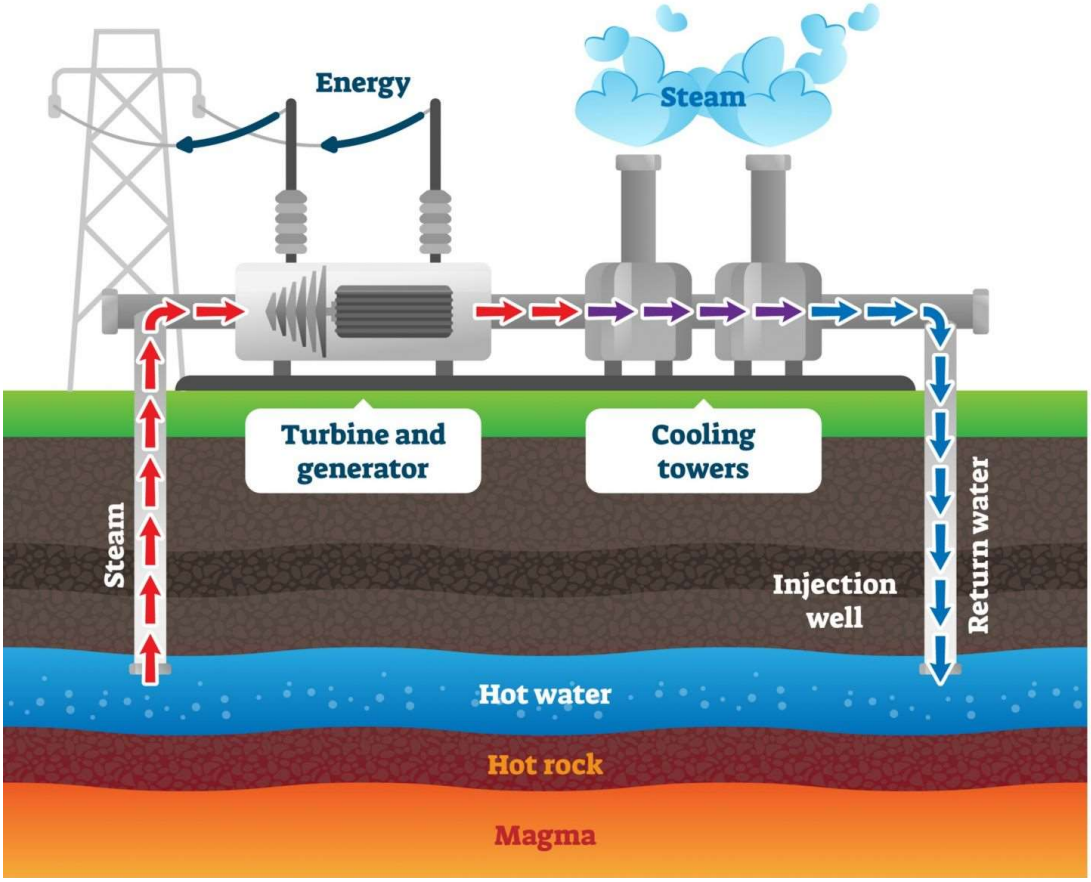

Figure 1. 1 Geothermal reinjection system (Bakerhughes, 2023).

Axelsson (2012; 2013; 2022), Diaz et al. (2016) and Kamila et al. (2021) delineate several criteria for the selection of reinjection zones. The main factor is that there should not be too direct of a hydrological connection between production and reinjection zones. If that is satisfied, reinjection could be located inside the main production area or on the edge of the production zone. Alternatively, reinjection may be located above or below a reservoir system or at a far distance from the production zone.

Axelsson (2012; 2022) and Kamila et al. (2021) briefly states the historical background of how reinjection emerged as a resource management tool. The Ahuachapan high-temperature geothermal system in El Salvador was the first field in which reinjection started in 1971 (Steingrímsson et al., 1989). Around the same time, reinjection was also performed in the low-temperature sedimentary geothermal system in the Paris Basin, France. A little later reinjection started at the Geysers in California, USA, and in Larderello, Italy, in 1970 and 1974, respectively, with the aim of disposal of condensed steam. It was later realized that reinjection improved the reservoir performance and longevity of geothermal systems. Presently, reinjection is an integral part of the utilization management of numerous geothermal systems, and is performed in more than 100 geothermal fields, including Icelandic ones such as Hellisheiði, Nesjavellir, Svartsengi, Krafla and Þeistareykir.

Despite the importance of reinjection in field management, reinjection may have negative impacts on geothermal operations (Axelsson et al., 2005), Axelsson (2012; 2013; 2022), Diaz et al. (2016) and Kamila et al. (2021). Induced seismicity is one of the main challenges, which is caused by reinjection through increased pore pressure. Other risks include cooling of production wells (cold-front breakthrough), scaling or corrosion in surface pipelines and injection wells, or rapid clogging of aquifers next to injection wells, especially in sandstone reservoirs. The injection rate and amount of injected fluid has an effect on the magnitude of negative impacts.

Reinjection activities in the Hellisheiði geothermal field began during commissioning of the first phase in 2006 (Gunnarsson, 2011). A mixture of the separated brine used in the heat exchangers has a temperature of 80°C and the steam condensate exiting high and low pressure turbines was reinjected into the Gráuhnúkar area situated at the southwest edge of Hellisheiði (Gunnarsson, 2011). However, this reinjection zone isn't used any more as a high temperature anomaly was observed in some of the wells drilled in that location, which was later switched to serve as a production zone (Gunnarsson, 2011). Large scale reinjection activity was launched in the Húsmúli reinjection zone situated on the western edge of the Hellisheiði geothermal fieldin 2011. Even though intense seismic activity started almost immediately in the area (Kristjánsson et al., 2016), this area serves as the reinjection zone for roughly 550 kg/s of separated brine and condensate. Therefore, it is important to understand the long-term consequences of continued reinjection in this area on production temperatures in nearby production wells.

1.2 Objective of Study and Thesis Organization

The aim of this study is to develop a geothermal reservoir model calibrated by tracer data in order to predict the timescales and magnitude of cooling due to long-term reinjection within the Hellisheiði geothermal field. The area of interest for this study is the vicinity of reinjection wells HN-09, HN-12, HN-14, HN-16, and HN-17 at Húsmúli, which are

apparently in hydraulic communication with nearby production wells HE-31, HE-33, HE-44 and HE-48 on Skarðsmýrarfjall (Kristjánsson et al., 2016).

This study analyzes tracer test data using a two-part modelling approach. The first approach consists of a three-dimensional model, which is calibrated both against natural state temperatures of wells HE-31, HE-33, HE-44 and HE-48 and tracer tests when tracer was injected into well HN-16 and monitoring in the previously mentioned wells. The model is used to study the future evolution of production well temperatures due to long term reinjection. The second approach involves analyzing tracer test data using a one-dimensional single fracture model, which can be used to estimate the parameters of flow channels and ultimately predict the thermal breakthrough of the reinjected fluid in the reservoir system of the production area. The tracer data utilized in this one-dimensional model is the same as that used in the three-dimensional numerical model.

The three-dimensional numerical geothermal reservoir modelling including the tracer return simulation was performed by a newly developed software tool named ***Volsung*** (Franz et al., 2019). ***Volsung*** (Section 4.5) provides a graphical user interface (GUI), enabling model pre-processing, execution, and post-processing in a single program. It has been validated using test models from the Stanford 1980 Geothermal Model Intercomparison Study (GMIS), and results from this simulator compare well with results of the TOUGH2 (Pruess et al., 1999) geothermal reservoir simulator. The software implements different approaches including Multiple Interacting Continua (MINC), and different equations of state (EOS) (Franz et al., 2019). The three-dimensional numerical reservoir simulation modelling work performed here incorporates two major sequential simulation tasks: 1) natural state simulation and 2) tracer test simulation. The simulation of natural state (i.e. pre-exploitation) conditions is done by choosing appropriate boundary conditions and geologic structure, reflecting the conceptual understanding of the reservoir system. The purpose of the natural state model calibration is to specify the initial conditions for modelling of tracer recovery. Leapfrog Geothermal 4.0 modelling tool (Seequent, 2020) is used to set up and retrieve the numerical grid from the 3D geological model of Hellisheiði area (Gunnarsdóttir and Poux, 2016). The PyTOUGH scripting package (Croucher, 2021) was used to refine the mesh developed on the Leapfrog interface. The conceptual model of the study area is based on measured downhole temperatures, as well as a literature review of previous studies of the greater Hellisheiði area.

In addition to the numerical modelling, one-dimensional analytical model simulation of tracer recovery is performed using ***TRINV*** (Section 5.5), developed at ISOR for the purpose of inverse modelling of tracer test data. The model uses tracer recovery data, collected at monitoring wells and assumed reservoir properties, including the number and approximate length of "flow-channels" conveying tracer-rich fluid from reinjection well to monitoring well, to estimate flow parameters such as flow velocity and fracture geometric parameters. After calibrating the parameters of the flow channels in this way, the rise of cooling of the production reservoir due to long term reinjection can be estimated for different scenarios.

Previous studies of large-scale tracer tests conducted in Hellisheiði during 2013 to 2015 are reported by Kristjánsson et al. (2016), Gunnarsson and Aradóttir (2014), Snæbjörnsdóttir et al. (2018), Tómasdóttir (2018) Ratouis et al. (2019) and Mahzari et al. (2021). This study focuses on a later tracer test performed during 2018-2021 based on a different reinjection well. On 11 July 2018, 99.6 kg of 2,6-NDS (2,6-Naphthalenedisulfonic acid) was injected into borehole HN-16. The injection continued for only a couple of hours, and tracer recovery

was measured at monitoring wells (HE-31, HE-33, HE-44, and HE-48) until 16 October 2021.

Overall, the ultimate objectives of this study are:

- Analyzing and interpretation of tracer data and prediction of cooling danger of the reservoir and the production wells situated at Skarðsmýrarfjall field due to long-term reinjection at the Húsmúli area, using one dimensional and three-dimensional models.
- Construction and calibration of a pre-exploitation natural state model of the Húsmúli subfield to extract initial state conditions of thermophysical variables used in numerical simulations of tracer tests.
- Comparison of 1-D analytical and 3-D numerical model predictions of temperature response due to long-term cold-water reinjection.

The thesis is organized in six sections including this chapter. The first chapter introduces reinjection activities and objectives of the study. The second chapter deals with tracer test theory and fluid transport in a reservoir system using a network of fractures. The third section describes geological and geophysical investigations of the study area, including the possible structural network of fractures that control fluid and tracer flow in the reservoir system. The fourth section describes the methodology used to perform the study, including conceptualization of the field, model set-up, simulation procedures, governing equations and working principles of the software used for model simulation. Chapters five and six present results and discussions, respectively, emphasizing model outcomes and interpretation of the results. Finally, chapter seven offers concluding remarks and future recommendations focusing on how to move forward in understanding and managing reinjection in the area.

Finally, this thesis hopefully constitutes an important contribution to the research and development operations ongoing in the Hengill geothermal system, such as to the Carbfix project.

2 Tracer Transport Analysis

2.1 Tracer Testing

Tracer testing is commonly used in all branches of surface and subsurface hydrology, as well in petroleum science and pollution and nuclear waste storage studies. As discussed by Axelsson et al. (2005) and Axelsson (2013; 2020) geothermal tracer testing can be used as part of a monitoring system to predict reservoir reaction to production and reinjection activities in a field. A tracer test is accomplished by injecting a chemical tracer into a hydrological system and monitoring its recovery, through time, at various observation points. The outcome is used to study flow-paths, quantify fluid-flow, and specifically in geothermal utilization to predict thermal breakthrough due to reinjection into a hot reservoir. The methods employed in geothermal applications have mostly been adopted from groundwater and petroleum reservoir engineering studies.

Tracer testing has various important applications in the geothermal industry (Axelsson et al., 2005). The main purpose in conventional geothermal development is to study connections between injection and production boreholes as part of reinjection research and management. The results are consequently used to predict the possible cooling of production boreholes due to long-term reinjection of colder fluid. In Enhanced Geothermal System (EGS) development, tracer testing has a comparable purpose, even though it is rather aimed at evaluating the energy extraction efficiency and longevity of such operations through studying the nature of connections between reinjection and production boreholes.

Tracer tests in geothermal applications are unique compared to their application in other branches of science (Axelsson et al., 2005) as its power lies in the fact that the thermal breakthrough time (onset of cooling) is usually several orders of magnitude (2–4) greater than the tracer breakthrough time. Geothermal tracer tests are mostly conducted through boreholes and can involve (i) a single borehole injection-backflow testing, (ii) a test involving one borehole-pair (injection and production) as well as (iii) several injection and production boreholes. To prevent major transients in the flow-pattern of the reservoir which would make the data analysis more difficult, the geothermal reservoir should preferably be in a semi-stable pressure state prior to a test.

In most cases a fixed mass of tracer is injected “instantaneously”, i.e., in as short a time as possible, into the injection borehole(s) in question. Samples for tracer analysis are most often collected from producing boreholes, while down-hole samples may need to be collected from non-discharging boreholes. The duration of tracer tests and corresponding sampling plans are site specific.

According to Axelsson (2020), the tracer selected needs to meet a few basic criteria: It should (a) not react with or absorb to reservoir rocks (b) be thermally stable at reservoir conditions (c) not be present in the reservoir (or at a concentration much lower than the expected tracer concentration) (d) be relatively inexpensive (e) be easy (fast/inexpensive) to analyse and (f) be environmentally benign. In addition, the tracer selected must adhere to prevailing phase (steam or water) conditions. Tracers in geothermal applications can be either intended for the liquid phase or the gas phase or for both phases. Liquid phase tracers can be halides like iodide (I^-) or bromide (Br^-), radioactive like iodide-125 ($_{125}I^-$) and iodide-131 ($_{131}I^-$),

fluorescent dyes such as fluorescein and rhodamine, aromatic acids such as benzoic acid and naphthalene sulfonates. Gas-phase tracers include fluorinated hydrocarbons, e.g. R-134a, R-23 and sulphur hexafluoride (SF6), and the two-phase tracers includes tritiated water (HTO) and alcohols such as methanol, ethanol and n-propanol.

2.2 Theory of Tracer Transport

In this study, analysis of the tracer test data is performed in two ways. The first approach involves using the three-dimensional numerical geothermal reservoir simulation tool named ***Volsung*** (section 4.1), which simulates multi-phase and multi-component geothermal fluid flow through porous and fractured media using an integral finite difference method, similar to the industry-standard ***TOUGH2*** code (Pruess et al., 2012). The second approach uses a model of a one-dimensional single fracture, through the software ***TRINV*** (see section 4.5). For the purpose of simplicity and clarity, only the one-dimensional single fracture model of tracer transport will be elaborated in this section.

The one-dimensional model of tracer transport assumes that the flow between injection and production boreholes may be approximated by one-dimensional flow in flow-channels, as shown in Figure *2.1*.

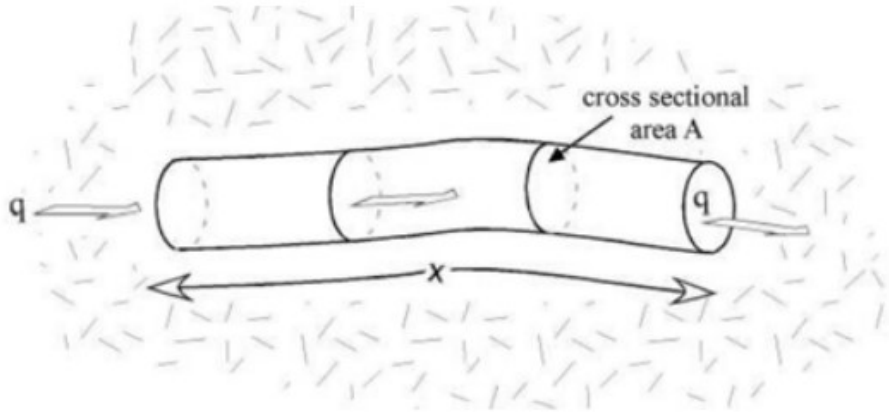

Figure 2.1 A schematic figure of a flow-channel with one dimensional flow, connecting an injection borehole and a production borehole (Axelsson et al., 2005).

The flow-channels may be parts of near-vertical fracture-zones or parts of horizontal interbeds or layers. Furthermore, the channels may be envisioned as being delineated by the boundaries of these structures, on one hand, and flow-field streamlines, on the other hand.

In other cases, these channels may be larger volumes involved in the flow between boreholes. In some cases, more than one channel may be assumed to connect an injection and a production borehole, for example connecting different feed-zones in the boreholes involved.

(Axelsson et al., 1995; 2005) the differential equation describing solute concentration in the channel if a fraction q of the injected water q_{in} flows through the channel and if molecular diffusion is neglected is,

The basic equations describing solute flow in porous media are the following:

$$F_x = F_x^{advection} + F_x^{dispersion} \quad (1.1)$$

where F_x denotes the mass flow rate of the solute (kg m^{-2} s^{-1}) in the x-direction given by

$$F_x^{advection} = u_x \cdot \phi \cdot C \quad (1.2)$$
$$F_x^{dispersion} = -\phi \cdot D_x \cdot \frac{\partial C}{\partial x} \quad (1.3)$$

where u_x denotes the fluid particle velocity (m s^{-1}), ϕ the rock porosity (-), C the solute concentration (kg m^{-3}) and D_x the dispersion coefficient (m^2 s^{-1}):

$$D_x = \alpha_x \cdot u_x + D^* \quad (1.4)$$
$$D_y = \alpha_y \cdot u_y + D^* \quad (1.5)$$
$$D_z = \alpha_z \cdot u_z + D^* \quad (1.6)$$

where α is the dispersivity of the material (m) in x, y and z directions and D^* is the coefficient of molecular diffusion (m^2 s^{-1}).

The differential equation for solute transport is derived by combining the above flow-equations and the conservation of mass of the solute involved. For a homogeneous, isotropic, and saturated medium the differential equation is (Axelsson et al., 1995; 2005):

$$\frac{\partial}{\partial_x}\left[D_x \frac{\partial C}{\partial x}\right] + \frac{\partial}{\partial_y}\left[D_y \frac{\partial C}{\partial y}\right] + \frac{\partial}{\partial_z}\left[D_z \frac{\partial C}{\partial z}\right] - \frac{\partial}{\partial_x}[u_x C] - \frac{\partial}{\partial_y}\left[u_y C\right] - \frac{\partial}{\partial_z}[u_z C] = \frac{\partial C}{\partial t} \quad (1.7)$$

where u is the average fluid velocity in the channel (m s^{-1}), given by $u = \frac{q}{\rho A \phi}$, with q the injection rate (kg s^{-1}), ρ the water density (kg m^{-3}), A the average cross-sectional area of the flow-channel (m^2) and ϕ the flow-channel porosity.

Based on the assumption of instantaneous injection of a mass M (kg) of tracer at time t = 0 into the reinjection well, the tracer concentration at the observation well can be estimated using the formula (Javandel et al., 1984 and Axelsson et al., 1995; 2005);

$$c(t) = \frac{uM\rho}{Q} \frac{1}{2\sqrt{\pi D t}} e^{-(x-ut)^2/4Dt} \quad (1.8)$$

Where $c(t)$ is the tracer concentration in the production borehole fluid, Q the production rate (kg s^{-1}) and x the distance between the boreholes involved.

The parameters u and D can be derived from experimental data, by fitting the equation to the data. The relative mass recovery RR can be calculated as a function of time t in a closed system for 1-dimensional case by defining the ratio of tracer recovered (M_R) in an observation well to the mass injected into a reinjection well, as follows (Axelsson et al.,1993) cited in (Axelsson et al., 1995):

$$RR(t) = \frac{M_R}{M} = Q \int_0^t \frac{C(t)dt}{M} \quad (1.9)$$

Axelsson et al. (1995; 2005) states that the goal of tracer testing is to predict thermal breakthrough and temperature decline during long-term reinjection in a geothermal reservoir system. This cooling mainly depends on the surface area and porosity of the flow-channel.

Figure 2.2 presents a model used to calculate temperature changes along the flow channel and hence the production well cooling predictions. It simulates a flow path along a fracture-zone, an interbed or permeable layer. In the model, b indicates either the width of the fracture-zone or the thickness of the interbed or layer, whereas h indicates the height of the flow-path inside the fracture-zone or its width along the interbed or layer. The flow-channel cross-sectional area is then given by $A = hb$. To estimate h and b on the basis of the main outcome of the tracer test interpretation, $A\phi$, the flow path porosity has to be averaged over the entire channel and the ratio between h and b is either approximately known or has to be assumed.

The theoretical response of this model is derived through a formulation that considers coupling between the heat advected along the flow-channel and the heat conducted from the reservoir rock to the fluid in the channel (Axelsson et al., 1995; 2005), see equation 1.2.

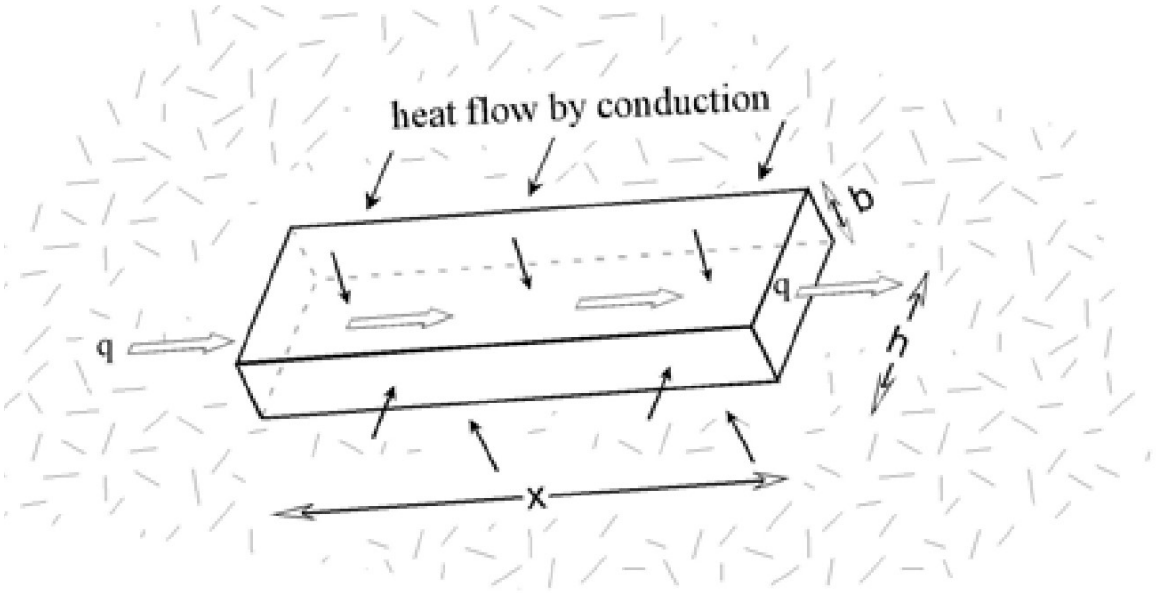

Figure 2.2 A model of a flow-channel, along a fracture zone or a horizontal interbed or layer, used to calculate reinjection related cooling predictions (Axelsson et al., 1995; 2005).

$$T(t) = T_o - \frac{q}{Q}(T_o - T_i)\left[1 - \mathrm{erf}\left\{\frac{kxh}{c_w q\sqrt{k\left(t-\frac{x}{\beta}\right)}}\right\}\right] \qquad (1.10)$$

where $\beta = \left(\frac{qC_w}{(\rho c)_f hb}\right)$ and $(\rho c)_f = \rho_w c_w \phi + \rho_r c_r (1-\phi)$, $T(t)$ is the production temperature, T_o is the initial reservoir temp, T_i is the injection temperature, q is the injection rate, Q is the production rate, k is the thermal conductivity of reservoir rock, κ is the thermal diffusivity of rock, and ρ and c are the density and heat capacity of water (w) and rock (r), respectively.

3 Study Area Description

3.1 Hengill Volcanic System

The Hengill volcano is part of the Icelandic volcanic rift zone, located at a triple junction in SW-Iceland where two active rift zones, namely the East Volcanic Zone (EVZ) and the West Volcanic Zone (WVZ), meet a seismically active transform zone, or the South Iceland Seismic Zone (SISZ) (Bjornsson et al., 1986) as shown in Figure 3.1.

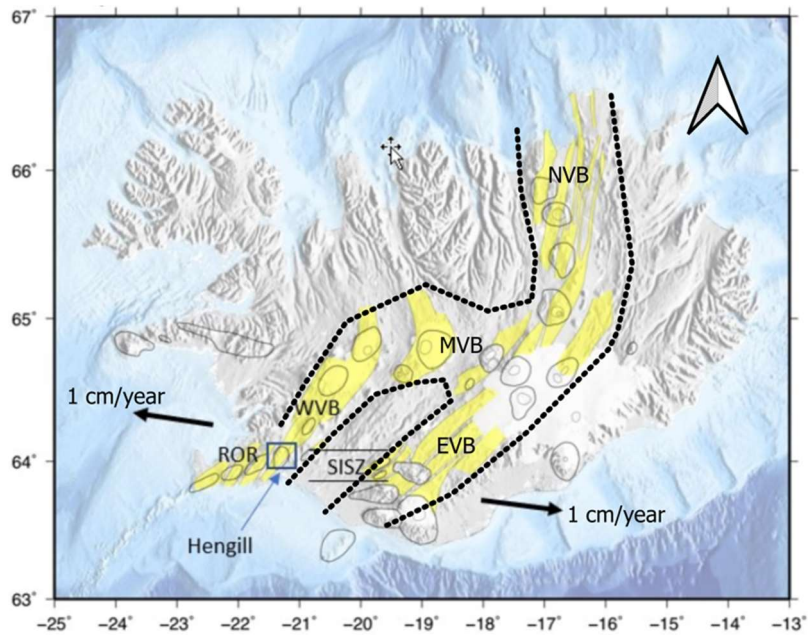

Figure 3.1 Map of Iceland showing the location of Hengill Volcano, the active rift, volcanic, and SISZ. The blue black box shows the location of the Hengil Volcano. WVB = Western Volcanic Belt, ROR = Reykjanes Oblique Rift, MVB = Middle Volcanic Belt, EVB = Eastern Volcanic Belt, NVB = Northern Volcanic Belt, SISZ = South Iceland Seismic Zone. Calderas are represented by black circles while fissure swarms are depicted by yellow. Picture is modified from Hjörleifsdóttir et al, (2021).

A 3-5 km wide and about 40 km long fissure swarm, where rifting is most active and with maximum volcanic accumulation, are the main geological components in the central part of the Hengill volcanic system (Franzson et al., 2010). The area is known for having numerous hot springs and fumaroles. It is one of the most extensive geothermal spots in Iceland, covering an area of about 110 km^2. Even though scientific studies and exploration of the area date backs to the 1960s, resource assessment through modelling only started in 1986. Hellisheiði and Nesjavellir power plants are the two geothermal power plants in operation in the Hengill region with a combined electrical generation capacity of 423 MW_e and thermal power capacity of 420 MW_{th}, where the capital city, Reykjavik, is receiving the hot water for space heating services. Besides, the Hveragerði field is also part of the Hengill system situated southeast of the center of the Hengill area, where the local community is utilizing the geothermal resource for direct use purposes and as a tourist attraction.

3.2 Geology of Hellisheiði Geothermal System

The Hellisheiði geothermal system is a liquid-dominated fractured geothermal system (Gunnarsson, 2011) situated in the southern part of the Hengill central volcano shown in Figure 3.2. Its bedrock consists of hyaloclastites, lava flows, and intrusions, mainly dykes (Gunnarsson and Mortensen, 2016). The hyaloclastite, which is bounded by a Holocene lava flows, dated to be 2 to 9 thousand years of age, is the dominant geological formation in the area (Gunnarsdóttir and Poux, 2016). The subsurface rocks show a large variation in porosity, i.e the porosity in hyaloclastites is high, while it's lower in the lava layers and lowest in intrusive rocks. The entire reservoir formation of the system is extremely heterogeneous. Húsmúli is the main reinjection site of the Hellisheiði geothermal field, situated in the southwest part of the Hengill central volcano. It is an interglacial lava shield (Ágústsson et al., 2015) and one of the oldest geological formations in the area, with an age of about 115,000 years (Sæmundsson et al., 2010). This lava shield can be traced in boreholes below the superimposed hyaloclastic units to the east where the formation is intersected by normal faults.

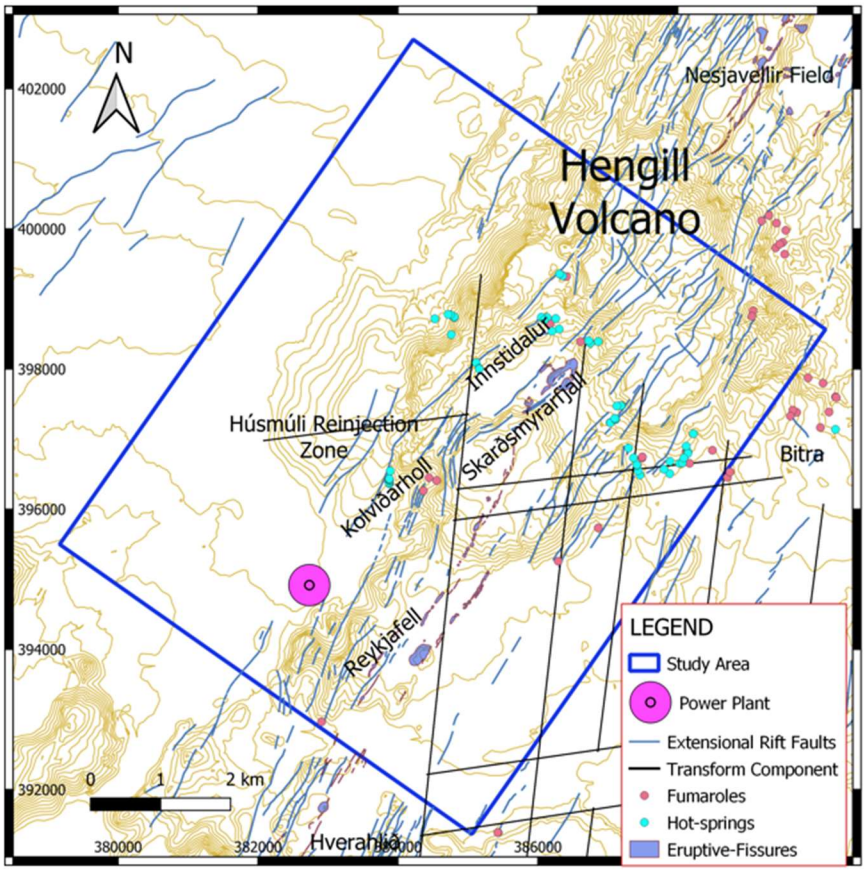

Figure 3.2 Location of the Hellisheiði geothermal field. The area of interest for this study is shown by a blue rotated rectangle (data source: Reykjavík Energy).

In the Hellisheiði geothermal field, over 61 wells have been drilled, from 1,000 meters to 3,000 meters in depth, of which 44 are production wells that supply steam to a flash steam power plant and 17 are reinjection wells (Ratouis et al., 2019; Hjörleifsdóttir et al., 2021). The Hellisheiði geothermal power plant is a combined heat and electrical power generation plant (CHP) which was commissioned in 2006 and expanded stepwise in 2008 and 2011,

with a total output of 303 MW_e and 133 MW_{th}, making it the largest geothermal combined heat and power plant in Iceland.

3.3 Geophysical Exploration

Geophysical exploration is among the main techniques of geothermal resource exploration and assessment in areas where such resources are suspected. Temperature, permeability and the chemical composition of the geothermal fluid are the essential properties which characterize a geothermal reservoir system (Hersir and Árnason, 2009). Despite the availability of different types of geophysical methods for geothermal exploration, mainly two (3.3.1 and 3.3.2) have provided the main geophysical information used in this thesis. These have been applied at different and successive times in the Hengill area, providing significant contribution to the model developed here. These are elaborated as follows.

3.3.1 Resistivity Measurements

Resistivity measurements play a great role in delineating geothermal reservoirs, locating recharge zones and estimating physical parameters like porosity of the reservoir system (Nyambayar, 2006). Porosity and the pore structure of the rock, amount of water (saturation), salinity of the water, temperature, water-rock interaction and alteration, pressure as well as the steam content in the water are the variables influencing resistivity (Hersir and Árnason, 2009). In Iceland, since 1991, the combined use of TEM and MT soundings has been found to be most effective, with some results shown in Figure 3.3, helping to resolve complex structures like those associated with the Húsmúli area (Árnason et al., 2010).

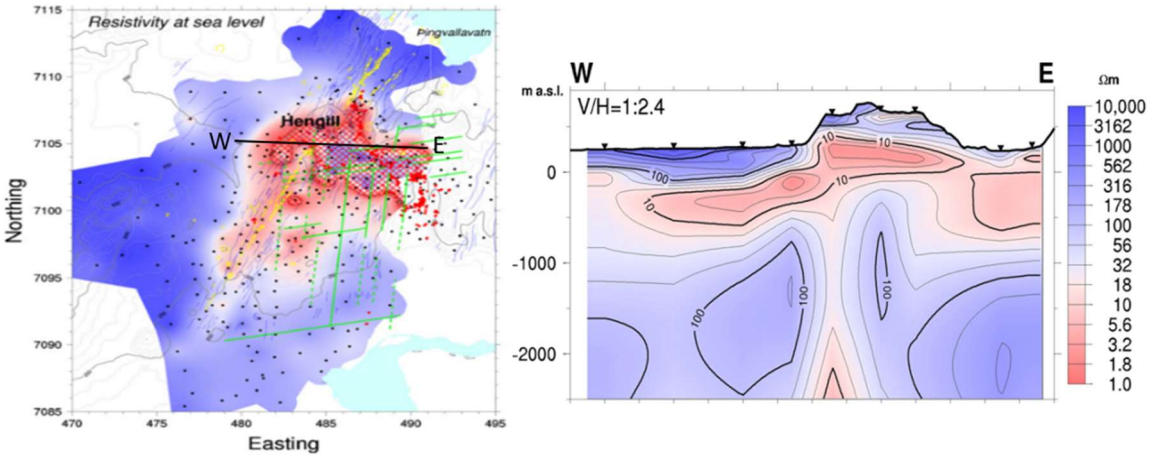

Figure 3.3 Resistivity cross-section of the Hengill volcanic system in an East-West direction (right) and resistivity-map for 2000m depth (left), based on TEM and MT measurement. The orientation of the cross-section and location of Hengil is shown on the right. The high resistivity formation goes to SW of Hengil along the fissure swarm. Source: Árnason et al. (2010)

The latest study of the Hengill system was carried out by Reykjavik Energy (OR) and Iceland GeoSurvey (ISOR) based on combined TEM and MT soundings in 2006. High temperature mineral alteration and a high resistivity core are located at shallow depth (400-800 m below

the ground surface). However. at greater depths, high resistivity rock is enclosed by low resistivity rock that stretches to the NW and SE of Hengill mountain (Árnason et al., 2010).

3.3.2 Seismicity and Tectonic Structures

Due to its location at the intersection of North American/Eurasian plate boundary, tectonic activity is widespread in Iceland and specifically in the Hengill volcanic system (Bjornsson et al., 1986; Árnason et al., 2010; Franzson et al., 2010; Ágústsson et al., 2015; Karson et al., 2018;). The two tectonic regimes that seem to prevail in the Hengill area (Franzson et al., 2010), as shown in Figure 3.4, consist of (1) the transform component concentrated in the eastern part of Hengill, which is linked with the SISZ, and (2) the fissure zone emerging from dilationary rifting.

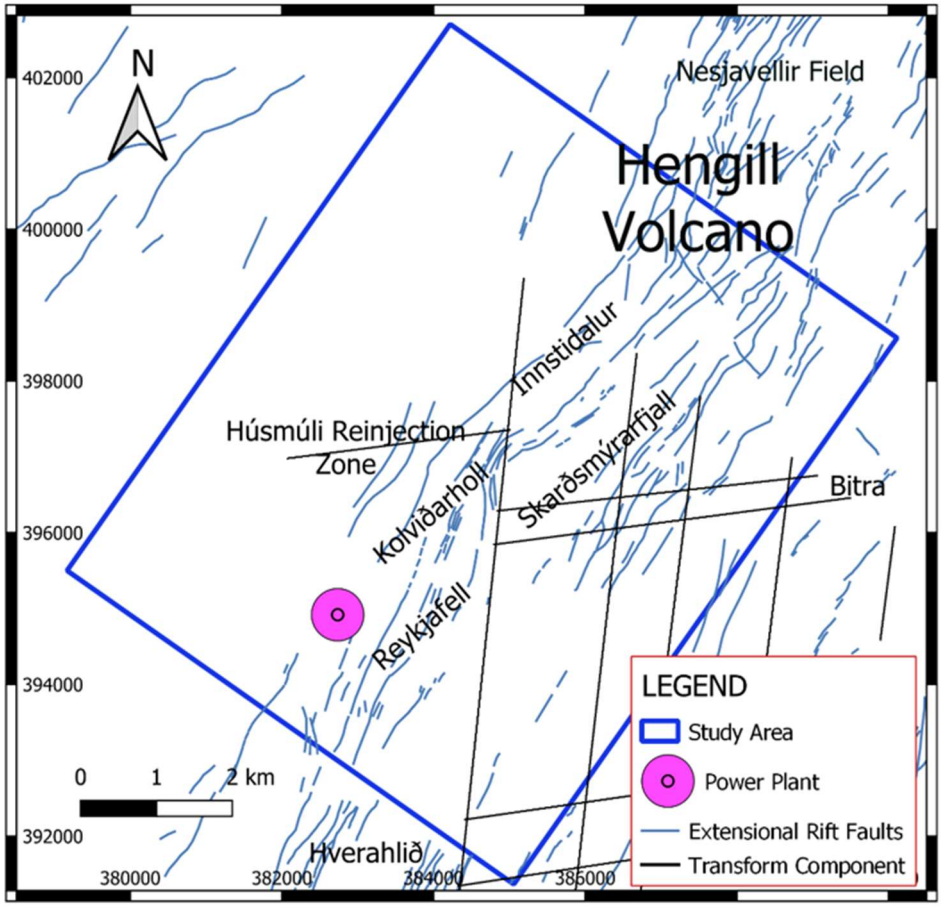

Figure 3.4 Tectonic structure prevailing in Hengill area, showing the faults associated with dilationary rifting (represented by light blue color trending NE) and the transform fault system (represented by solid black lines).(Data Source: Reykjavík Energy and Iceland GeoSurvey).

The tectonic character reflects the tectonic setting of the Reykjanes Peninsula, which is an oblique rifting segment of the plate boundary in SW-Iceland. NE trending grabens and volcanic fissures producing crater rows and hyaloclastite ridges are the most striking features on the Reykjanes Peninsula. North-trending faults of varying age showing right-lateral, strike slip displacements are superimposed on these structures, which are reflected by

earthquakes up to magnitude 6.3 ML in the peninsula (Halldórsson, 2014; Ágústsson et al., 2015).

In the Hellisheiði-Hengill area, major earthquake activity seems occur every 20 to 40 years (Ágústsson et al., 2015). However, after full scale drilling operations started in the 2000s, following reconnaissance drilling conducted in the 1980s and 1990s, earthquake occurrence became more frequent, with the main reasons believed to be associated with drilling and reinjection activities. These phenomena affect the existing fault structures that are activated by stress perturbations associated with the injection operations in the Húsmúli area. These have different orientations, which causes the nature of the fractures to be quite complicated. Ágústsson et al. (2015) suggest that increased pore pressure and block rotations are probably the cause of the displacements on the non-optimally oriented faults with respect to the regional stress field. An intense seismic swarm was triggered at Húsmúli, due to full scale reinjection, launched in September 2011, that amounted to 550 l/s (Ágústsson et al., 2015).

3.4 Geochemical Exploration

During surface exploration and production, geochemical studies play a major role in understanding the characteristics of the geothermal resource (Óskarsson and Ármannsson 2015). Óskarsson and Ármannsson (2015) further claim that the most important application of geochemistry in exploration of geothermal is chemical geothermometry, as it helps to interpret chemical composition of fluids in terms of reservoir temperature. The most common geothermometers include the silica (SiO_2) geothermometers, which are based on the solubility of silica minerals, such as quartz or chalcedony, and gas geothermometry involving reactive geothermal gases like CO_2, H_2S, H_2 and CH_4 (D'Amore and Arnórsson, 2000).

In Iceland, basaltic rocks show sequences of alteration mineral assemblages that change with increasing depth and temperature (Kristmannsdóttir and Tómasson, 1978; Kristmannsdóttir, 1979; Franzson, 1998). The primary mineralogy of the rocks in Hengil volcanic system consists of olivine and plagioclase phenocrysts with plagioclase, pyroxene, olivine, Ti–Fe oxides and glass in the groundmass (Sæmundsson, 1967, 1992), as cited in Scott et al.,(2014). Cutting analysis from the production wells (HE-31, HE-33, HE-44 and HE-48) drilled in Skarðsmýrarfjall area of Hellisheiði geothermal field incorporated in this study suggests that secondary minerals such as quartz, epidote, chlorite, prehnite, wollastonite, and actinolite are abundant(Snæbjörnsdóttir et al., 2018). Three local up flow zones within the Hellisheiði reservoir are identified based on the distribution of hydrothermal alterations (Franzson et al, 2005). In addition, isotopic analysis of fluids from of Hellisheidi field indicates that the isotope composition of the deep circulating fluid ranges from -7.3 ‰ to -6.5 ‰ and -62 ‰ to -65 ‰ for $\delta^{18}O$ and $\delta^{2}H$, respectively (Mutonga, 2007).

3.5 Structural Flow Paths for Tracers

With the aim to define hydrological flow paths and evaluate the risk of thermal breakthrough between injection and production wells (Kristjánsson et al., 2016), the first tracer test in the Hellisheiði geothermal field was undertaken in 2013 using naphthalene sulfonic acids as tracers. The tracer analysis of samples collected was performed by using fluorescence

detection at the ÍSOR chemical laboratory by high-performance liquid chromatography (HPLC). Due to their affordability, easy detectability with fluorescence spectroscopy, environmental benignity and thermal stability, naphthalene sulfonates have proven to be effective tracers in high temperature geothermal reservoirs (Rose et al., 2000). Six boreholes close to the Húsmúli reinjection area, of which five are reinjection wells and one failed production well, were selected for the task using six Naphthalene Sulfonic acids, namely 1,5-NDS, 1,3,5-NTS, 1,3,6-NTS, 2,6-NDS, 2,7-NDS and 1,6-NDS. Fourteen wells adjacent to the selected injection wells were sampled and analyzed for the selected naphthalene sulfonic acids before the injection of the tracer, which resulted in the occurrence of none of the chemicals in any of the wells. Following the tracer injection, Kristjánsson et al. (2016) clearly illustrated the phenomenon of tracer transport, the tracer from well HN-17 appeared first at well HE-31, just after a couple of weeks, and consequently at well HE-48 after 18 days and finally the tracer from well HE-17 took 53 days to reach well HE-44 (Figure 3. 5).

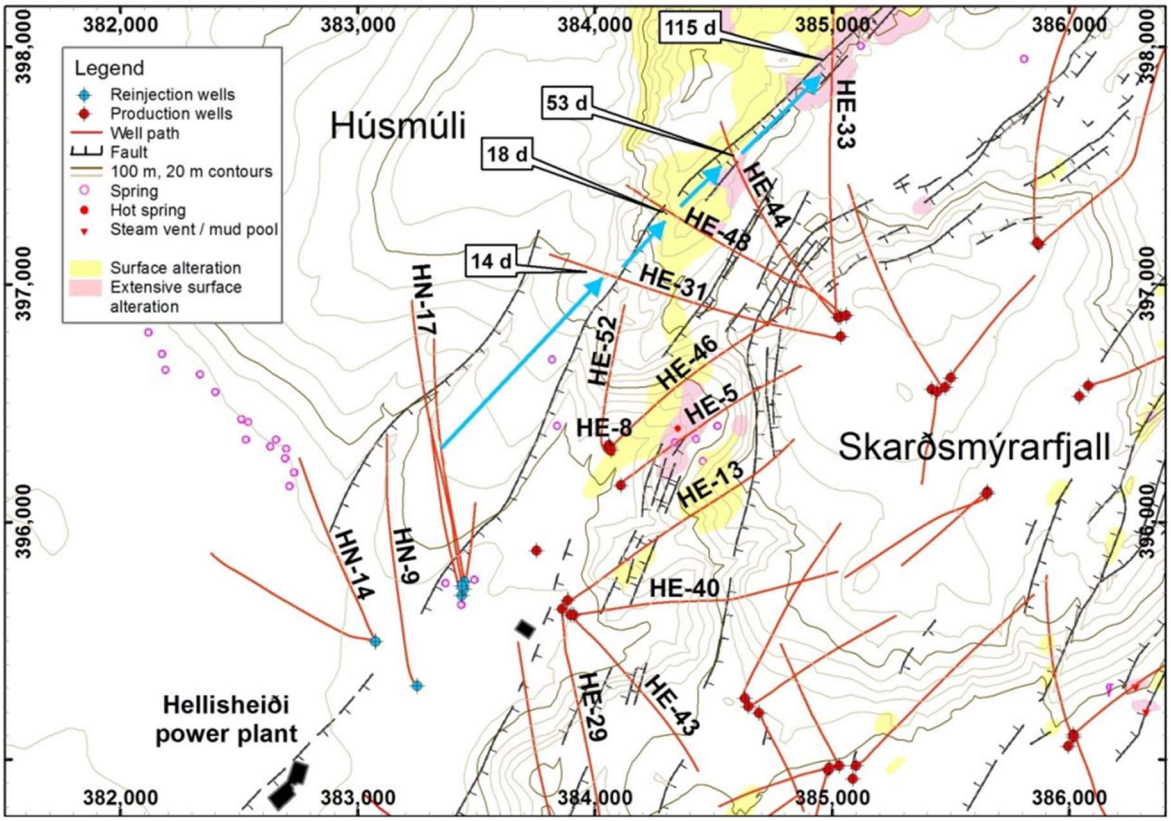

Figure 3. 5: Map showing tracer transport from reinjection well HN-17 to production wells HE-31, HE-33, HE-44 and HE-48. Blue arrows show direction of travel of the tracer while boxes shows time of arrival of the tracer in days. (Source: Kristjánsson et al., 2016)

Interpretation of the 2013 full scale tracer test study in the Hellisheiði geothermal field is presented by Khodayar (2013) and Kristjánsson et al. (2016), supported by available data such as seismic event data, subsurface data and aerial photographs. It should be pointed out that the parallel faults and eruptive fissures of the NE rift are the main structural targets for drilling in Hengill. These two studies explored some findings on the fracture sets that control the permeability in the vicinity of Húsmúli wells, connectivity of wells, and features of these fracture sets (see Figure 3.6) by analyzing and interpreting results of the tracer experiments

in selected wells and correlation of the structural elements with the feed-zones of these wells. Khodayar (2013) further analyzed the faults reactivated during the re-injection at Húsmúli, results of televiewer logs interpretation in HN-11, HN-12, HN-14, and HN-16, correlation with pressure maps prior to production and fluid mass extraction due to the production, selected GPS and gravity measurements and review of some regional tectonic data due to the location of Húsmúli and the surroundings of the junction of the rift and transform zones.

Further, Ratouis et al. (2019) clearly summarized the possible potential structures that control the tracer flow path at the study area, which are a composite of six fracture sets (Khodayar et al., 2016) striking NNE, ENE, NS, NW and E-W, classified as either carriers or barriers for the tracer flow paths (Figure 3.6). The ENE set (structure 1-5) is the most favorable flow path for the tracer and appears to be the main tracer carrier. These fractures extend from the reinjection zone to the edge of the Skarðsmýrarfjall production zones and intersect wells HE-31, HE-48, HE-44, and HE-33, facilitating a relatively short travel time between them and reinjection wells HN-16 and HN-17. The NS faults (structures 6-8) are also good carriers and channel the flow to and from the ENE faults. The NW fractures

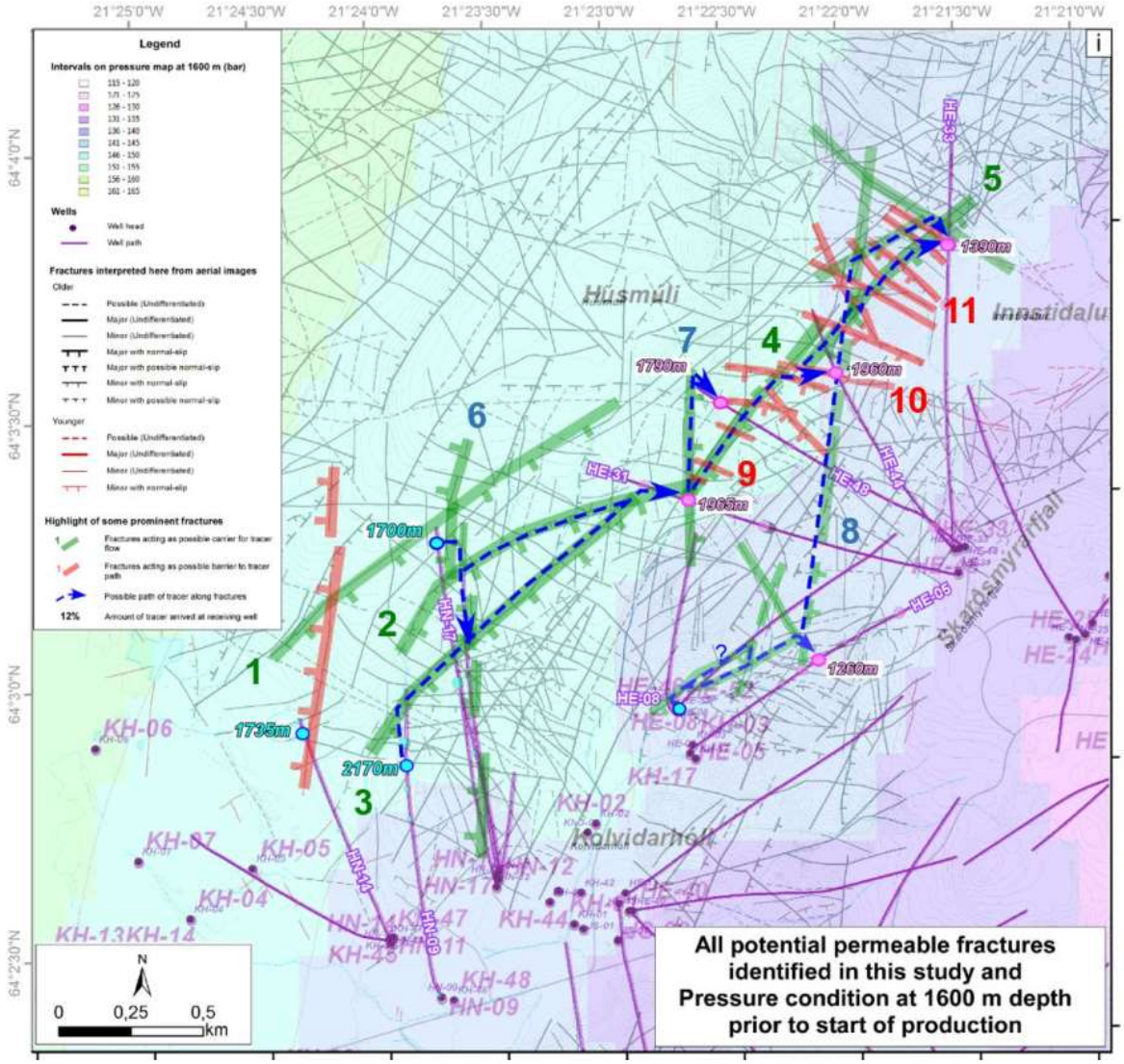

Figure 3.6 All potential permeable fractures that are possible tracer flow paths from individual injection wells to production wells (Khodayar et al., 2015 and Ratouis, et al., 2019).

(structures 9-11) are southwestward dipping and run perpendicular to the tracer flow direction and act as barriers for the tracers coming from the southwest, resulting in a delay of the tracer travel time across the fault. Accordingly, if the flow path is parallel to the fracture plane and runs on the hanging wall block of the fault, the structure acts as a carrier, facilitating the travel path and a short travel time. But if the tracer flow path is perpendicular to the fracture plane, even with a favorable dip direction and on a hanging wall, the extensional fracture acts as a barrier, thus delaying the travel time (Ratouis et al., 2019). The ENE, WNW, NW, and E-W faults are the Riedel shears of the SISZ while the NNE set, which plays a dominant role in fracture permeability and earthquake activity, belongs to the rift (Khodayar, 2013; Khodayar et al., 2015).

3.6 Previous Reservoir Models

Geothermal modelling studies of the Greater Hengill Volcano go as far back as the 1980s (Bodvarsson et al., 1990), when the focus was on the Nesjavellir field situated to the north of Hengill. The size of this early model was 12 by 12 km, and it consisted of 4 layers and 250 grid elements. The estimated initial pressure and temperature distributions of the system, and a limited production history, were used for calibration purposes. Accordingly, the capacity was estimated to be 300 MW_{th} of thermal energy for a 30-year exploitation period as the plan was only to produce hot water at Nesjavellir for the Reykjavík area The first phase of the development of the Nesjavellir plant was 100 MW_{th} thermal, commissioned in 1990 and expanded to 150 MW_{th} in 1991.

This first model simulated the geothermal system quite well, in view of modelling capabilities at the time and the short production history available. However, the model overestimated pressure drawdown rates, which resulted in underestimated production rate of wells. In 1992 the model was adjusted considerably in size, from 12×12 km to 100×100 km, increasing the external permeability and re-gridding the mesh close to new wells to match the production rate of the field recorded from 1986 to 1992. This model predicted that the system was capable of sustaining an additional 100 MW_{th} thermal energy compared to 300 MW_{th} in the first model (Bodvarsson, 1993).

Further updating of the Nesjavellir reservoir numerical modelling was performed in 1998 (Bodvarsson, 1998). It had been decided at this time to start electricity generation at Nesjavellir. The modelling work used the previous model with some adjusting of the permeability and porosity of the system, which resulted in an output estimate of 60 MW_e and 200 MW_{th} thermal utilization for another 30 years. To study the feasibility of adding another 30 MW_e electrical and 100 MW_{th} thermal unit to the existing power plant, the model was recalibrated once again in 2000 (Bjornsson et al., 2003) and the fourth 30 MW_e electrical unit added in 2005, bringing the total plant capacity to 120 MWe and 300 MW_{th} being operated now a days.

Further geothermal field development was started in the Hengill area in the year 2001, Hjörleifsdóttir et al. (2021) focusing on Hellsheiði field situated south of Nesjavellir, hence new reservoir model (Bjornsson et al., 2003) of the greater Hengill system became necessary. The new model was calibrated by incorporating temperature logs amounting to 1100 measurements, pressure logs amounting to 450 measurements, lithology, thermal alteration and fluid chemistry over a 38 years time span, used as initial values for the new

model. Finally, considering the existing Nesjavellir model parameters as an initial guess, two NE striking volcanic fissures, which intersected the Hengill volcano ~2000 and ~5500 year ago, act as primary conduits for subsurface fluid flow in the model of the region. A single up-flow zone was assumed to be situated underneath the Hengill volcano, feeding hot fluid to both Nesjavellir and Hellisheiði, the Hveragerdi field may also receive fluid from that same upflow zone so that the model mesh allows for a transverse flow structure already suggested by geophysical and geological studies. Nesjavellir rock properties are reflected across the entire Hengill volcano in this model. Work on this model, which is shown in Figure 3.7a, started in 2003. It encompasses a total area of 100×100 km with a total thickness of 2500 m, ranging from 300 m a.s.l., to 2200 m b.s.l., having eight different layer thickness ranging from 100 m to 500 m. The model consists of 4,358 elements with varying size and 15,000 connections.

In 2010, a model of the Hengill geothermal reservoir was again developed to incorporate four upflow zones of the system situated in the areas of Nesjavellir, Hellisheiði, Bitra and Hverahlíð (Gunnarsson et al., 2010) performed using the TOUGH2/iTOUGH2 simulation package. The model (Figure 3.7b) has a total area of 10,000 km^2 (100×100 km) and total thickness of 2700 m depth, ranging from 400 m a.s.l. to 2300 m b.s.l. classified into nine layers of different thickness with a total number of 8694 elements of different sizes. The numerical modelling was performed based on geological survey data and production data of the wells with the aim to calibrate host rock parameters of the model, and finally used to estimate the production capacity of the field for future power and thermal production.

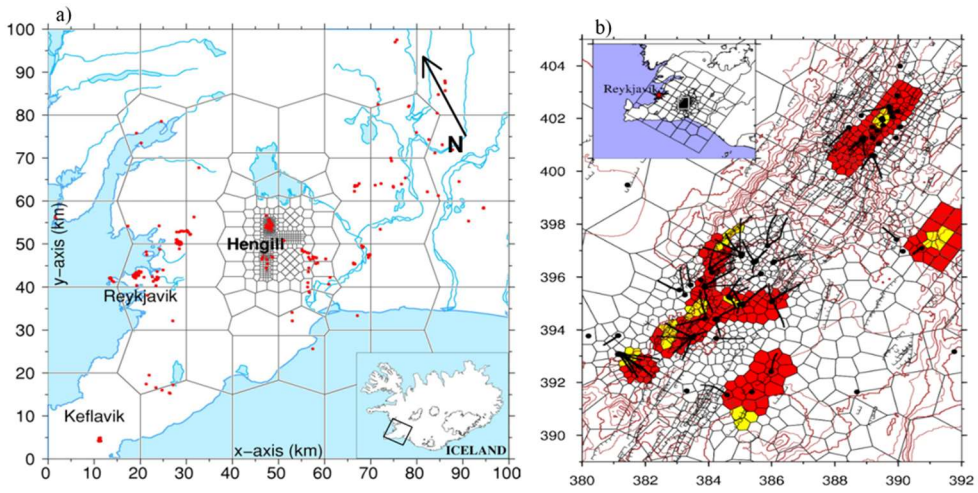

Figure 3.7 Numerical model layout of the Hengil volcanic system a) constructed by Bjornsson et al. (2003) in 2000 and (b) developed by Gunnarsson et al. (2010) in 2010. The red dots in a) show wells while the colored areas in b) show the location of heat sources in the 2010 model, where red color indicates places where only heat is introduced while yellow color indicates places where hot fluid is injected at the bottom of the model.

Furthermore, numerical modelling works aimed at determining the possible flow paths, using tracer test data, continue to be developed on a small scale for individual fields of the Hengill volcano. Among others, the modelling work done by (Kristjánsson et al., 2016) to define the potential structural flow paths for tracers and source faults of earthquakes in the Húsmúli area of Hengill, set up a cornerstone for further modelling works. The recent research performed by Gunnarsson and Aradóttir (2014) based on 8 reinjection wells,

Snæbjörnsdóttir et al. (2018) based on reinjection well HN-16, Tómasdóttir (2018), Ratouis et al. (2019), and Mahzari et al. (2021) based on reinjection well HN-17, are a few studies that clearly illustrate the possible major and minor flow paths in the fracture network of Hellisheiði field based on tracer test data. Gunnarsson et al. (2018) uses well HN-16 as reinjection well and CO_2 as second component in their modelling study of the area.

All the models outlined above are executed with the TOUGH2/iTOUGH2 coding system. However, utilization of data from recent tracer tests, i.e. from mid-2018, performed in the Hellisheiði field along with a new reservoir numerical modelling tool, i.e ***Volsung***, as well as making comparison with the one dimensional single fracture ***TRINV*** tool with final objective of cooling prediction, is what mainly makes the present study different from the above-mentioned researches.

4 Methodology

This section consists of five sub sections describing the software and methods used to build the models used in this study, how to proceed with calibration of model parameters based on the Hengill system natural state and specifically the tracer recovery simulation process applied through the numerical model and the simpler analytical model as well. The first section introduces step by step the governing equations used by the numerical model simulator. The second section deals with the conceptual model and its components and their relevance. The third section elaborates step by step the numerical model development while the fourth section describes the procedures to be followed during natural state and tracer simulation in three-dimensional numerical model. Meanwhile, the fifth and last subsection introduces tracer test simulation on basis of a one-dimensional analytical model.

4.1 Volsung Geothermal Reservoir Simulator

Volsung (Franz et al., 2019; Franz and Clearwater, 2021) is a geothermal fluid flow simulation package family that has enhanced data visualization, incorporating different simulators for running fully coupled geothermal reservoir, wellbore, and surface network models as well as inverse modelling. In the geothermal industry, the TOUGH2 software package (Pruess et al., 2012) has been the industry-standard numerical simulator for the last couple of decades. Recent years have seen the development of additional simulation software packages including TOUGH2's successor TOUGH3 (Jung et al., 2018), Waiwera (O'Sullivan et al., 2019), TIM (Yeh et al., 2013), in addition to ***Volsung*** (Franz et al., 2019; Franz and Clearwater, 2021). PyTOUGH (Croucher, 2021) is also a Python program widely used for pre-processing and post-processing of TOUGH data files.

The governing equations used to simulate multi-phase and multi-component flow of heat and fluid mass through porous and fractured media using the integral finite difference method is described in detail in the user manual of ***Volsung*** (Franz and Clearwater, 2021). The software uses its own internal computational engine called ***Fafnir*** in order to perform the computations in a way that is comparable with TOUGH2. Like TOUGH2, all thermophysical properties of the fluid required for the computation of fluid flow are computed within an Equation of State (EOS) module. All secondary variables are calculated using a set of primary variables (X). A factor of $N_p = N_c + 1$ is necessary to choose the primary variables where N_p is the number of primary variables per element and N_c is the number of fluid components, e.g. $N_c = 1$ for pure water or $N_c = 2$ if a second component like CO_2 is present.

Volsung uses the thermodynamic steam table tool, i.e. IAPWS-IF97, to calculate the required initial primary persistent thermodynamic variables (defined as variables that remain independent even as phase conditions change, so that they can be used throughout the single and two-phase regions) from the input which helps the user to skip time consuming and complicated calculations of partial pressure of mass fraction of the NCG by entering the fluid composition using the set of persistent thermodynamic variables of either pressure, specific enthalpy and fluid mass fraction components (i.e., p, h, X) or pressure, temperature and mass fraction components (i.e., p, T, X). ***Volsung*** is fully capable of running different EOS and offers flexibility to switch simulations from one EOS to another.

The new reservoir simulator ***Volsung*** in its working interface called Brynhild, is very flexible in its capability to accept different data inputs. The data input for ***Volsung*** is prepared in different forms beginning from either creating the entire model, i.e. the grid geometry and rock parameters on its own interface or importing fully or partially the TOUGH2 model input and geometry files done on LEAPFROG (Seequent, 2020) using the new flow button or prepared using Python script library like PyTOUGH (Croucher, 2021) or AUTOUGH2. The most interesting part of ***Volsung*** is that it doesn't need further tools for visualization of the output, like TOUGH2 does. All results are viewed through its 3D visualization interface tool, with the possibility of exporting an output listing file to LEAPFROG software to view in three dimensions.

Like TOUGH2, TIM and Waiwera, ***Volsung*** uses the finite volume method (FVM) to solve the governing equations of conservation of mass and heat for transport of heat and mass in porous and fractured media of a geothermal reservoir system. The equation for the mass and heat balance in the fractured media of the reservoir system is described by the following equations:

$$\frac{dM_i^k}{dt} = V_i^{-1} * \left(\sum_j A_{ij}\, F_{ij}^k + Q_i^k\right) \qquad (4.1)$$

with M_i^k being the mass/heat accumulation term of component k (H_2O, CO_2, air, tracer, etc.) in element i, V_i is the volume of element i, A_{ij} is the interface area between element i and element j; the summation goes over all neighbours j to the element i. F_{ij}^k is the component flux between the elements, which is symmetric, i.e. $F_{ij}^k = -F_{ji}^k$, and Q_i^k is the component source or sink rate.

here the term M is split into mass and heat accumulation terms as follows:

For mass accumulation: $M^k = \phi \sum_\beta S_\beta \rho_\beta X_\beta^k$ (4.2)

For heat accumulation: $M^{Nc} = (1-\phi) C_R \rho_R T + \phi \sum_\beta S_\beta \rho_\beta u_\beta$ (4.3)

where ϕ denotes porosity, β denotes the fluid phase (e.g., liquid, gas), R denotes the rock, T denotes temperature, C denotes heat capacity and u denotes specific internal energy of the phase. The phase parameters S, ρ and X^k denote the phase saturation, phase density and phase component mass fraction of component k, respectively.

The term Q_i^k (sources and sinks) in equation (4.1) appear in many forms within a reservoir simulation. The common way to specify the flow rate is in the form of using mass flow rate w, dry heat rate q, specific enthalpy h and component mass fraction X. They relate back to the component source/sink rate:

For the mass flow rate: $Q_i^k = \pm w . X^k$ (4.4)

For the heat flow rate: $Q_i^{Nc} = \pm w . h \pm q$ (4.5)

where the symbol ± denotes injection/extraction of mass/heat in to/out of the element, i.e. + if reinjection and - if extraction.

Fluid fluxes between two computational elements are calculated using linear Darcy flow in its discretized form as follows:

$$F_{ij,\beta} = -k_{ij}.\frac{k_{r\beta}.\rho_\beta}{\mu_\beta}\left(\frac{P_{i,\beta}-P_{j,\beta}}{D_{ij}} - \rho_{ij,\beta}.g_{ij}\right) \quad (4.6)$$

Where

- D_{ij} is the nodal distance between the two element centers;
- $P_{i,\beta}$ is the phase pressure of element i, which differs from the system pressure p in i by taking the capillary pressure into account, i.e. $P_{i,\beta} = P + P_{cap,\beta}$;
- g_{ij} is the force of gravity acting between the two elements, i.e. g_{ij} = cosαg where g is the gravitational acceleration and α the angle to the vertical between the two element centers; and
- k_{ij}, $k_{r\beta}$, μ_β and ρ_β represent the total permeability, relative permeability, dynamic viscosity and phase density, respectively.

Once the phase Darcy flux between two elements is computed, it is used to calculate the following:

The phase mass component flux; $F^k_{ij,\beta} = F_{ij,\beta}.X^k$ (4.7)

The total component flux; $F^k_{ij} = \sum_\beta F^k_{ij,\beta}$ (4.8)

The total flux; $F_{ij} = \sum_k F^k_{ij}$ (4.9)

On the other hand, the heat flux between two elements, which in its discretized form is:

$$F^{Nc}_{ij} = \sum_\beta h_\beta F_{ij,\beta} - \lambda\frac{T_i-T_j}{D_{ij}} - \epsilon.\sigma_{SB}\left(T_i^4 - T_j^4\right) \quad (4.10)$$

Where

- D_{ij} is the nodal distance between the two element centers;
- h_β is enthalpy of the phase component;
- λ is heat conductivity;
- T_i , T_j are temperature of elements i and j;
- ϵ is radiative emittance; and
- σ_{SB} is the Stefan-Boltzmann constant.

For numerical simulations, the governing equation of mass and heat should be discretized continuously over space and time to get a vector residual (R) that is approximately nil as follows:

$$R^k_i(t+\Delta t) = M_i(t+\Delta t) - M_i(t) - \frac{\Delta t}{V_i}\left(\sum_j A_{ij}F^k_{ij} + Q^k_i\right) \quad (4.11)$$

Iterations are done until all the residuals for all elements and components are reduced below a convergence tolerance. The basic acceptance criterion is:

$$\frac{\left|\tilde{M}_{i,p+1}^{k}(t+\Delta t)\right|}{\left|M_{i}^{k}(t)\right|} \leq \varepsilon_1 \qquad (4.12)$$

where ε_1 is the relative convergence criterion (typically 10^{-5}) and p denotes the iteration index of the Newton-Raphson method.

4.2 Conceptual Model Development

A good conceptual model is the basis for developing a numerical model, revealing the location of heat sources, tectonic structures like faults and fractures, alteration zones and other features. The conceptual model is an output of a combined study of geological, geochemical, and geophysical exploration, and helps for the assessment of a geothermal resource located within a particular area (Mortensen, 2017). Conceptual models are not used for calculations, but are rather descriptive or qualitative, appearing in either 1D, 2D or 3D forms (Mortensen and Axelsson, 2013). To be standalone, a conceptual model should incorporate surface mapping and analysis of subsurface geological data, remote sensing data, resistivity and magnetic information, chemical and isotopic content of fluid information in surface manifestations and reservoir fluid samples collected from wells, information on temperature and pressure conditions based on analysis of available well-logging data as well as various reservoir engineering information (Mortensen and Axelsson, 2013).The final aim of conceptual models is to highlight the distribution of thermodynamic variables like temperature and pressure, and hydrological parameters like permeability and fluid chemistry that are fundamental in delineating the direction of fluid flow and circulation within the reservoir part of a geothermal field.

In this thesis, the conceptual model is developed to represent the hypothetical reservoir system of Hellisheiði geothermal field in a simplistic way. The major components incorporated in this study are the host rock formation (extrusive and intrusive rocks) that constitutes the reservoir system, a 200 m thick cap rock at an elevation of sea level (Árnason et al., 2010) that prevents fluid circulation between the reservoir system at the bottom and cold ground water at the top, the heat sources, three NE strike rift parallel faults and one EW transform fault that control the flow and finally reinjection and production wells that drive the fluid convection. The heat source is believed to be at ~2.3 km b.s.l (Gunnarsson and Aradóttir, 2014) in the vicinity of an area that extends from wells HE-05, HE-31, HE-33, HE-44, HE-46 and HE-48 down to the southeast encompassing wells HE-06 and HE-09 (Gunnarsson et al., 2010), and is believed to be the solidified magma in the volcanic fracture that erupted some 2000 years ago (Steingrimsson, pers. comm., September 2022) as depicted in Figure 4.1.

The three major NE-striking faults (shown in Figure 4.1, Figure 4.3 and Figure 4.4) associated with dilationary rifting act as fluid conduits (Mahzari et al., 2021) between the reinjection and production wells and the one EW striking fault associated with the transform zone acts as a barrier (Ratouis et al., 2019, 2022) for the tracer that hinders it from flowing towards the production wells, as demonstrated by the tracer recovery at the monitoring wells. The tracer return at wells located to the northeast and lack of tracer at wells located to southwest clearly suggests that the permeability of both the host rock and the tectonic structures is anisotropic. The five reinjection wells (HN-09, HN-12, HN-14, HN-16, and HN-17) and six production wells (HE-05, HE-31, HE-33, HE-44, HE-46 and HE-48) (see

Figure 4.1) are also incorporated in the model to represent assumption of fluid inflow and outflow to/from the model through the feed zones of these wells.

4.3 Three-Dimensional Model Setup

The model size in the study is set to cover an aerial extent of 63.36 km^2 (i.e., 8.8×7.2 km). Figure 4.1 shows this area, including the six production wells in parts of the Skarðsmýrarfjall field and five reinjection wells in the Húsmúli reinjection area.

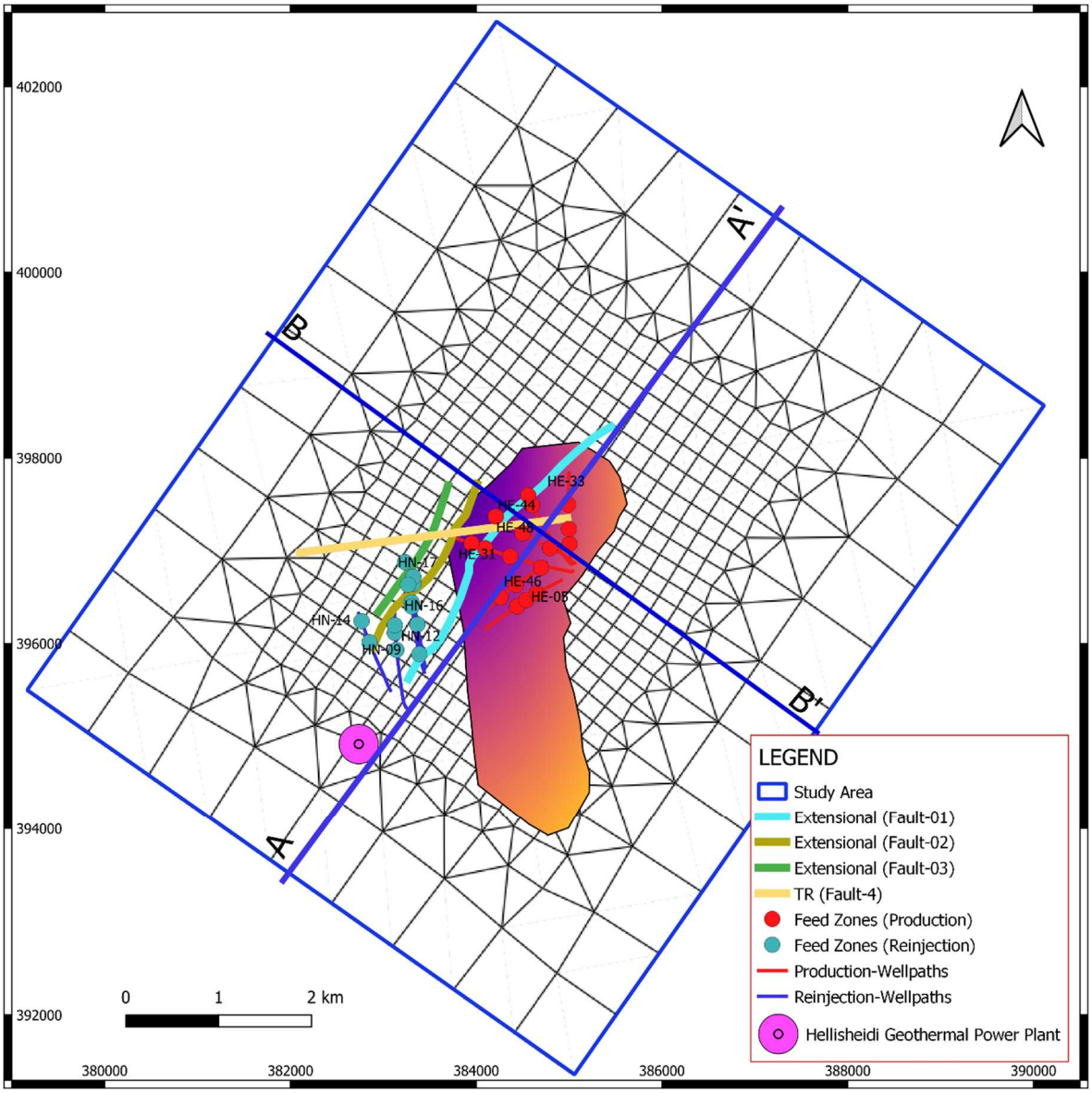

Figure 4.1 Model grid set up of the study area. Extensional faults are depicited by red, green and blue solid lines. The cross section lines labeled by AA' and BB' are used for display of model outputs like vertical rock assignments (refer to Figure 4.2), temperature distribution (refer to Figure 6.2) and tracer distribution over time (refer to Figure 5.7).

The grid is set up in 4 steps of refinement and tilted 35° to align with the main fluid conduits or NE trending faults in the area. The topographic surface in the model is based on the 3D geological model developed by Reykjavik Energy (OR) for the Hellisheiði Geothermal area created in Leapfrog Geothermal (Gunnarsdóttir and Poux, 2016). Refinement in the grid size from ~800 m block size at the boundary to ~200 m at the main area of interest was done using PyTOUGH (Croucher, 2021). The grid has a total of 9578 elements and 28,517 connections. Except for the topographic surface, all the rock formations are made flat for their entire horizontal extent. The number of layers of the model including the topographic surface layer is 15, each with a thickness of 200 m. Although grid generation was performed using Leapfrog and PyTOUGH, rock type assignment was done manually using ***Volsung***. The depth of the model is chosen to be adequately deep to include the measured depth of the wells and the fractured zones of the reservoir, which ranges from 600 m a.s.l to a depth of 2600 m b.s.l, encompassing the deep feedzones and the whole depth of wells where fluid circulation is believed to be taking place.

The model rock type assignment shown in Figure 4.2 is based on the stratigraphic arrangement of the Hellisheiði field (Gunnarsson and Aradóttir, 2014) resulting from well cuttings based on binocular microscope analysis; however, the geometry and placement of the cap rock is based on electrical resistivity models of the area. Accordingly, the model is classified into the shallow cap rock, the cold ground water system, the cap rock of the geothermal system, geothermal reservoir rocks comprised of the post-glacial lava flows and hyaloclastites, and intrusive basement rocks. Horizontal cross section of each rock type is shown in Appendix 3. The top layer is represented by a couple of 200 m thick layers associated with a shallow clay cap (Árnason et al., 2010) followed by another low resistivity layer, which corresponds to the cold ground water system that appears to be at an average depth of 200 m below ground surface (Gunnarsson and Aradóttir, 2014), represented by a 200 m thick layer. The next layer is the less permeable cap rock of 200 m thickness at sea level (Árnason et al., 2010), which prevents fluid circulation between the ground water and geothermal system.

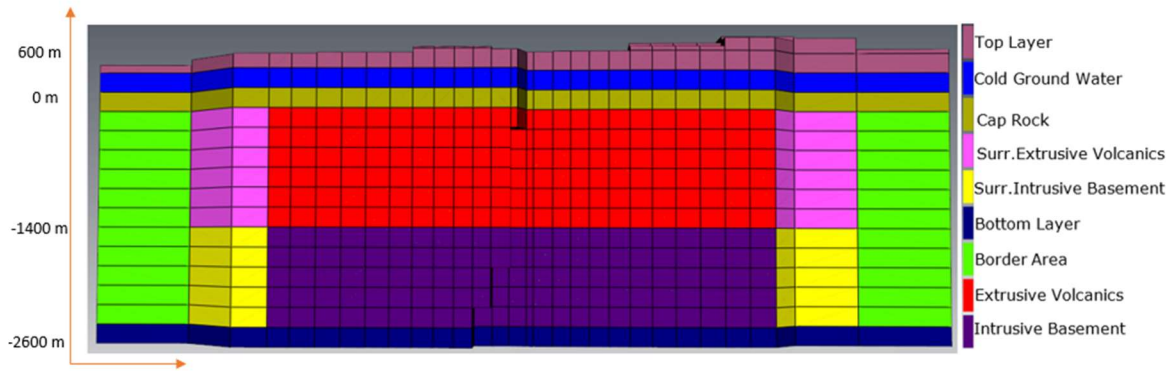

Figure 4.2 Rock type assignment of model built in Volsung across cross section A-A' (see Figure 4.4).Top layer started at 600 m.a.s.l down to 200 m.a.s.l while cold ground water system and cap rock are represented by 200 m thick layer each aligned horizontally across the entire model. On the other hand the main host rocks, i.e, extrusive volcanics and intrusive basement started from -200 m.b.s.l down to 1400 m.b.s.l and from 1400 m.b.s.l down to 2400 m.b.s.l respectively.Finally, the bottom layer used to support the model is 200 m thick.

The geothermal reservoir system is allocated by two rock types namely extrusive volcanics or the hyaloclastites (from depth of 200 m b.s.l to 1400 m b.s.l) and intrusive basement (from depth of 1400 m b.s.l down to 2400 m b.s.l) as clearly mentioned in Franzson (1998) is located between the bottom layer and cap rock layer of the model and is enclosed by surrounding formations and border area with lower permeability. Hyaloclastites are formed by magma-water interaction during glacial periods and are highly heterogeneous, ranging from crystalline pillow basalts with only minor amounts of volcanic glass to pure volcanic glass (tuffs) (Gunnarsson and Aradóttir, 2014, Snæbjörnsdottir et al., 2018). The intrusive rocks are "associated with interglacial periods where lavas erupted in the highlands and flowed to the lowlands" (Gunnarsdóttir and Poux, 2016), which is believed to be base of Hengill volcanic system is created before establishment of the Hengil central volcano, belonging to another central volcano called Grensdalur 5 km east of Hengill (Franzson, 1998). The deepest part of the model is the 200 m thick bottom layer at 2500 m b.s.l, which represents the low permeability formation that controls fluid migration between the reservoir system and the underlying heat source.

To make the model representative of the reservoir's complex network of fractures, the NE-striking parallel fault structures (Khodayar et al., 2016) and the EW-striking transform fault that control the fluid flow in the reservoir system are incorporated into the model (see Figure 4.3). The three extensional parallel structures are believed to be the main favorable flow paths of tracer (Mahzari et al., 2021) from well HN-16 to wells HE-31, HE-33, HE-44 and HE-48, as based on the Hellisheiði 3D geological model (Gunnarsdóttir and Poux, 2016) while the fourth fault acts as a barrier to tracer circulation due to its perpendicular alignment with the parallel faults. These faults are identified in the hyaloclastite formations (Hersir et al., 2009) and have a near-vertical dip spanning the entire model depth.

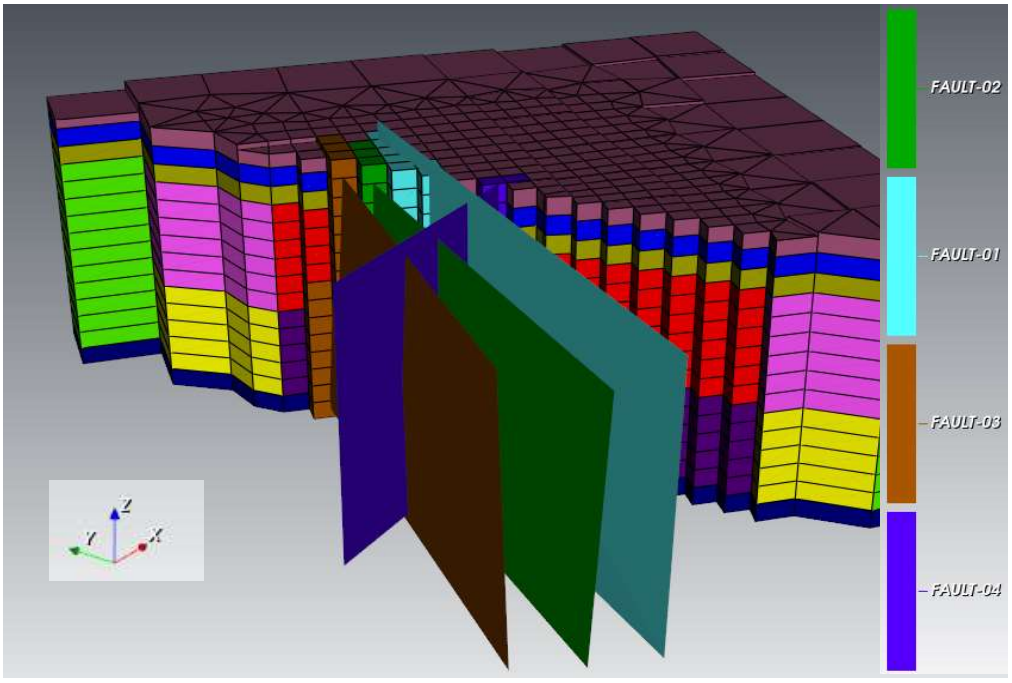

Figure 4.3 NE and EW trending faults and their intersection in the 3D model. The faults are extracted from the Leapfrog 3D geological model of the Hellisheiði geothermal field (Gunnarsdóttir and Poux, 2016) as dxf.file and integrated into the numericals model.

While initial permeability values of the rocks are shown in Table 4.1, the physical properties of rocks such as density (2650 kg m^{-3}), porosity (10%), heat conductivity (2.1 W m^{-1} K^{-1} based on Clauser and Huenges, 1995) and heat capacity (1000 J kg^{-1} K^{-1} based on Bouhifd et al., 2007) are assigned as constant. Due to the fact that Hellisheiði's reservoir system is characterized by complex fracture networks (Khodayar, 2013 and Khodayar et al., 2015), the two dominant rock formations namely intrusive and extrusive rocks are assigned dual porosity (Barenblatt, 1960; Warren and Root, 1963) where the blocks of rock are further categorized into fracture and matrix elements. While the fractures support the permeability of the rock, the matrix on the other hand, provides the volume where the fluid is stored (Goloshibin, 2006). Permeability for the fracture is assigned higher than that of the matrix's and the flow between blocks of the matrix occurs through the fractures. The fracture ratio (10%), fracture spacing (150 m), fracture porosity (90%) and matrix porosity (5%) are taken into consideration as clearly mentioned by Ratouis et al. (2019; 2022).

Table 4.1 Initial Permeability values utilized in the model. The values for the top layer, cold ground water, cap rock and bottom layer are retrieved from the work of Gunnarsson and Aradóttir (2014). However, the values for the faults, intrusive basement, extrusive volcanics, surrounding and border areas are the guess of the current author.

	Permeability (m^2)			
Rocks	**X**	**Y**	**Z**	**Matrix**
Top Layer	10^{-15}	10^{-15}	10^{-15}	
Cold Ground Water	10^{-14}	10^{-14}	10^{-14}	
Cap Rock	10^{-17}	10^{-17}	10^{-17}	
Extrusive Volcanics	10^{-14}	10^{-14}	10^{-14}	10^{-18}
Surrounding of Extrusive Volcanics	1.5×10^{-17}	1.5×10^{-17}	1.5×10^{-17}	
Intrusive Basement	10^{-15}	10^{-15}	10^{-15}	10^{-18}
Surrounding of Intrusive Volcanics	10^{-17}	10^{-17}	10^{-17}	
Border Area	10^{-18}	10^{-18}	10^{-18}	
Bottom Layer	10^{-18}	10^{-18}	10^{-18}	
Extensional Faults	10^{-13}	10^{-13}	10^{-13}	
Transform Fault	10^{-13}	10^{-13}	10^{-13}	

O'Sullivan (2015) suggests that the best way of utilizing boundary conditions to represent convection and conduction in a natural state model simulation is to assign source terms for heat and mass to the bottom layer of the model. Hence, the heat source in this study is chosen to be at 2300 m b.s.l. (Gunnarsson and Aradóttir, 2014) in the vicinity of the production borehole, as the higher downhole temperature of these wells is believed to indicate the presence of "hot fluid up-flow heated by a complex of dikes and sills associated with an eruptive fissure active during the Holocene" (Scott et al., 2014) underneath theSkarðsmýrafjall production wells (Gunnarsson et al., 2010). Accordingly, hot fluid is injected at a constant rate into the 2nd deepest layer of the model in this area. The lateral or side boundaries of the model are closed except the NE side, due to recharge (regional ground water flow) into the model domain (Aradottir et al., 2012), which is instead represented by a constant pressure boundary condition. Lastly, top boundary of the model is assigned by

constant pressure and temperature connected all the way to the ambient atmospheric condition.

4.4 Three-Dimensional Model Simulation

For this study, EOS1 is implemented as the equation of state module, which assumes pure water as the fluid component (Component 1 representing the geothermal fluid) and steamtable of (IAPWS 2014) is assumed. An extra component representing the tracer (Component 2) is used for making the tracer simulation. All the data utilized in the modelling procedure is supplied from Reykjavík Energy. The model is simulated in two consecutive stages: 1) natural state simulation and 2) tracer transport simulation.

4.4.1 Natural State Model Simulation

The natural state model describes the field in its original condition, prior to the extraction of fluid mass. Volsung simulates the natural state for a long period of time (hundreds of thousands or millions of years) until all thermodynamic variables like temperature, pressure and enthalpy converge to steady-state values. Calibration of rock parameters (mainly the permeability) and calibration of heat inflow either hot fluid or dry heat injection to the deepest layer of the model is carried out until the outputs of the model matches with measured downhole formation temperatures. The output of this stage, a ***SAVE file***, is used as the initial condition for thermodynamic variables for the tracer recovery simulation. In this study, the convergence criteria was reached after the simulator has run for a period exceeding 100,000 of years and all the thermodynamic primary variables like temperature, pressure and enthalpy had reached a steady-state. The output is believed to represent the state of Hellisheiði reservoir in 2011 when full scale reinjection was launched in the Húsmúli area, in the NW part of the field. The natural state simulation was started from a cold start i.e a pressure magnitude of 100 bar and temperature magnitude of 15°C was assigned for every rock formations in the entire model.

4.4.2 Tracer Return Simulation

The second task of the numerical simulation is the tracer return simulation, which is performed as component 2 simulation using EOS1. The simulation begins on 11th of July 2018, when 99.6 kg of 2,6-NDS tracer was injected for a couple of hours into well HN-16 and is run until the end of 2021. During simulation, all production and reinjection wells including HN-16 are at flowing conditions. The tracer appeared at production wells HE-31, HE-48 and HE-44 after 10, 15 and 42 days of travel time, respectively, since the onset of reinjection (Figure 4.4). The tracer arrived at well HE-33 after 454 days of travel in an extremely small amount.

To reduce the influence of tracer injected before 11/07/2018 in the reservoir system including the 2014 tracer injection carried out at HN-16 and tracer injection in 2013 at wells HN-17 and HN-09, the tracer background value is subtracted. Furthermore, to avoid convergence problems during the simulation due to different orders of magnitude between the mass of the main component H_2O and the injected tracer the amount of injected tracer was scaled to a higher amount, i.e. by a factor of 10^4.

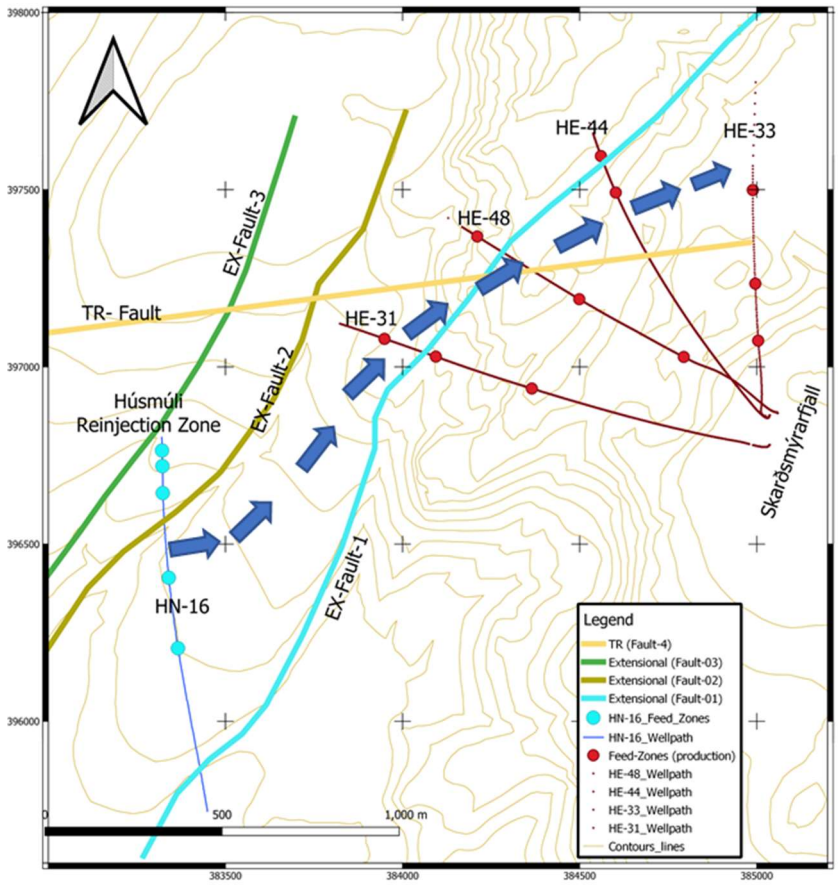

Figure 4.4 Horizontal tracer flow direction and arrival time at the observation wells. Note that the arrows don't show the exact flow path of the tracer but rather the general direction of flow. The tracer enters the system from well HN-16. The fractional contribution of different feed zones in wells involved is listed in Appendix 1.

The tracer transport simulation (Figure 4.6) is conducted by two approaches, i.e. single porosity and dual porosity. The single porosity approach considers the transport of tracer from reinjection well to production wells to be due to advection process (Axelsson, 2013), where the fluid flows via pore spaces from area of high-pressure potential to area of low-pressure potential. This helps to check whether the induced pressure gradient is sufficient to conduit the tracer from reinjection well to production wells and produce the expected return curves (Tómasdóttir, 2018).

The second approach classifies the reservoir into two interacting continua namely matrix and fracture system which avoids averaging parameters over the entire volume of a block (Ratouis et al., 2019). The manual calibration process is carried out either by modifying the permeability anisotropy of the rock or adjustment of other parameters like rock porosity, fracture ratio and fracture space. This is carried out until the tracer response of each observation well in the model attains the measured return curves. The shape of the tracer recovery curves, observed in the field, and shown in Figure 4.5 indicates that a fracture network is most likely present between well HN-16 and wells HE-31 and HE-48, which causes the tracer to move faster and reach its peak values, while the recovery curve at production well HE-44 looks like mostly matrix-dominated flow, which causes the tracer to flow more slowly and take longer to penetrate and reach the well. However, the data for HE-33 suggest that communication is limited due to possible presence of a barrier fault that

hinders the flow of fluid. A total of 41.2 kg of tracer was recovered from the four production wells, accounting for 41.3% of the total injected chemical.

Figure 4.5 Tracer recovery curves for observation wells (HE-31, HE-33, HE-44 and HE-48).

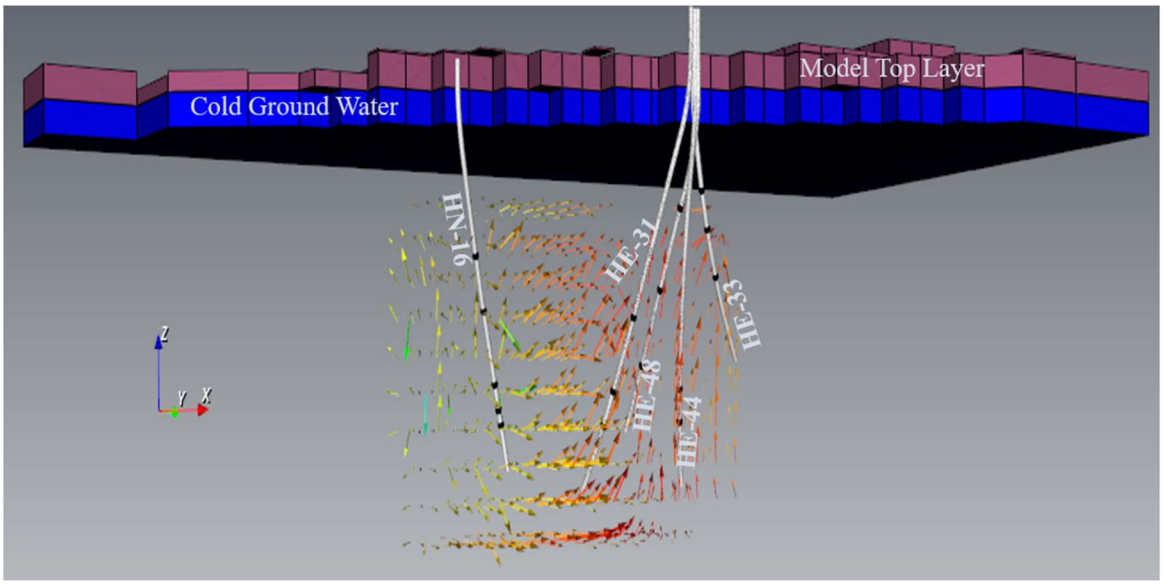

Figure 4.6 Vertical cross-section of model showing tracer transport simulation along cross section AA' see figure 4.4). The vector flow field of the tracer is indicated by arrows.

The anisotropy of the fault structures is introduced by assigning higher permeability along (parallel to) the fault plane and lower across (perpendicular to) the fault plane (Ratouis et al.,

2019). As these structures are the dominant controls on flow in the reservoir, this helps to represent preferential flow paths of the tracer in the reservoir system.

Finally, long term danger of cooling of the reservoir system because of cold fluid reinjection is predicted up to 2060 assuming that past mass flow rates continue. The temperature decline of the system modelled using numerical simulation is finally compared to the results of the 1-D tracer simulation software TRINV discussed below.

4.5 One-Dimensional Model Simulation

This section presents the tracer recovery modelling and associated cooling predictions performed using a simple one-dimensional modelling software named ***TRINV***, developed at Orkustofnun (predecessor of ÍSOR) for the purpose of modelling tracer recovery and thermal breakthrough for single and multiple flow channel simulation of geothermal reservoir systems. ***TRINV*** is part of the *ICEBOX* software package and used to solve equation (1.8) inversely by a non-linear least square method (Axelsson et al., 2005) for tracer recovered through monitoring wells, and ultimately used to predict cooling in the reservoir system of the well field, due to reinjection. The fundamental basis for this software is the theory of tracer transport (section 2.2) in porous and permeable fractured medium. The tracer recovery is controlled by the flow channel properties (Axelsson et al., 2005) such as flow channel length (x), flow channel cross-sectional area ($A\phi$) and flow channel dispersivity (α_{L}), along with production and injection rates.

On the other hand, along with assumptions on the surface area and porosity of the flow-channel, the flow channel properties and mass recovery are used to predict the danger of cooling of the production reservoir with time. A flow channel is defined as the conduits of the fracture network (Axelsson et al., 2005) for the injected 2,6-NDS tracer migration from the feed zone location of the reinjection well (i.e. HN-16) on its way to the feed-zones of the most affected production wells (i.e. HE-31, HE-44 and HE-48), see Figure 4.4. The application of this model helps characterizing the effects of mechanical dispersion and diffusion in the tracer transport, lack of which is the main drawback of conventional numerical geothermal models.

4.5.1 Tracer Return Simulation

TRINV analyzes the results of a tracer test for a single injection-production well pair, and one, two or three flow-paths or conduits. It assumes that a fixed mass of tracer is injected into the system at time t=0 and that the concentration of recovered tracer is then measured in observation well(s) at different times. The *TRINV*-tool uses measured tracer concentration values at monitoring wells as simulation input. In this study up to three flow conduits are considered in the analysis as this enables a better match with the field values.

Table 4.2 Basic parameters used in the TRINV simulation of 2,6-NDS tracer return in wells HE-31, HE-44 and HE-48, i.e. the wells that show substantial tracer recovery due to their good connection with the reinjection well of HN-16.

Production Wells	HE-31	HE-44	HE-48
Average production rate (kg/s)	75	50	54
Average reservoir temperature (°C)	265	243	257
Porosity (%)	5	5	5
Concentration Unit	kg/m^3	kg/m^3	kg/m^3

The *TRINV*-tool determines not only the tracer recovery in the production wells but also estimates the properties of each flow channel (Axelsson et al., 2005) such as flow channel cross-sectional area ($A\phi$), length of flow channel (x), flow channel dispersivity (α_L) and fluid-velocity (same as tracer-velocity) in the channels. Observed tracer return time series values (see Figure 4.5), injection rate (Figure 4.7) of both brine and condensate fluid at the reinjection well, the temperature of the reinjected fluid (Figure 4.8), the mass of tracer injected, length of the flow channels from the feeders of reinjection well to feeders of production wells and the production rate of the observation wells are the input values for *TRINV* (Table 4.2). Since the fluid injected into well HN-16 is a mixture of condensate and brine water, which have different temperatures, i.e. average temperature of the brine is 60°C and of the condensed steam is 20°C, an average injection fluid temperature of 40°C is used. The same is true for the water injection rate, which is taken as the time-averaged value of the injection flow rates.

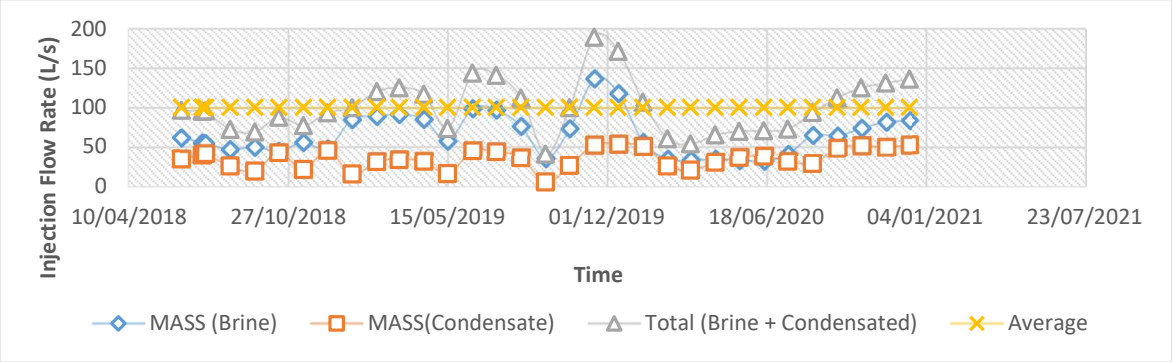

Figure 4.7 Mass flow rate of injected fluid into reinjection well HN-16. Data source: Reykjavík Energy.

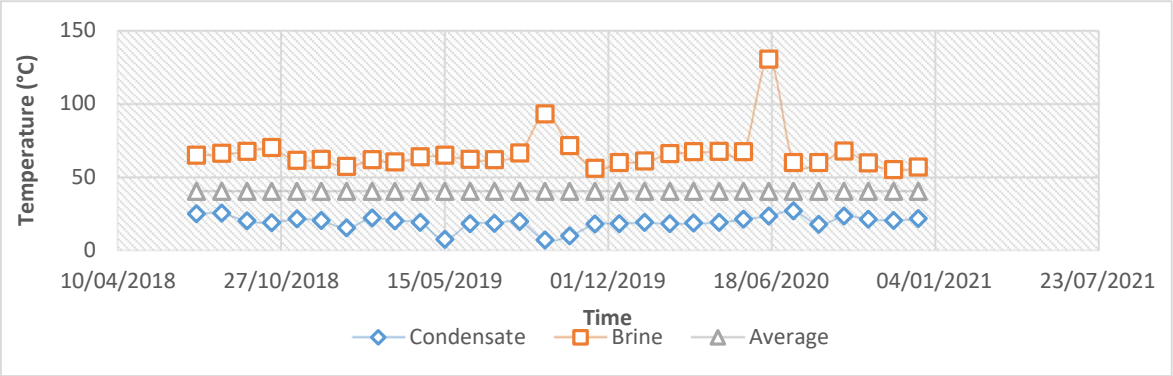

Figure 4.8 Temperature of injected fluid into reinjection well HN-16. Data source: Reykjavik Energy.

4.5.2 Cooling Predictions

Following simulation of tracer return, the resulting parameters are used to estimate the temperature decline during long-term cold-water reinjection. The mass fraction and cross-sectional area for each flow channel are the decisive parameters (Axelsson et al., 2005) in calculating the cooling impact of the cold-water reinjection on the production wells. Mass fraction describes the fraction of the cold water injected into the reinjection well, which migrates through the flow channel, eventually affecting the production well by cooling. While the cross-sectional area defines the size of the opening of the conduit, its aspect ratio, i.e. the ratio of height to width for the fracture has to be assumed/estimated. Kristjánsson et al. (2016) conclude that using a small aspect ratio is “overly conservative”, a higher aspect ratio which represents fault-like conduits in the reservoir system is utilized in this study.

5 Results

This chapter elaborates the results of both the numerical model development and simple TRINV model calculations. The temperature profiles of geothermal wells in the natural state numerical model are illustrated in the first section while tracer recovery simulation results of the corresponding wells are presented in the second section. The outcome of the one-dimensional simple modelling of the same wells is discussed in sub-section three. The modelled thermal response of the reservoir, due to cold water injection using both the numerical model and the simple one-dimensional model, is outlined in the last subsection (5.4).

5.1 Natural State Temperature Model

Natural state modelling of geothermal systems assumes that the mass and heat inflow into the model equals the outflow of heat and mass from the model, and that the system is at a "steady-state". As described in section 3.1, primary thermodynamic variables (temperature, enthalpy, pressure, and steam fraction) converge to steady-state values after a length of time (generally 10^6-10^7 years) depending on the physical behavior of the model and number of elements in the model. When the change in thermodynamic primary variables between time-steps becomes negligible, the size of the time-steps increases, and the model has attained a steady-state condition. The model developed in this work takes on average about 300,000 years to reach a steady state.

Manual model calibration is made against downhole formation temperature of wells HE-31, HE-33, HE-44, and HE-48, measured during the warm-up period immediately following the completion of the corresponding drilling operation in 2007/8. These boreholes are located in the Skarðsmýrarfjall area, close to where the heat source in the numerical model is located. Initially, hot fluid mass of 1 kg/s with an enthalpy of 1500 kJ/kg was injected to serve as the heat source in the second deepest layer, extending from the southeast part towards the zone underneath the production wells. The formation temperature resulting from this magnitude of heat energy input, besides utilizing the initial isotropic permeability distribution, clearly shows a significantly lacking fit with the field data (see Figure 5.1). In all the four wells, the down hole formation temperature is extremely underestimated and reflects inversion type of temperature profiles where boiling point temperature is recorded at approximately 500 m b.s.l. in all wells.

As this test appeared to produce unsatisfactory correlation between model output data and field data, the permeability structure of the very important rock formations such as the extensional and transform component fault structures, the basaltic intrusive and hyaloclastite extrusive rocks, along with strength of the heat sources, were tuned manually to achieve a formation temperature match between model predictions and field data. Eventually, a considerable correlation (Figure 5.2) is gained by elevating the rate of hot fluid mass injection and enthalpy to 25 kg/s and 1650 kJ/kg, respectively, and by switching the isotropic permeability to an anisotropic one. The ultimate values obtained are presented in Table 5.1.

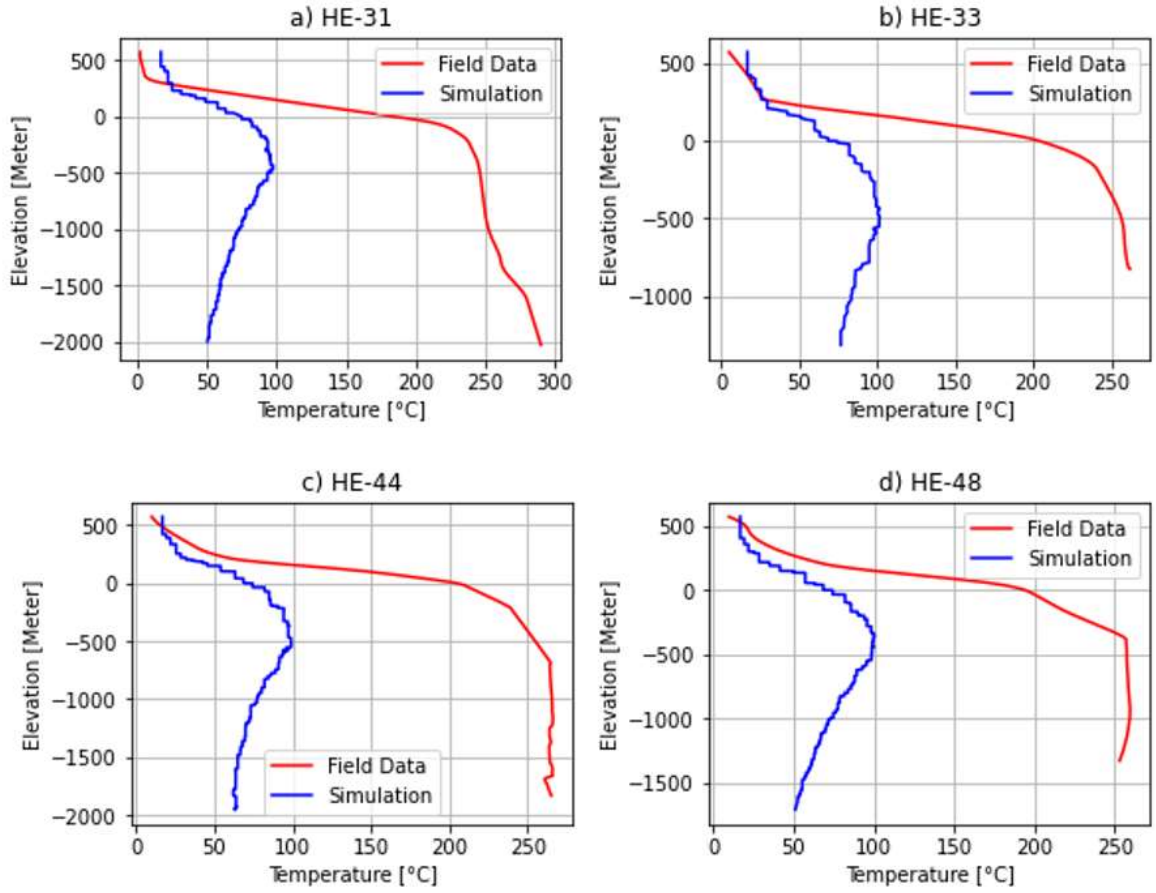

Figure 5.1 Observed and modelled downhole formation temperature profiles of production wells. a)HE-31, b)HE-33, c) HE-44, and d) HE-48.Note:This output is based on initial permeability values listed in Table 4.1.

The anisotropic permeability of extrusive rocks is modelled to be 2×10^{-14} m^2 in the vertical and y-directions, while it's 10^{-14} m^2 in the x-direction. Besides that, the anisotropic permeability distribution for the intrusive rocks is of the order of 10^{-14} m^2 horizontally and the order of 10^{-15} m^2 vertically. Similarly, the horizontal and vertical permeability distribution of the faults is estimated to be of the order of 10^{-15} m^2 and 10^{-16} m^2, respectively. Matrix permeability of both the volcanic extrusive and intrusive rocks is unchanged at 10^{-18} m^2.

Table 5.1 Calibrated anisotropic permeability values of the natural state model. Note: Only the rock formations taken in to account during calibration process are listed.

	Permeability (m^2)			
Rock types	X(SW-NE)	Y (E-W)	Z (Vertical)	Matrix
Extrusive volcanics	10^{-14}	2×10^{-14}	2×10^{-14}	10^{-18}
Intrusive basement	10^{-14}	1.5×10^{-14}	8.5×10^{-15}	10^{-18}
Faults (ex. and transform)	10^{-15}	10^{-15}	10^{-16}	

As apparent in Figure 5.2, the modelled downhole temperature of all the four production wells of the model fits the measured temperature trends fairly well, despite the slight underestimation of temperatures in the cap-rock. While there is a fair match between model result and measured formation temperature for well, HE-31 (Figure 5.2a), in the depth-range of 500-1500 m, the model predicts a slight temperature reversal below 1500 m, which is not reflected in the measurements. The downhole temperature of the entire depth of well HE-33 (Figure 5.2b) is underestimated to a small extent but the trend is in good agreement, as both the model and field data show a small degree of inversion. The overall trend of the modelled downhole temperature profile for well HE-44 (Figure 5.2c) is captured in the model, but temperature is only exactly matched at an elevation of 500 m b.s.l. The downhole temperature of HE-48 (Fig. 5.2d) is underestimated by the model down to a depth of 500 m b.s.l., the model closely matches the measured temperatures at greater depths. These results indicate that the initial reservoir temperature distribution in this part of the Hellisheði geothermal field is reasonably captured by the numerical model.

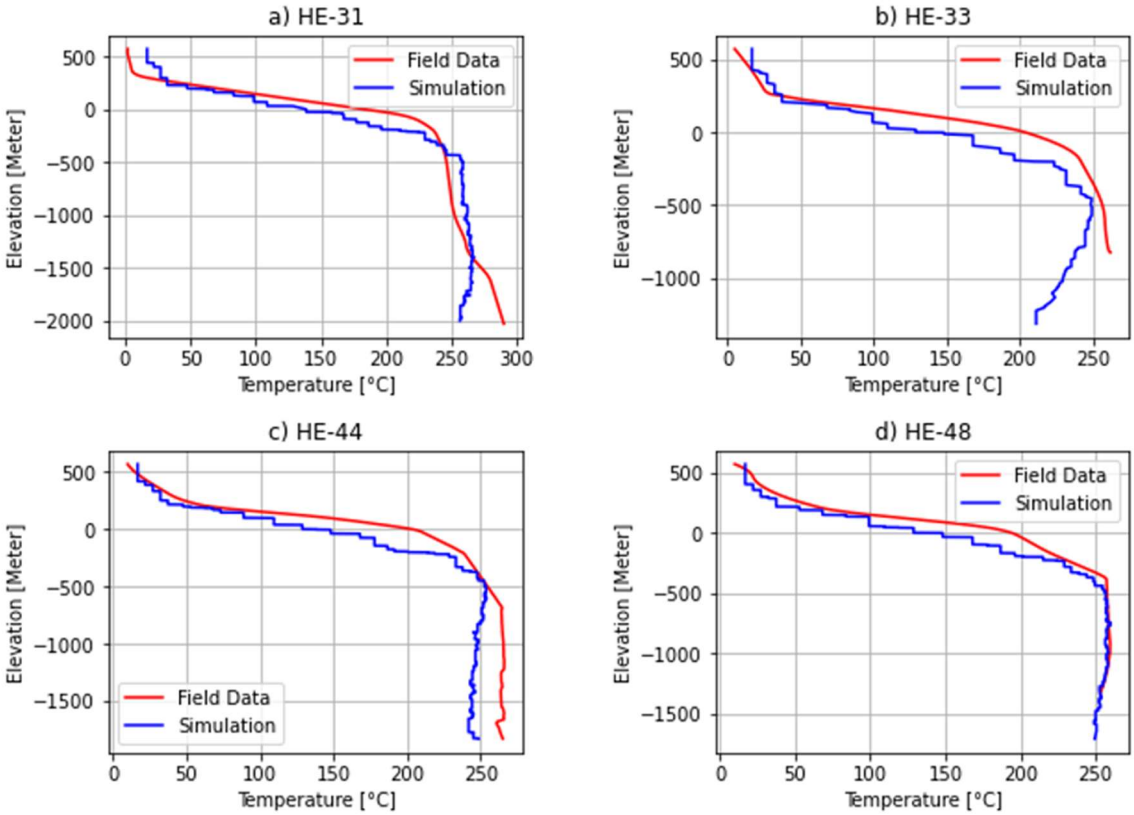

Figure 5.2 Down-hole formation temperature of wells a) HE-31, b) HE-33, c) HE-44 and d) HE-48. Model data is indicated by blue color and measured data is indicated by red color. Note:This output is based on thecalibrated permeability values presented in Table 5.1.

The slight discrepancies observed may result from the fact that these wells were drilled after >30 other wells had already been drilled in the area, which may have resulted in a disturbance of the reservoir temperature, during measurement time and hence the estimated formation temperature couldn't minimize the extent of the gap with the measured formation temperature. Besides, all the assigned rock types in the model are sorted in a manner with fully horizontal and uniform thickness throughout the entire model, which is different from reality where elevation and thickness varies greatly, which eventually leads to a slight

mismatch of model and field values. Overall, in terms of temperature, the correlation between model results and measured data is strong.

5.2 Tracer Test Model

The tracer test studied here was initiated July 11th, 2018, when 99.6 kg of 2,6-NDS were injected for a couple of hours into reinjection well HN-16, located in the Húsmúli area. Sampling at monitoring wells continued up to the 31st of December 2021. The appearance of the tracer at wells HE-31, HE-44, HE-48, and HE-33 indicates that the path of the tracer flow is linked with the extensional faults, which are aligned in a NE direction.

The numerical model simulation of the tracer transport during this period of the tracer test initially used the permeability and porosity distribution estimated during calibration of the natural state model. The initial results, based on the natural state model, are shown in Figure 5.3, which clearly shows that the tracer concentration is underestimated at all the monitoring wells. This implies that the tracer doesn't make its way to these wells at detectable levels in the model but diffuses throughout a very large volume.

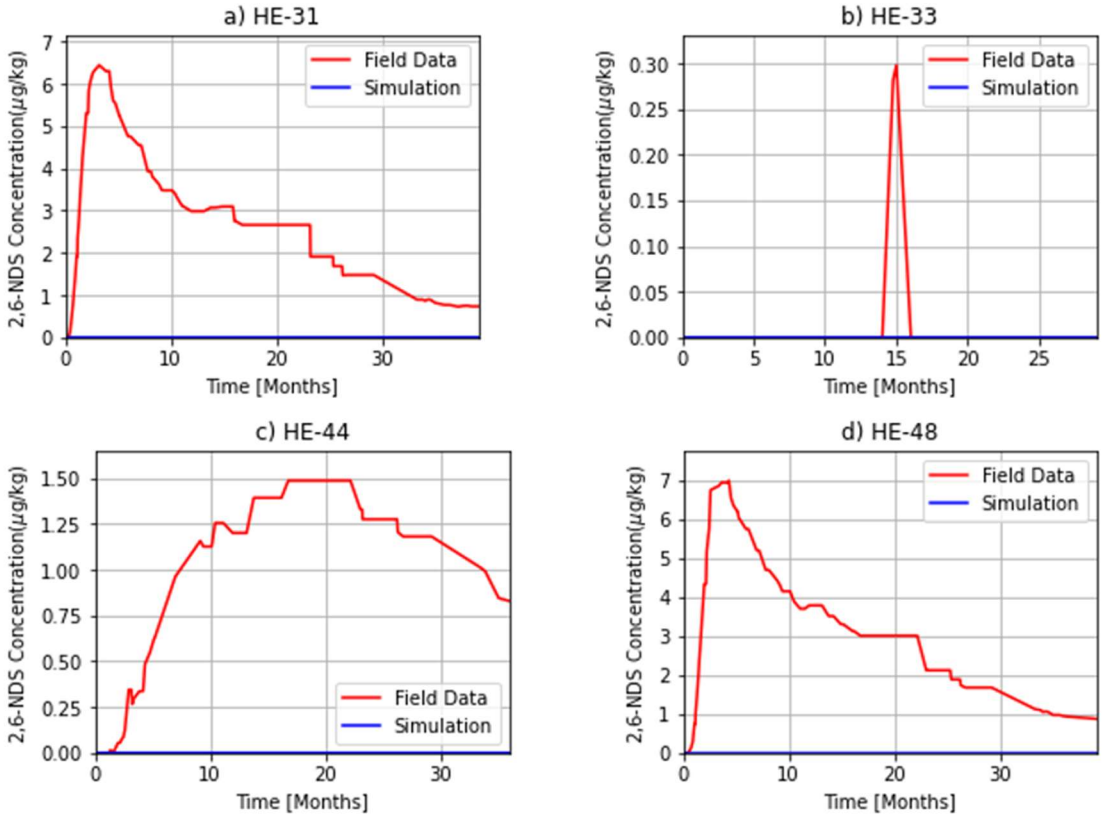

Figure 5. 3 Single porosity model tracer return data (blue curve) and field data (red curve) based on natural state numerical model parameters for a) well HE-31, b) well HE-33, c) well HE-44 and d) well HE-48.Note:This output is based on the calibrated permeability values listed in Table 5.1.

Further attempts show that even after increasing permeability along the fault plane by three orders of magnitude, the single porosity model still underestimates tracer return at the

monitoring wells. Overall, the single porosity nature of the fault structures, and the permeability and porosity values used for the initial natural state model calibration, clearly don't reproduce the tracer recovery curves measured in the field.

Since modification of the hydrological properties of the fracture zones didn't result in a good correlation with the observed tracer recovery using the single porosity approach, a change in model set-up was required to capture the tracer response in the field. Hence, all the model fault structures were changed to being dual-porosity, as previous studies by Ratouis et al. (2019; 2022) and Mahzari et al. (2021) have shown that the dual-porosity approach was necessary to reproduce rapid tracer breakthrough patterns. The dual-porosity model was tested first by using permeability and porosity values obtained during the natural state model, while additionally assuming matrix permeability and porosity 10^{-16} m^2 and 5%, respectively, with a fracture spacing of 150 m and fracture ratio of 10%. However, the model results still showed no tracer return in the monitoring wells. After increasing the permeability of faults along the fault plane (i.e. along the y-direction for the extensional faults and x-direction for the transform fault) to 10^{-12} m^2 or 10^{-11} m^2 respectively, the shape and magnitude of concentration in the modelled tracer recovery curves, changes significantly (Figure 5.4), but it still does not match the field data.

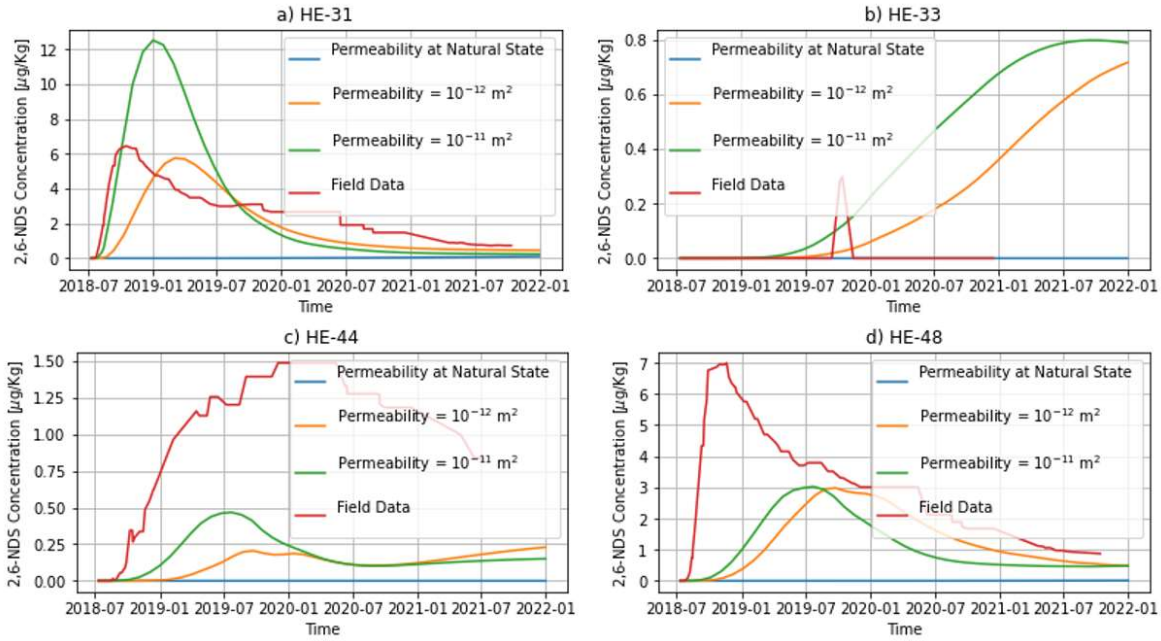

Figure 5.4 Modelled tracer return curves of the monitoring wells with dual porosity incorporated as well as different permeability values for the fault structures along fault planes for a) well HE-31, b) well HE-33, c) well HE-44 and d) well HE-48.

A considerably better match between measured and simulated tracer response (Figure 5.5) is achieved by manual calibration of the permeability of the extrusive volcanics, intrusive basement and all the fault structures as shown in Table 5.2 as well as using the porosity (fracture and matrix) value of 5%. The fracture spacing was, however, kept at 150 m as well as a fracture ratio of 10% and 2% for the rocks and faults, respectively. The better match (Figure 5.5) clearly demonstrates the tracer flow is confined along the NE oriented fault structures. The outcome of the tracer test simulation reveals that a good correspondence between measured and model data is obtained for wells HE-31 (Fig. 5.5a) and HE-48 (Fig. 5.5d). The shape, the peak, and the tails at both ends are captured reasonably well by the

model, while the timing of the peak is delayed by some days in the model. In addition, the overall shape of the tracer recovery in well HE-44 (Fig. 5.5c) is in good agreement with the measured one, but the magnitude is slightly underestimated in the simulation. The model overestimates tracer concentrations in well HE-33 (Fig. 5.5b) in the model, likely due to the fact that the transform fault component in the dual porosity model diverts the tracer flow too strongly towards this well. A sample of visualization of tracer transport throughout the simulation time in the constructed model is shown in Figure 5.6 and Figure 5.7 both at a horizontal reservoir slice at 1000 m.b.s.l and vertical cross section along the fault orientations respectively.

Table 5.2 Final calibrated permeability values utilized in the tracer test model simulation.

	Permeability (m^2)			
Rocks	**X**	**Y**	**Z**	**Matrix**
Extrusive volcanics	10^{-16}	5×10^{-14}	5×10^{-15}	10^{-16}
Intrusive basement	10^{-16}	2.5×10^{-15}	5×10^{-16}	10^{-16}
Extensional faults	5×10^{-15}	2.5×10^{-12}	10^{-15}	10^{-16}
Transform fault	5×10^{-16}	10^{-16}	10^{-16}	10^{-16}

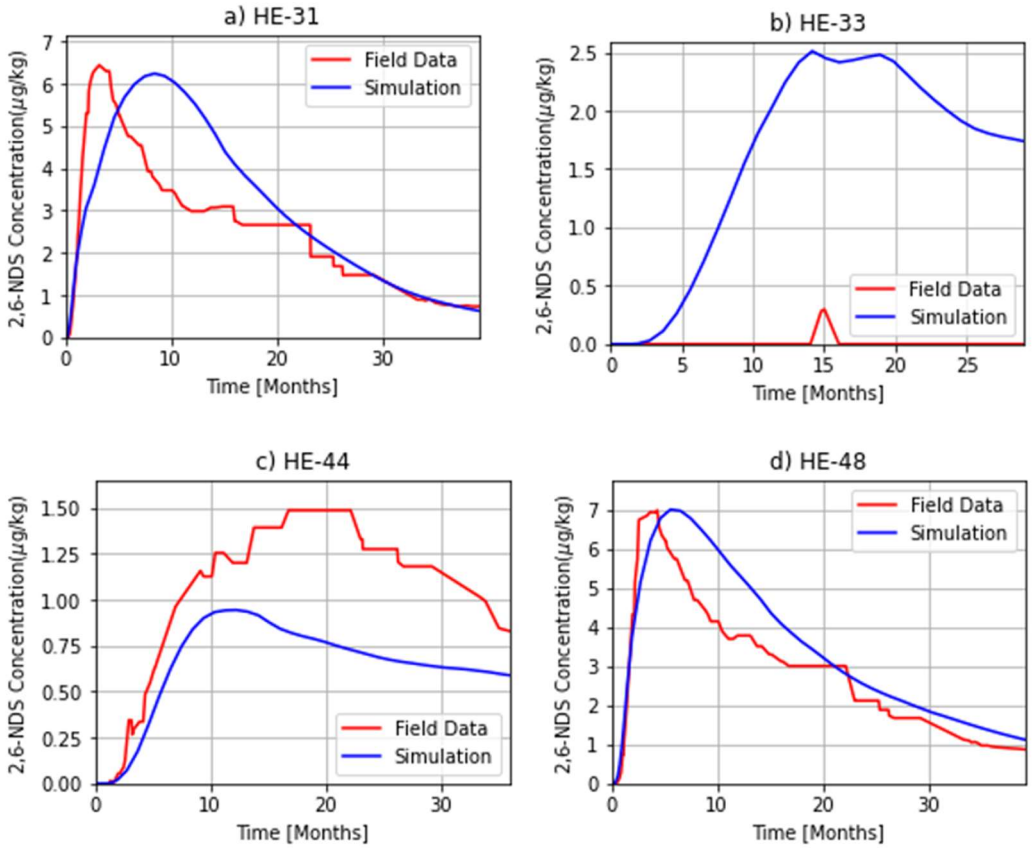

Figure 5.5 Simulated tracer return curves obtained using dual porosity in the numerical model. Modelled data (blue) and field data (red) for a) well HE-31, b) well HE-33, c) well HE-44 and d) well HE-48.Note:This output is based on the permeability values listed in Table 5.2.

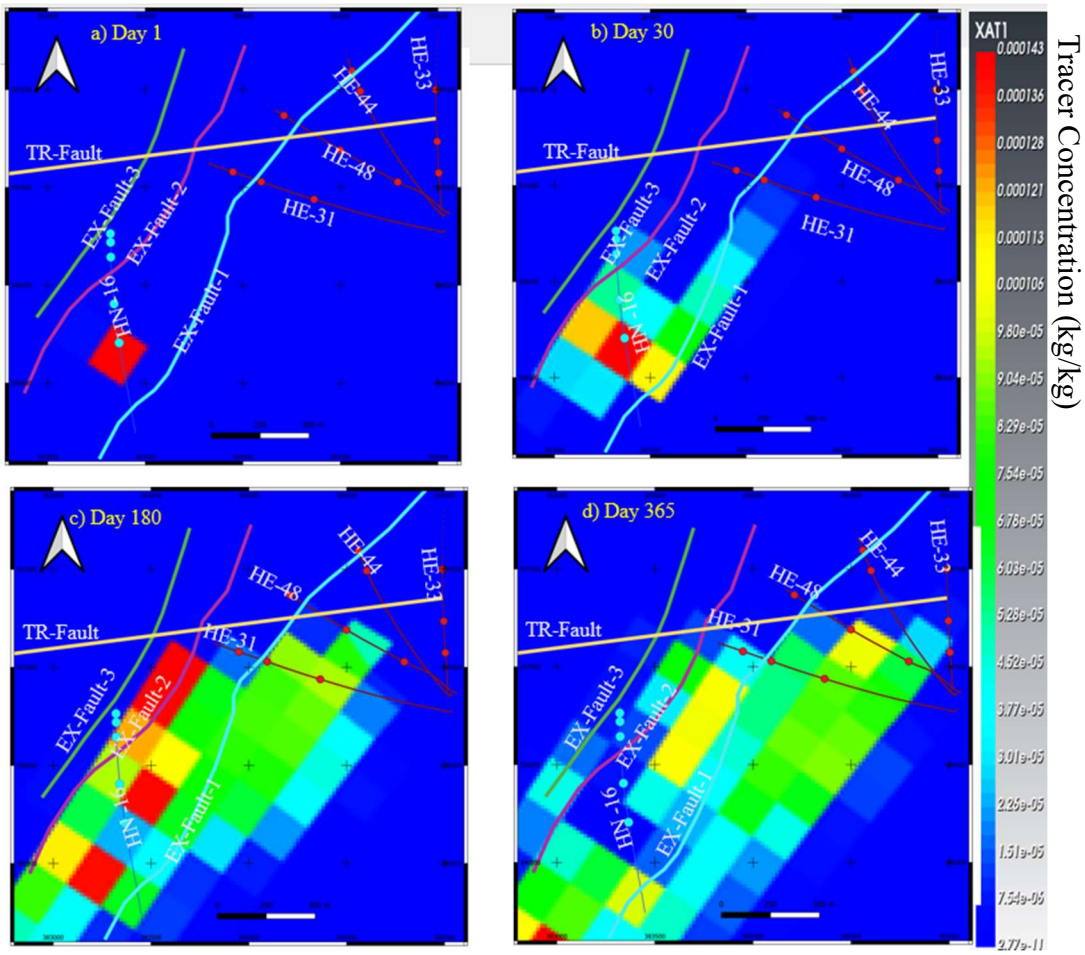

Figure 5.6 Tracer distribution at elevation of 1000 m b.s.l. according to the dual porosity numerical model after a) 1st day, b) 30 days, c) 180 days, and d) 365 days. XAT1 on the legend indicates the upscaled tracer concentration in kg/kg.

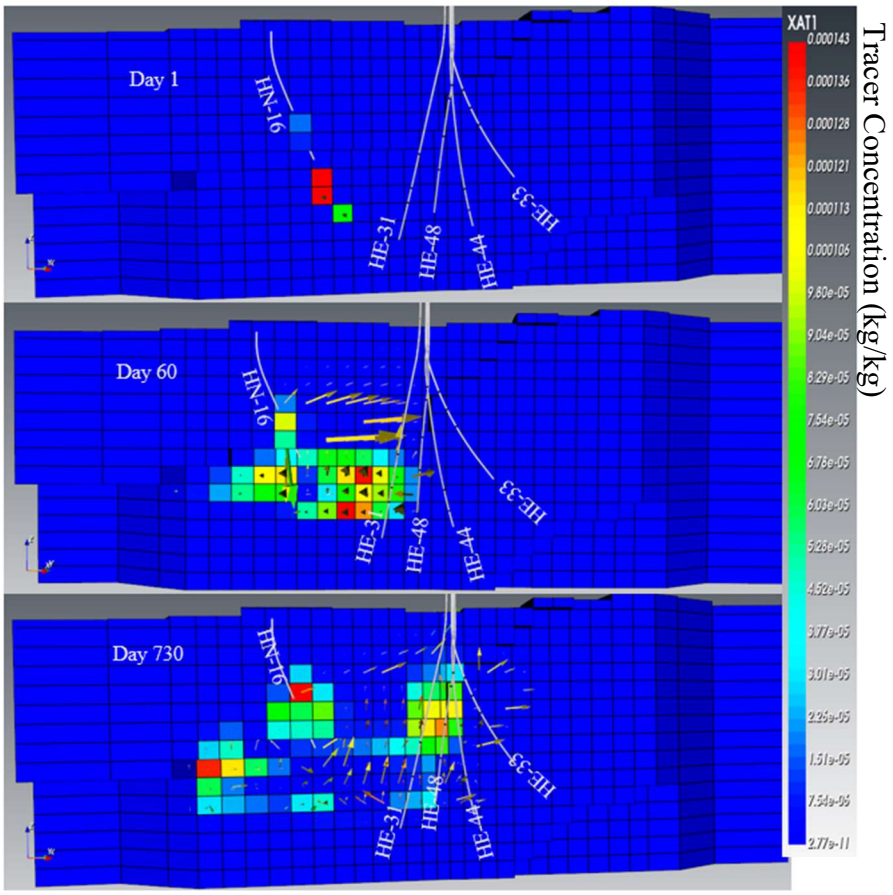

Figure 5.7 Vertical cross section of the numerical model showing tracer progression through time along cross section A-A' (see Figure 4.4) at different times, i.e. a) after 1 day, b) after 60 days, and c) after 730 days. The arrows in the figure show the tracer vector flow field. XAT1 on the legend indicates the scaled up tracer concentration in kg/kg.

5.3 Permeability Comparison Between Natural State and Tracer State Model

A comparison between the calibrated permeability values obtained from calibration of the natural state and tracer state models is presented in Table 5.3 and Figure 5.8. It is clearly seen that the anisotropic permeability structure in the tracer state model is significantly different from the natural state model. The permeability along the plane of the extensional faults, which are the main conduits for the tracer transport, is increased from 10^{-15} m^2 to 2.5×10^{-12} m^2 . Similarly, the permeability perpendicular to the strike of the extensional faults is increased from 10^{-15} m^2 to 5×10^{-15} m^2, and the vertical permeability increased from 10^{-16} m^2 to 10^{-15} m^2. For the transform fault structure, the vertical permeability is the same in both models, but the permeability in x and y directions is altered from 10^{-15} m^2 during natural state calibration to 5×10^{-16} m^2 and 10^{-15} m^2 in the tracer state model, respectively. In addition, the permeability of extrusive volcanics along y-direction is increased from 2×10^{-14} m^2 to 5×10^{-14} m^2. On the other hand, the vertical and horizontal permeability of the intrusive basement is decreased by two orders of magnitude in x-direction and one order of magnitude in y-direction and z-directions. Matrix permeability of the both the intrusive and extrusive rocks indicate a two order of magnitude increase being necessary, raising it from 10^{-18} m^2 to 10^{-16}

m^2. At last, the porosity value of the rock formations was also reduced from 10% during natural state to 5% during tracer state modelling.

Table 5.3 Comparison of calibrated permeability values (m^2) of rock formations between the natural state and tracer state models. Note that only the rock types where permeability values have been altered are presented here.

Rocks	Natural state model				Tracer state model			
	X	Y	Z	Matrix	X	Y	Z	Matrix
Extrusive volcanics	10^{-14}	2×10^{-14}	2×10^{-14}	10^{-18}	10^{-16}	5×10^{-14}	5×10^{-15}	10^{-16}
Intrusive basement	10-^{14}	1.5×10^{-14}	8.5×10^{-15}	10^{-18}	10^{-16}	2.5×10^{-15}	5×10^{-16}	10^{-16}
Extensional faults	10^{-15}	10^{-15}	10^{-16}		5×10^{-15}	2.5×10^{-12}	10^{-15}	10^{-16}
Transform fault	10^{-15}	10^{-15}	10^{-16}		5×10^{-16}	10^{-16}	10^{-16}	10^{-16}

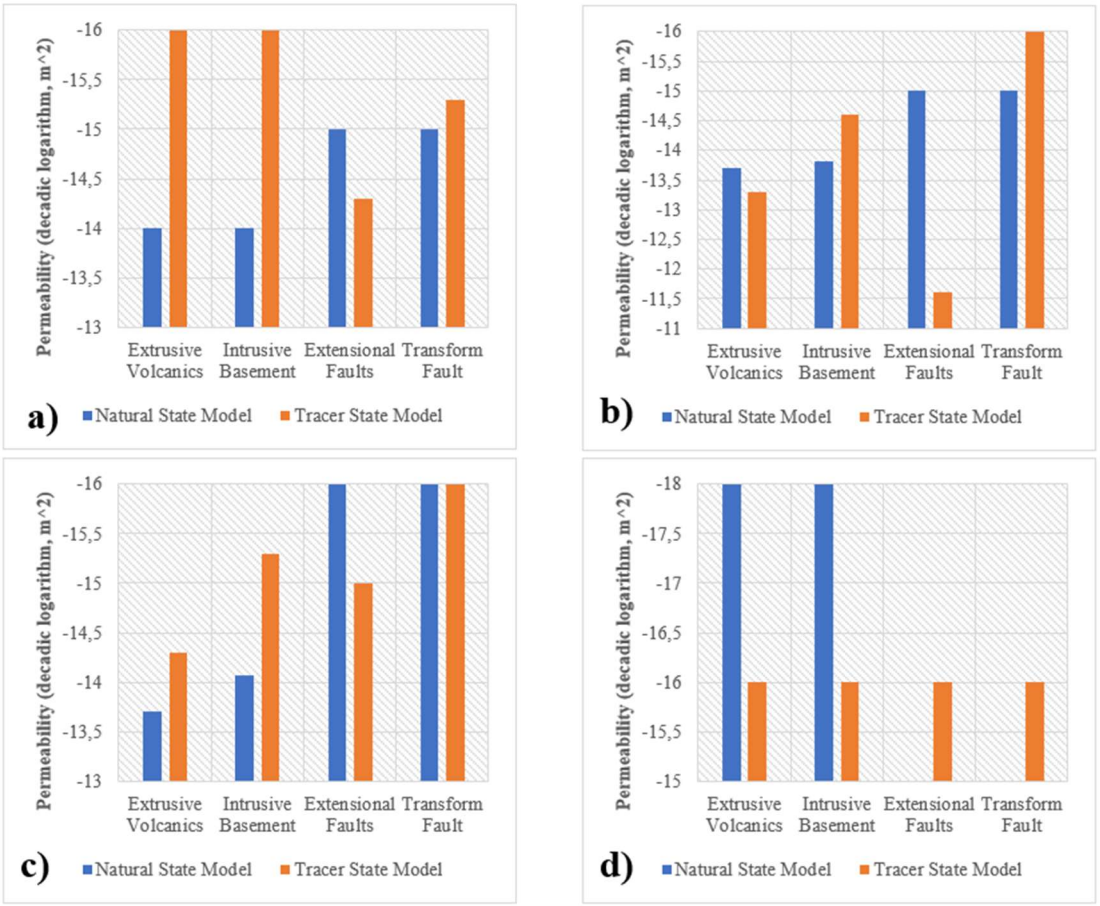

Figure 5.8 Comparison of calibrated permeability values (on logarithmic scale) between natural state model (depicted by blue) and tracer test model (depicted by orange). a)X-permeability (E-W orientation), b)Y-permeability (SW-NE orientation), c)Z-permeability (vertical oreintation), and d) matrix permeability.

The question is why the porosity and permeability structure of the natural state model needs to be altered during tracer state model calibration. Firstly, this is clearly due to the fact that natural state conditions in geothermal systems can be simulated without taking the details of geomechanical forces associated with changes in stress from the rock formation and water flow, because of the behaviour of water flow in fault structures, which can affect pore connectivity in the surrounding rock, eventually generating permeability change (Heffer, 2002; Kitamura et al., 2010; Mahzari, et al., 2021). Since it is expected that the stress and fractures combine to exert a strong influence on the permeability tensor and shape of the permeable volume (Batir et al., 2012). For instance, Zhao et al. (1996) claim that "when the pore pressure in these rocks is increased, the effective confining pressure decreases, which in turn decreases the Poisson's ratio and increases permeability". If these conditions apply in the deep crust, water can then move into the fault zone where it will reduce the strength of the fault.

The effect of both production and reinjection water in the Hellisheiði reservoir system changes the system of flow dynamics in-place during the pre-exploitation state, which eventually can cause repeated earthquakes (Ágústsson et al. (2015); Vogfjord and Hjaltadottir (2007) cited in Hjörleifsdóttir et al. (2021)). The rate of seismicity increased drastically when injection started in Húsmúli in September 2011 (Hjörleifsdóttir et al., 2021). The circulation of the new addition of water in the system is now considered to be the main contributor to the seismic reaction. This is most likely because the reinjected water in the Húsmúli area resulted in a sudden rise of the effective pressure available in the faults and pore spaces of the rock formation. The fluid pressure in the fractures and rock matrix arose from the reinjected water, which leads to brittle deformation of the intrusive and extrusive bodies and eventually triggers hydrofracturing that can affect the shape of the permeable medium and its permeability tensor. It is believed that this phenomenon reciprocated to some extent by the model developed here.

Other argument for why alteration of permeability of rocks happened is due to thermal expansion (when subject to an increase in temperature) or contraction (when subject to decrease in temperature) which leads to change in aperture (Lin, 2002; Gunnarsson, 2020) of fractures of the rocks and structures.

Overall, the interplay between fluid flow, rock alteration, and the stress state can affect the rock permeability structure in a hydrothermal system (Scott and Driesner, 2018). However, as this topic is out of the scope of this study, for in-depth understanding of the relevant science, the author strongly recommends that the reader refers to further literature on the subject. In addition, further research is encouraged into the secret of how permeability and porosity of rocks change due to stress arising from abundant fluid pressure in pore spaces and fractures.

5.4 TRINV 1D Simple Model Tracer Test Results

The tracer test recovery data was further simulated using the TRINV one dimensional simulator tool (refer to section 4.5) to match and interpret the measured tracer returns at production wells HE-31, HE-44, and HE-48. These are the wells through which the 2,6-NDS tracer is mainly recovered, with well-defined return curves. Since there are only a couple of tracer recovery data-points for production well HE-33, it is not incorporated in this analysis.

The simulation results for the tracer migration using single channel and two channel flow, shows a satisfactory fit with field data. Yet, the correlation using three flow channels is superior, hence only the results of that case are presented here. Figure 5.9 presents the 2,6-NDS tracer return curves of wells HE-31, HE-44, and HE-48 simulated with *TRINV* using three flow channels to each production well. The results of this simulation for the three relevant production wells are summarized in *Table 5.4*.

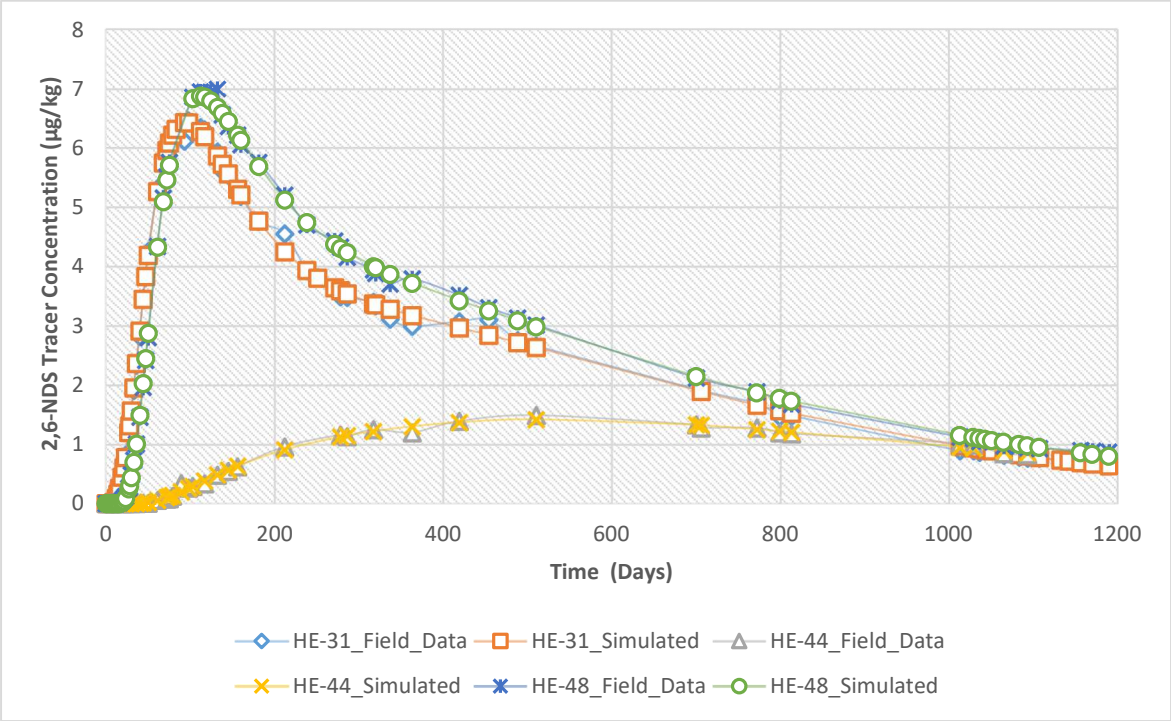

Figure 5.9 Observed and simulated (TRINV) recovery of 2,6 NDS (injected into well HN-16) through the production wells HE-31, HE-44 and HE-48.

The tracer recovery simulated through the TRINV-model, in each of these wells, corresponds well with the measurements in terms of overall shape of curve as well as time and magnitude of the peak recovery. The simulation is, in fact, much better than with the numerical model. As shown in *Table 5.4*, the estimated dispersivity of the tracer through all the three flow channels, which represent the zone of the complex fracture network, for all the three boreholes, reflects values in the range of 1 to 410 m, while the velocity of the tracer seems to be as slow as of the order of 10^{-5} m/s.

On the other hand, the cross sectional area of each of the flow channels are varied. The cross sectional area of HE-31 varies from 116 m^2 (the second flow channel) to1530 m^2 (the third flow channel). Besides, the cross sectional area of HE-48 varies from 0.216 m^2 (first flow channel) to 451 m^2 (third flow channel). Furthermore, HE-44's cross sectional area varies from 2.84 m^2 (third flow channel) to 209 m^2 (the first flow channel). The bigger cross-section of a flow channel allows much fluid to pass through while smaller cross-section allows less fluid to be conveyed.

There are two possibilities of flow channel length determination when using *TRINV*. Either the software can be fed the actual measured distance between feed zones or the software can automatically adjust the flow channel length. As the location of aquifers in the wells involved

is uncertain and the geometry of the flow-channels is unknown, feeding the software with fixed distances was found to be unreliable and instead the software was obliged to estimate the dimension on its own.

Table 5.4 TRINV simulated model parameters for the tracer (2,6-NDS) return to wells HE-31, HE-44 and HE-48, using three flow channels.

Wells	Channel	Length [m]	Mass [kg]	Velocity [m/s]	Dispersivity [m]	Area [m²]	Height [m]	Width [m]	Mass Fraction [%]	Recovery based on Field Data [kg]
HE-31	1	1110	8.55	2.24e-5	140	387	482	16.1	8.58	
	2	856	8.65	7.55e-5	269	116	264	8.79	8.68	
	3	1010	8.9	5.9e-5	40	1530	958	31.9	8.94	
	Total recovery [kg]		**26.1**							**19.26**
HE-44	1	1920	6.48	3.14e-5	410	209	290	14.5	6.51	
	2	1520	0.69	8.1e-5	224	8.64	58.8	2.94	0.69	
	3	1600	0.05	1.87e-5	1	2.84	33.7	1.69	0.05	
	Total recovery [kg]		**7.22**							**5.57**
HE-48	1	1536	0.03	2.26e-4	1	0.13	8.69	0.29	0.03	
	2	1227	6.13	1.08e-4	241	57.6	186	6.2	6.15	
	3	1112	10.8	2.43e-5	228	451	521	17.4	10.8	
	Total recovery [kg]		**16.9**							**16.08**

The estimated distances show that all the aquifers of production well HE-31 are located at approximately 1 km range, reflecting the shortest distances involved in the case of the three production wells, while the distances to the aquifers of well HE-44 range from approximately 1.5 to 2 km, which are found to be the longest distances. Finally the feedzone locations of well HE-48 are found to correspond to an approximate distance of 1 to 1.5 km. The variation of distance among the flow channels suggests that the shortest ones are the most direct flow paths, or even a kind of short circuit connections, while those involving the longest distance reflect indirect flow paths, or even tortuous paths, which the reinjected fluid needs to flow to reach its final destination.

5.5 Cooling Predictions

The long-term impact of the cold fluid injection is further analyzed for the purpose of predicting cooling of the production area. This task is performed by the two models, i.e. the numerical model and the 1D model (TRINV). The cooling forecasts are calculated using both models up to the year 2060, with the aim of understanding the impact of long-term cold-water reinjection on the geothermal system and its management during long-term utilization.

5.5.1 Numerical Model Results

The eventual temperature decline of the production wells can be seen through modelled downhole temperature profiles (Figure 5.10). Greater temperature decline at well HE-31 appears mostly in the depth range of 900 m b.s.l. down to 1800 m b.s.l., while a small

temperature decline is modelled in well HE-48 in the depth range of 1000 m b.s.l. to 1500 m b.s.l. On the other hand, for wells HE-33 and HE-44, the modelled downhole temperature remains without any visible reduction.

The overall outcome of temperature evolution of the numerical model for the production wells (Figure 5.10) infers that the temperature drop due to cold water reinjection, which in total amounts to 286 kg/s (average 2021 value) into the five reinjection wells (namely HN-09, HN-12, HN-14, HN-16 and HN-17), situated in the Húsmúli reinjection field, is imminent. The reservoir temperature of well HE-31 is predicted to drop from 265°C in 2021 to 236°C in 2060 after 39 years of reinjection. Reservoir temperature of HE-33 is predicted to gradually decrease from 252°C to 250°C. The predicted decline of the reservoir temperature surrounding well HE-44 slowly falls from 244°C to 235°C after 39 years of cold-water reinjection. A decline of approximately 13°C is finally predicted in the reservoir

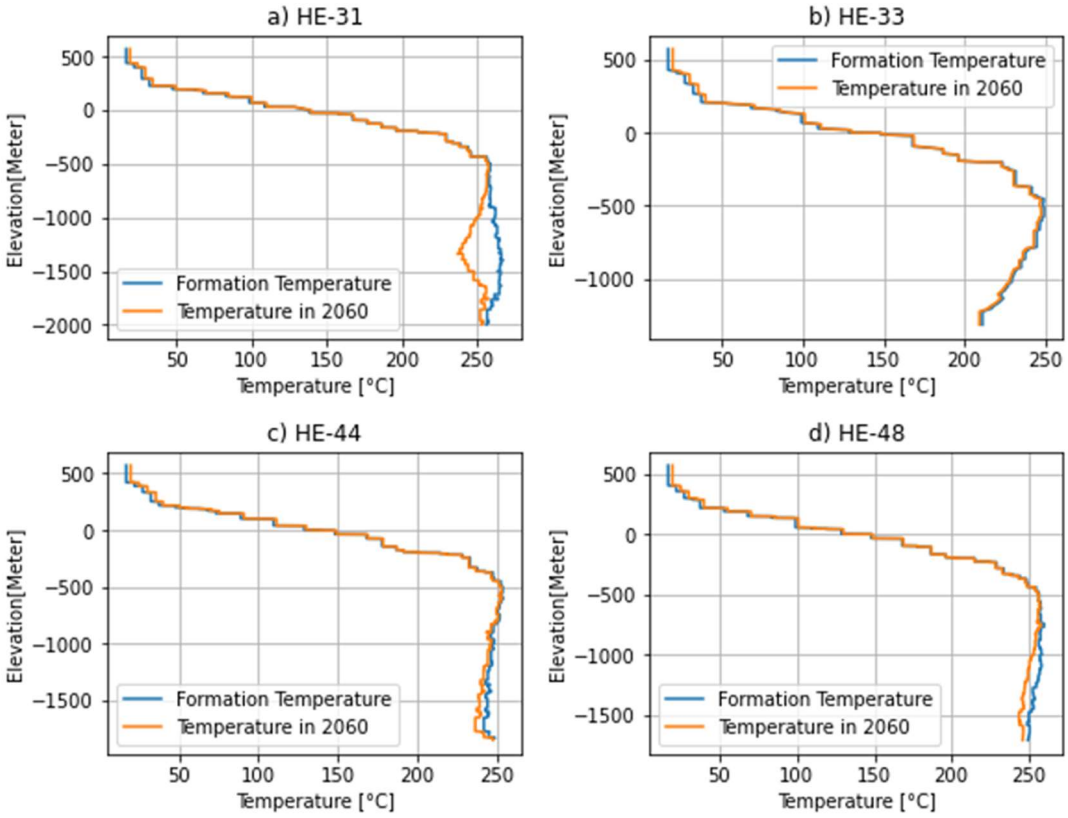

Figure 5.10 Downhole temperature simulated by the numerical model at the end of 2060 and estimated formation temperature of production wells a) HE-31, b) HE-33, c) HE-44, and d) HE-48.

surrounding well HE-48 from 2021 to 2060. Overall, the numerical model predicts that only a minor temperature decline will be seen over 39 years of geothermal energy production, except in the case of well HE-31 (Figure 5.11).

In addition, the modelled reservoir enthalpy also shows a visible decline over 39 years of production (Figure 5.12). The predictions for wells HE-31 and HE-48 show considerable decline while those for wells HE-44 and HE-33 show a slight and gradual change over time. The predictions for well HE-31 show the greatest decline in enthalpy, which falls from 1160 kJ/kg at the beginning of the reinjection period to 1020 kJ/kg after 39 years of geothermal fluid production, due to long-term cold-water reinjection. On the other hand, HE-33 has the

smallest reservoir enthalpy decline, which is in the range of 1100 to 1080 kJ/kg over the entire reinjection period. The reduction of enthalpy for HE-44 amounts to only 40 kJ/kg and for HE-48 is twice that, over the entire period of cold-water reinjection. The two wells last mentioned, share a similar trend in predicted enthalpy decline.

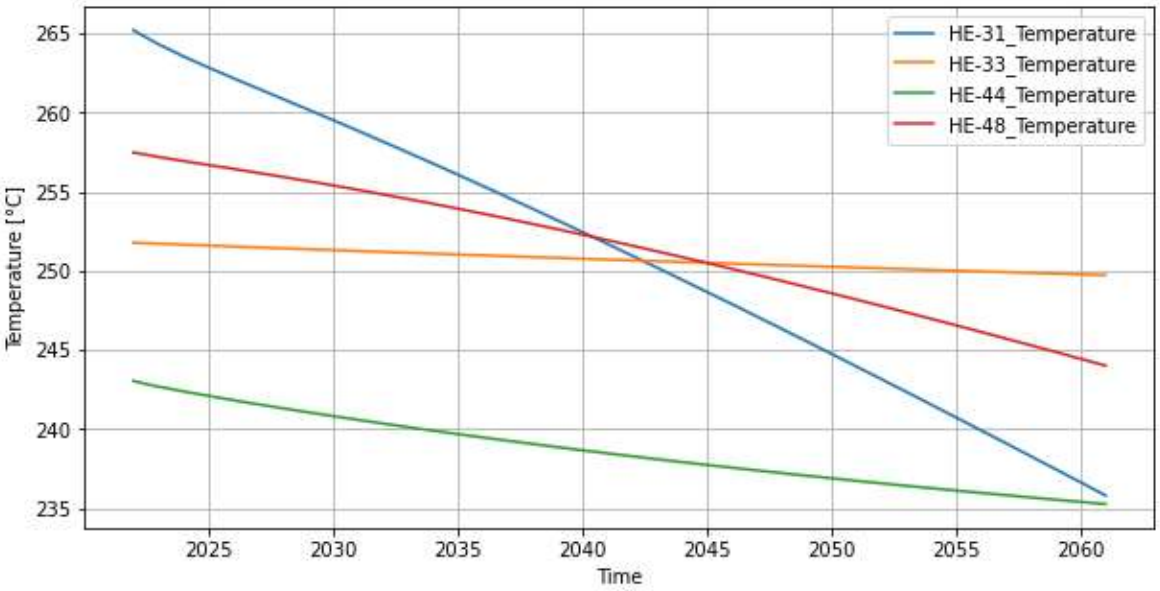

Figure 5.11 Temperature response of reservoir of production wells due to long term reinjection modelled by the numerical model.

It should be mentioned that the gradual decline of temperature and enthalpy from cold water reinjection is counteracted by reservoir pressure increase, caused by the reinjection. The modelled pressure response (Figure 5.13) at the production wells, shows steady conditions over the entire period of simulation.

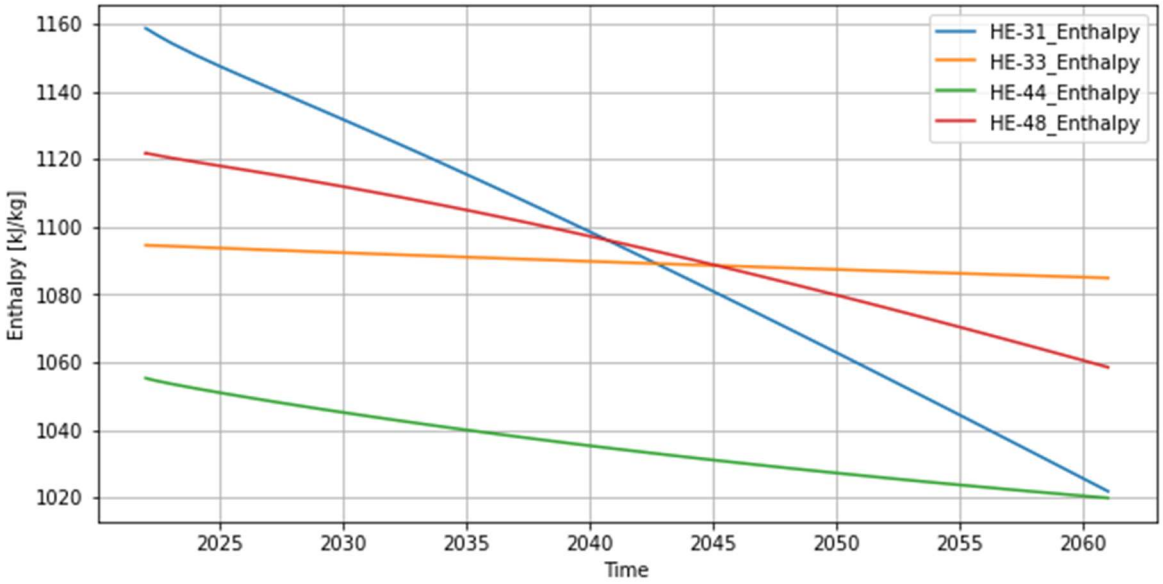

Figure 5.12 Enthalpy response of reservoir of production wells due to long term reinjection, predicted by numerical model.

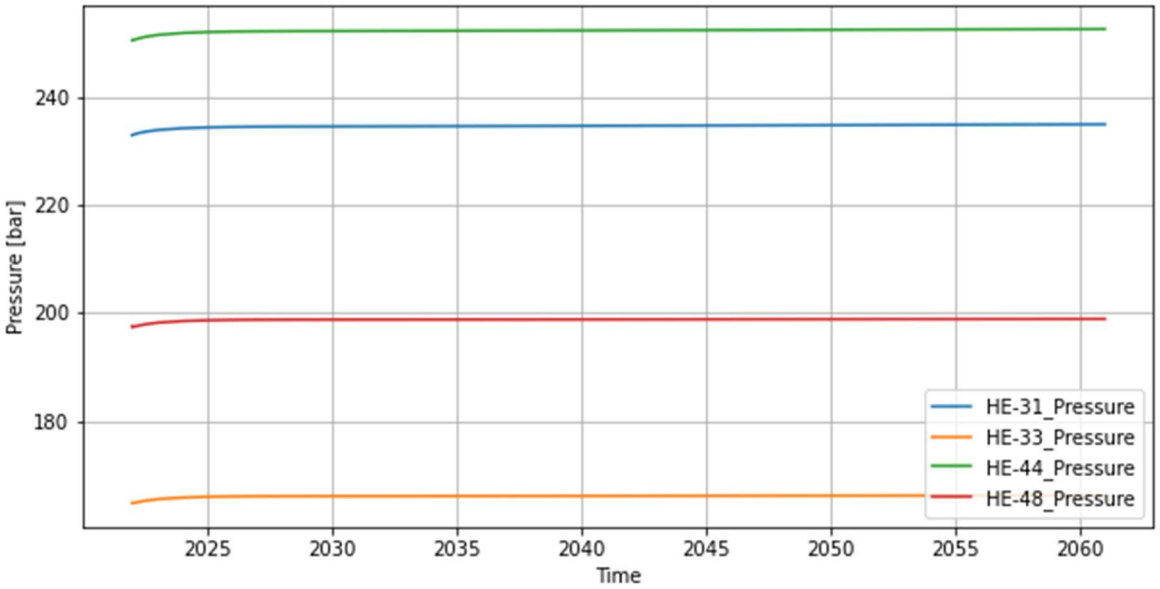

Figure 5.13 Pressure response of reservoir of production wells due to long term reinjection, modelled by the numerical model.

Two more scenarios to forecast thermal breakthrough in the simulation are considered in this study. First by reducing the amount of water injection to half, i.e. to 143 kg/s, and second by abandoning fully the reinjection operation. The aim is to compare the temperature decline of the productive reservoir system for different scenarios, over different time scales. A total temperature decline of about 15°C, 2°C, 10°C and 4°C (Figure 5.14) is modelled over 39 years of production, for wells HE-31, HE-33, HE-44, and HE-48, respectively, if the reinjection is reduced to half. On the other hand, a temperature decline of 5°C, 3°C, 11°C and 3°C is predicted for the production wells HE-31, HE-33, HE-44, and HE-48, respectively, if the reinjection is completely ceased. Total temperature decreases and time scale temperature evolution over 39 years of production period is sketched (Figure 5.15) in for the three scenarios considered.

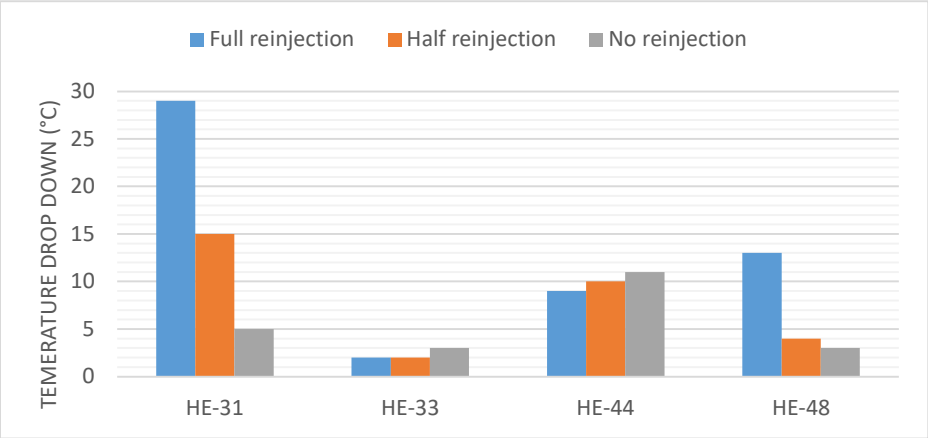

Figure 5.14 Total temperature dropdown of wells over 39 years of production period for the three senarios.

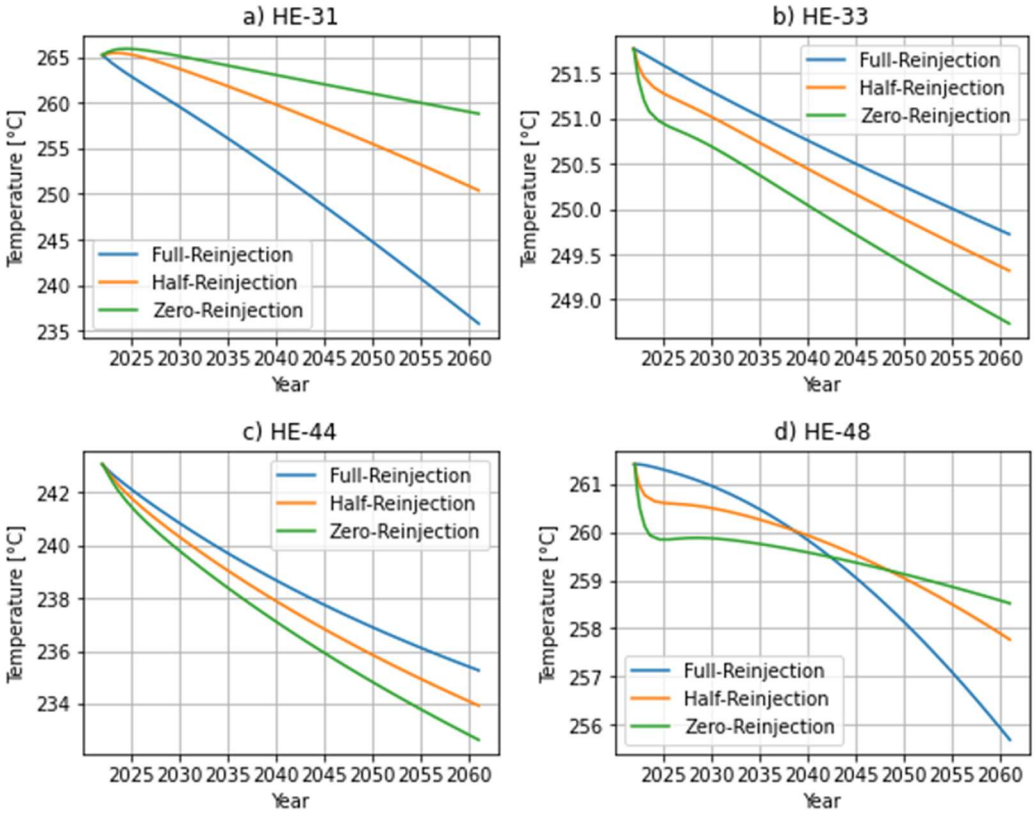

Figure 5.15 Time scale temperature response of production wells predicted by the numerical dual porosity model due to long term cold water full reinjection (286 kg/s),half reinjection (143 kg/s) and no reinjection (0 kg/s) at different time scales for a) well HE-31, b) well HE-33, c) well HE-44 and d) well HE-48.

5.5.2 Simple 1D Model (TRINV)

The predicted temperature decline calculated by the TRINV model for the three selected wells, i.e. HE-31, HE-44 and HE-48, is presented in Figure 5.16. The cooling prediction is estimated for a production and reinjection period of 39 years, i.e. from end of 2022 to 2060, assuming that the past injection and production rates are maintained. Fluid and heat propagation is modelled through three conducting fractures (flow-channels) between reinjection and production wells, with aspect ratio (height to width) of 30:1 for the cross-sectional areas, for wells HE-31, HE-44 and HE-48, respectively. This aspect ratio is believed to be representative of vertical fault structures present in the area. The result shows that wells HE-31 and HE-48 will likely face imminent but gradual cooling danger during their production period, while the results for well HE-44 show no vulnerability to cold front propagation. As is clearly seen in the figure, the reservoir temperature of wells HE-31and HE-48 drops from 265°C to 248°C and from 257°C to 245°C, respectively, while HE-44 shows almost no cooling within 39 years of production, up to the end of 2060.

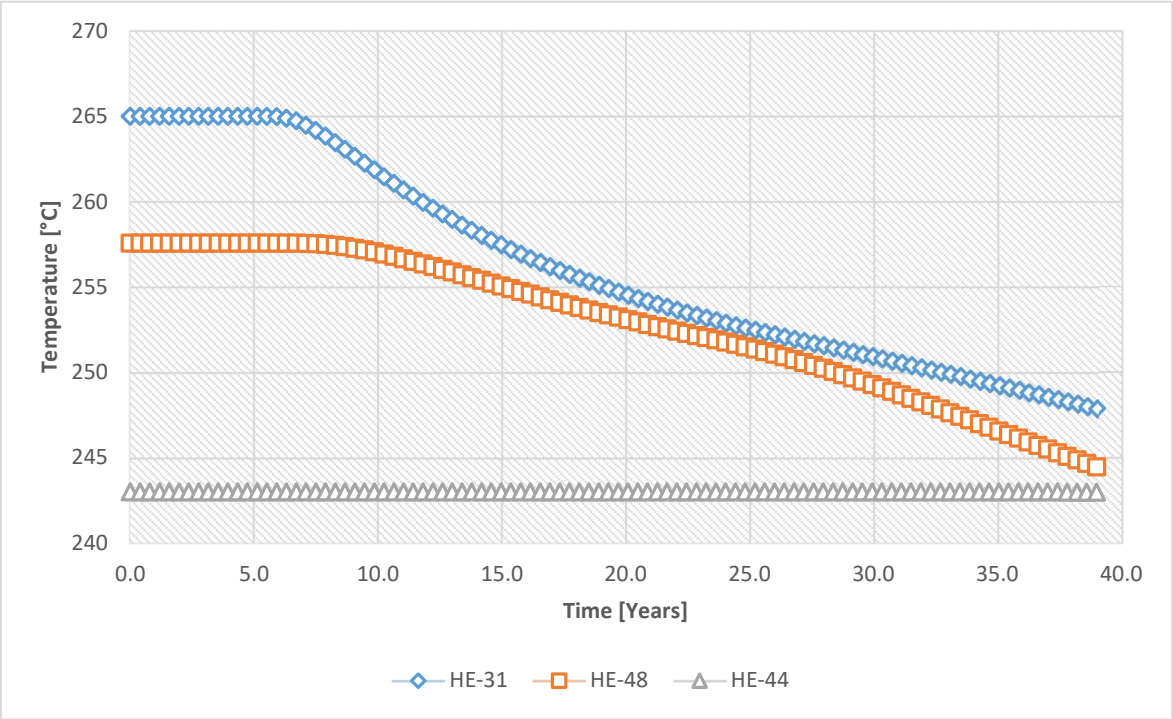

Figure 5.16 Temperature decline of production wells during reinjection into well HN-16, modelled by TRINV, using three flow channels for each well-pair. The aspect ratio of height to width of the flow channels is assumed to be 30:1. The prediction period extends from 2022 to 2060, or over 39 years.

5.5.3 Comparison of Numerical and Simple Model Cooling Predictions

Thermal front propagation is predicted for almost four decades by both models in this study. The onset of cooling due to reinjection estimated by tracer inverse model is slower than in the numerical model for all the tracer affected wells (Figure 5.17). Well HE-31 is the well that is estimated to be the well mostly affected by the reinjection, by both models, but the difference between predictions is 12°C. A very similar temperature decline (1°C difference) over the entire period of reinjection is predicted by both models for well HE-48. For well HE-44 there is no temperature decline predicted by the simple model over the forecast period but a 9°C drop estimated by the three-dimensional model. The pattern of cooling predicted for the production wells using the numerical model shows that the cooling starts concurrently with the reinjection. On the other hand, in the one-dimensional model, the onset of cooling only appears after some years of production. For instance, in well HE-31 the decline starts after 6 years of production and in HE-48 the thermal front reaches the well after 8 years of production.

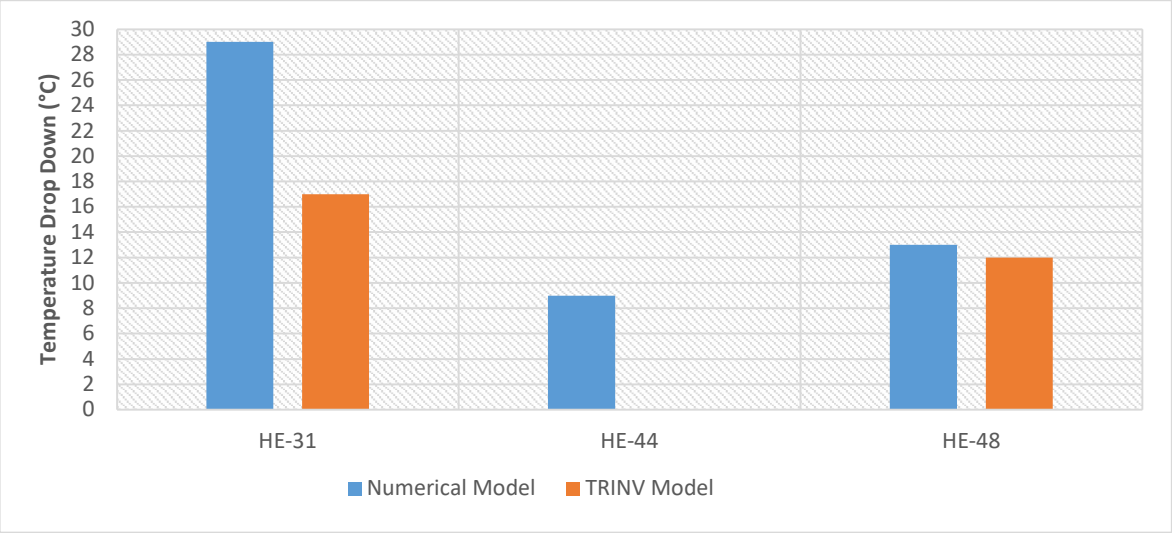

Figure 5.17 Temperature decline comparison for wells HE-31 and HE-48 due to long term reinjection over period of 39 years using dual porosity numerical model and TRINV simple model.

6 Discussion

This chapter presents an overview of the modelling results for the Hengill geothermal area presented in this thesis. The first subsection briefly discusses the implications of the numerical natural state model developed, while the second subsection reviews the numerical simulation of the tracer transport. Following that, the third subsection elaborates on the tracer test interpretation with the one-dimensional simple model (TRINV) and a comparison of the results of the numerical and analytical models. The fourth and last subsection discusses the effects of long-term cold-water reinjection on the temperature conditions in the geothermal reservoir system and the implications for future reservoir resource management and monitoring in the Hellisheiði geothermal field.

6.1 Natural State Temperature Model

In all the above-mentioned rock types (Table 5.3.1), the permeability in the SW-NE orientation (y-direction) was found to be prevailing over the one in the E-W direction (x-direction) as well as the vertical permeability tensor component. The model properties demonstrate that the fracture permeability of the extrusive and intrusive rocks is greater than that of the fault structures, however this circumstance is reversed in the tracer transport state. Despite this result being somewhat unexpected, it highlights that the pore pressure in the surrounding formation of these faults exerts a stress on the fault planes which may lead to consolidation of the fault's grain structure which ultimately leads to reduction in effective interconnected pore spaces which indirectly lowers their permeability. The temperature model shows that the temperature increases down to the bottom of the model (2600 m b.s.l.), in agreement with the belief that magmatic intrusions act as the source of heat for the hot fluid up-flow system. The 240 – 260°C temperature contour extends to the top of the extrusive volcanics in the central part of the model, where the production wells are situated. A maximum temperature of over 300°C is estimated by the model underneath the production wells, close to where the intrusive activity has taken place.

The temperature contours of the natural state model (Figure 6.1) clearly indicate a convective system with upward heat transport (Figure 6.2.a). The hot fluid (Figure 6.2.b) of the reservoir rises from underneath the intrusive volcanics and flows up to the resistive core. As the aim of this study is to predict temperature decline of the field due to long term reinjection, the model calibration was performed on basis of formation temperature.

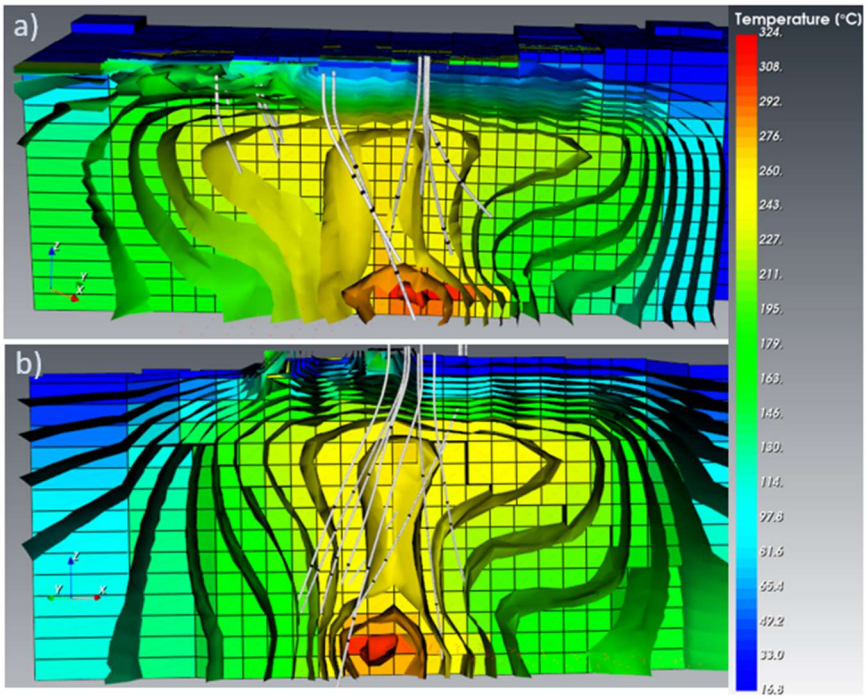

Figure 6.1 Formation temperature distribution in the study area, according to the numerical model along (a) cross-section A-A'and (b)cross-section B-B'(see Figure 4.1). Note that each layer is 200 m thick and the top and bottom layers are located at 600 m a.s.l. and 2600 m b.s.l., respectively. Feed zone locations in the wells are represented by small, black circles.

The results of the natural state model developed in this study show that the downhole temperature of the wells in the Hellisheiði geothermal field correspond well (refer to Figure 5.2) with measured data. Thus, the convective heat transfer upwards through the fractured basaltic lava formation from 2300 m b.s.l., where the up-flow is located (Gunnarsson and Aradóttir, 2014), is reasonably captured by the model, except mainly at shallow depths down to the cap rock. The lower temperatures in the cap rock, and above the cap rock, indicates that the host rock which consists mainly of Holocene lava flows (Franzson, 1998 and Snæbjörnsdóttir et al., 2018) that are highly affected by the circulation of cold ground water. Modelled formation temperatures in the deeper lithologies are influenced by the anisotropic permeability distribution in addition to the proximity of the convective plume in that zone. The more permeable rock characterized by fractured networks enables (Barenblatt, 1960), (Warren and Root, 1963) and (Goloshubin, 2006) the hot fluid circulation in the system, which in turn leads to heat energy transport to nearby the matrix of intrusive and extrusive rocks, and ultimately causes a temperature increase.

The two abundant rock formations (extrusive and intrusive, refer to Figure 4.5), assumed to constitute the reservoir system of the model, are found to have relatively elevated permeability, which is most likely due to the presence of fracture networks. These fracture

networks are incorporated through classification of the rocks into fracture and matrix formations (dual porosity) (Barenblatt, 1960) during the model construction. The fractured extrusive rock, which is believed to represent hyaloclastite formation found to be more permeable than the intrusive basement, which supposedly represent the basaltic lava intrusion in the model situated below 1400 m b.s.l. Generally, the permeability structure revealed through the modelling of these two rock formations has substantiated quite the heterogeneity and anisotropic nature, where the geothermal fluid circulation is distributed mainly in the NE and vertical directions and less in EW direction.

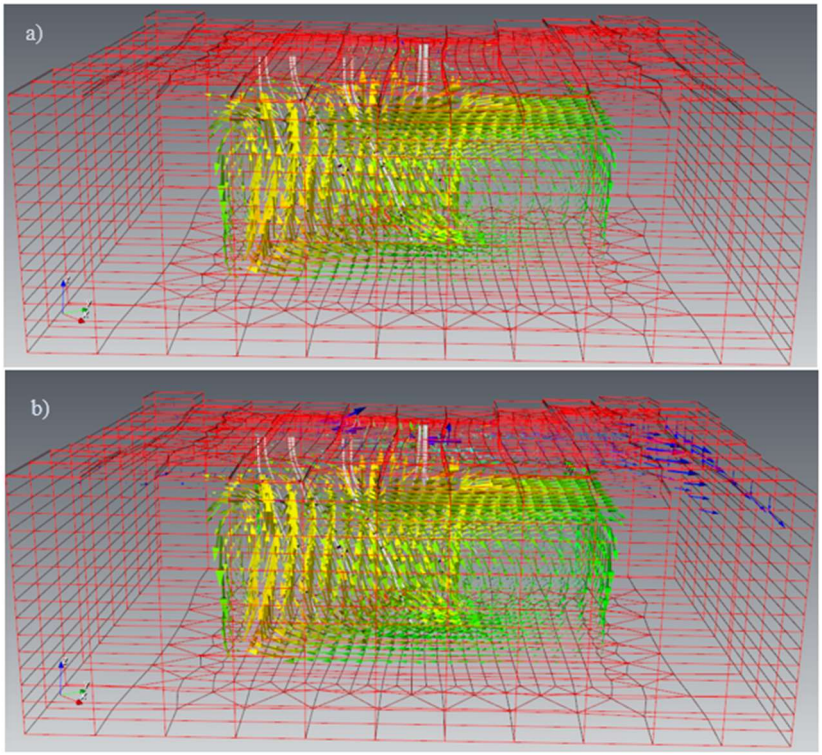

Figure 6.2 Vector flow field of heat (a) and mass (b) in the natural state numerical model along cross section A-A' shown in figure 4.1.

6.2 Tracer Test Model

The numerical model developed in this thesis is consistent with previous work of Snæbjörnsdóttir et al. (2018), Tómasdóttir (2018), Ratouis et al. (2019 and 2022) and Mahzari et al. (2021) showing that the geothermal system in the Húsmúli area is a heterogenous and highly fractured reservoir system, with a flow direction of the tracer mainly to the NE along the fault structures. The overall correspondence between the measured and simulated tracer test implies that the modelled direction and rate of tracer flow, spatial and temporal variations of tracer concentration, and mixing dynamics of the tracer in the reservoir are comparable with the actual tracer flow pattern in the reservoir system.

Although the tracer transport simulation initially assumed that the NE striking fault structure and the transform component faults were single porosity, consistent with the natural state model, mismatch between model predictions and measured results show that it is essential to represent the fault structures as well as the intrusive and extrusive volcanics with dual

porosity characteristics. This indicates that the matrix flow alone within the NE striking structures doesn't represent the dynamics of tracer flow to the monitoring wells.

Switching the nature of the faults in the model into dual porosity reflects the potential of the fault system to act as preferential flow paths for the injected fluid (Barenblatt, 1960) and (Warren and Root, 1963). Tracer concentrations calculated by the numerical model for monitoring wells HE-31 and HE-48, which show most rapid tracer breakthrough, are in good agreement with measured values. However, the timing of the concentration peak is delayed in the model calculations compared to the measurements. In addition, the tail end of the recovery curves (at late times) is generally well-captured by the model calculations, suggesting an increasing role for matrix-dominated flow.

The alignment of the fault structures plays a major role in creating favourable fluid conduits, leading to a direct connection (even a short-circuit), between injection well HN-16 and monitoring wells HE-31 and HE-48. Of course, the faults also connect wells HN-16 and HE-44 too, but they are located further away from the injection well and affected by a transform fault that cuts across the extensional faults. Well HE-33 is quite far away from the NE striking faults but in close contact with this transform component fault. The limited tracer recovery in this well indicates that this structure restricts further NE flow of the tracer and forces it to move marginally towards well HE-33. In other words, the transform component fault acts as a barrier for the tracer that emerges from HN-16. The amount of tracer recovered through this well is overestimated by the numerical model, but the timing of the peak agrees somewhat with the field data. The presence of multiple peaks in the modelled recovery suggests that the tracer arrives at this well via a couple of feed zones in the numerical model.

A depth slice at 1 km b.s.l. (Figure 5.7) shows that the tracer travels along the NE striking fault structures and is blocked by the EW striking fault structures from propagating further to the NE. The tracer is assumed initially to sink immediately to the aquifer locations of the reinjection well, where it enters the reservoir, instead of sinking towards bottom depth of the well. This means that initially the feed zones and surrounding formations are highly saturated by the tracer and then the tracer gradually propagates to the monitoring wells via the NE trending faults which is modelled by the NE permeability structure of the model. Finally, as the fluid gets heated up by the hot rocks of the geothermal system, it rises back and diffuses to the reservoir system closer to the surface, in the Skarðsmýrarfjall well field.

Overall, fluid flow in the Hellisheiði reservoir system is controlled by the NE trending permeability structures as well as the EW transform component fault, as the tracer distribution appears to be confined to these structures (Khodayar 2013; Khodayar et al., 2015; Ratouis et al., 2019). Permeability, porosity, and the fracture ratio in the reservoir system are the key parameters affecting the shape of tracer recovery curves. As flow in the system is controlled by pressure gradient and permeability, increasing permeability strongly influences the pathway along which the tracer is traveling. Increasing porosity and fracture ratio leads the return curve to have lower transport-speed and small peak concentration, while decreasing these values causes a faster response and higher peak concentration which is in line with Tomasdottir (2018).

6.3 TRINV 1D Model Results

Even though TRINV simulates tracer transport assuming one-dimensional transport, its flexibility to utilize several flow channels reflects the possibility that multiple fracture structures could be the conduits carrying the tracer from the feed-zones of reinjection wells to feeders of production wells. In addition to the degrees of freedom resulting from multiple flow channels, incorporating dispersion into the inverse model calculations allows a quite exact simulation of the tracer return data.

The outcome of the model in the present study of the Hengill area suggests that tracer propagation occurs via three flow channels. Incorporating this assumption into model calculations enables reproduction of the shape of the tracer return curve, the tracer peak and time of arrival of the peak, which is not the case if either single or double flow channels are assumed. Another reason for this good fit is the inclusion of dispersion effects (Horne and Rodriguez, 1983) due to velocity variations along the flow paths, e.g. fracture width variations on top of advection system transport of the tracer. This also includes tortuosity, which in the case of geothermal reinjection can involve the sinking of colder reinjected water to depth due to higher density and consequent rising when heated again.

The result shows that the injected tracer is dispersed and transported via each of the flow channels. The travel of the tracer to well HE-31 is equally distributed in all three flow channels. For well HE-48, the tracer travel is dominated by flow channels two and three, whereas for HE-44, the tracer is conveyed mainly via flow channel one. Following this analysis all these conduits are believed to be the porous and permeable fracture networks and the corresponding shortest routes between the injection well and the respective monitoring wells. On the other hand, the contribution of flow channels two and three for well HE-44 and flow channel one for HE-48 is believed to result from the tortuosity of the fracture-zones, reflecting longer and more indirect flow paths for the tracer (Axelsson et al., 2005).

6.4 Cooling Predictions

The fault structures play a key role in channeling the cold water reinjected into the reservoir system to production wells in the numerical model, as is also the case for the flow channels conducting the cold water towards the production wells in the case of the TRINV model. Both approaches in effect simulate the same conditions. Thermal front propagation predicted by the numerical model is at more gradual rate and somewhat smaller in magnitude than that of the TRINV model.

Figure 5.11 indicates that the reservoir temperature of well HE-31 is most affected by reinjection while well HE-33 is least influenced by the cold front propagation. The modelled reservoir temperature of well HE-48 also shows considerably greater temperature drop than well HE-44. The trend of the reservoir temperature decline due to the advancement of the thermal front around well HE-31 is most visible, while the influence of cold-water recharge on the reservoir surrounding well HE-33 is quite gradual over the 39-year prediction period. On the other hand, reservoir temperature predictions for wells HE-44 and HE-48 clearly imply a decline of 8°C and 14°C, respectively, over the same period. These results clearly suggest that there is direct communication with the reinjection wells due to the presence of

the NE striking fault structures. The cold-front transported via these structures, which first arrives in the vicinity of wells HE-31 and HE-48, and later at well HE-44, as demonstrated by the tracer test. The much smaller risk of cooling of the reservoir around well HE-33, due to long-term cold-water reinjection, suggests the presence of a barrier-like structure that impedes the fluid travelling from the area around well HE-44 towards well HE-33, consistent with the inferred transform fault structures. Total temperature drop and average annual reservoir temperature decline at each production well is summarized in Table 6.1

Figure 5.12 shows the enthalpy evolution over a 39-year period of reinjection and production from the producing wells, suggests a declining trend comparable to the temperature trend, which is expected as these variables are mutually related. The wells (HE-31 and HE-48) intercepted by the NE striking faults indicate a considerable decline in enthalpy whereas at wells HE-44 and HE-33, the predicted enthalpy decline is slight. The enthalpy decline signals clearly that the reinjected liquid propagates mostly via these structures, which has the capability to eventually cool the reservoir around the producing wells.

Figure 5.13 shows the modelled reservoir pressure response of the producing wells that demonstrate tracer recovery. The graph indicates that reinjection stabilizes reservoir pressure in the production wells over the simulation period, in concurrence with the hydraulic communication between the injection well and the production area.

Table 6.1 Average annual and cumulative temperature decline of the production wells considered, due to full cold water reinjection, predicted by the numerical model.

Well	**HE-31**	**HE-33**	**HE-44**	**HE-48**
Average annual reservoir temperature decline (°C)	0.76	0.05	0.25	0.35
Cumulative reservoir temperature decline over 39 years of production period (°C)	30	2	8	13
Average annual reservoir enthalpy decline (kJ/kg)	3.6	0.9	0.26	1.54
Cumulative reservoir enthalpy decline over 39 years of production period (kJ/kg)	140	35	10	60

Figure 5.15 shows the predicted temperature decline of the production wells studied over the 39-year (i.e. 2022 to 2060) production period for three reinjection scenarios (i.e. full reinjection, half reinjection and without reinjection) in the numerical model. As expected, the temperature decline due to full reinjection, is faster in the wells that show the greatest tracer response, i.e. wells HE-31and HE-48. Temperature decline is more gradual in the case of half reinjection and, of course, for no reinjection. On the contrary, for wells HE-33 and HE-44, the temperature decline in response to full reinjection appears as a more gradual decline than with half reinjection and no reinjection. It may be that cooler marginal fluids from surrounding boundaries are entering the reservoir and less reinjection allows more of them to flow in. Although this result is unexpected, it may highlight the importance of injection in stabilizing reservoir pressure and reducing cold recharge from surrounding areas.

Figure 5.16 shows the temperature forecast over a period of 39 years for the production wells, calculated by the one-dimensional TRINV tool. The impact of the reinjected fluid on wells HE-31 and HE-48 indicates a decline amounting to 16°C and 13°C, in production

temperature over the reinjection period, which corresponds to 0.41°C and 0.35°C average annual temperature decline, respectively. The prediction reflects that well HE-31, which has the greatest tracer recovery, is the well most affected by cold front propagation in the long term. Besides that, well HE-48 also shows cooling due to reinjection while the magnitude and trend is different from that of well HE-31. The field tracer data infers, that these two production boreholes which have significant recovery, are directly connected with the reinjection well through the NE striking fractures, causing a rapid migration of fluid from well HN-16 to wells HE-31 and HE-48. To elaborate more, the cold front propagation is dominated by flow channel number two in both of wells HE-31 and HE-48, as can be seen in Appendix 2, so the temperature decline caused by this flow channel is most significant. Their relative proximity, associated with short circuiting and/or direct flow paths from well HN-16, results in the cooling danger discussed.

According to the TRINV-predictions, there seems to be no cooling for the first 5-7 years of production but afterwards the cooling starts to come in gradually. In contrast, well HE-44 is the one which doesn't show any cooling in the predictions due to the cold reinjection into HN-16. This reflects the fact that the circulation of cooler reinjected fluid along the NE trending fault, is counteracted by perpendicular fractures trending EW, which divert the reinjected cold fluid. The general trend of temperature evolution in wells HE-31 and HE-48 is a gradual decrease over time after about 6 years of production, which is caused by the multiple flow channels (considered to be both straight and tortuous flow-paths) that connect pairs of aquifers in the reinjection well (HN-16), on one hand, and the production wells (HE-31, HE-44 and HE-48), on the other. Because these flow channels have different conduit-length as well as different fluid velocity, each flow channel has their own contribution (Appendix 2), which is surprisingly not of equal share in the thermal front breakthrough in the reservoir.

Previous work by Kristjánsson et al. (2016) on thermal breakthrough due to cold water reinjection into well HN-17, which is situated quite close to well HN-16, using the one-dimensional TRINV model for flow channels with an aspect-ratio of 30:1 and a porosity of 15%, predicts a total temperature drop of approximately 29°C, 27°C and 9°C, over 20 years of production for wells HE-31, HE-48 and HE-44, respectively. If this finding is projected to 40 years of reinjection as presented in this study, the production wells HE-31, HE-48 and HE-44 would face almost not very far from the predicted values i.e total temperature drop of approximately 30°C, 30°C and 10°C respectively (see Figure 6.3). The cooling of reservoir temperature is significantly appeared at the first 5 to 10 years of production period and remains to be very gradual decline throughout the production period. Kristjánsson et al. (2016)'s cooling prediction seems to be in close agreement with the estimate by numerical model and greater than of the estimate by TRINV for HE-31 in this thesis. On the other hand, the prediction calculated by Kristjánsson et al. (2016) is more than two times the prediction made by the numerical and TRINV models for HE-48 in this study. Finally, as there is no cooling estimated by TRINV for HE-44 in this study, the estimation by the numerical model is in reasonable approximate with the estimate of Kristjánsson et al. (2016). Overall, the cooling estimated in this study reflects slower speed of propagation than the estimates of Kristjánsson et al. (2016). This is further supported by a static downhole temperature measurement (presented in figure 6.4) carried out in well HE-31 at end of June 2022 after a period of 11 years of reinjection (reinjection in the Húsmúli area started in September 2011). The main reason for the difference in estimation is believed to be the application of different porosity values in the model calculations; while the porosity used by Kristjánsson et al.

(2016) is 15%, the porosity calibrated in this study is 5% both in the numerical and the TRINV model.

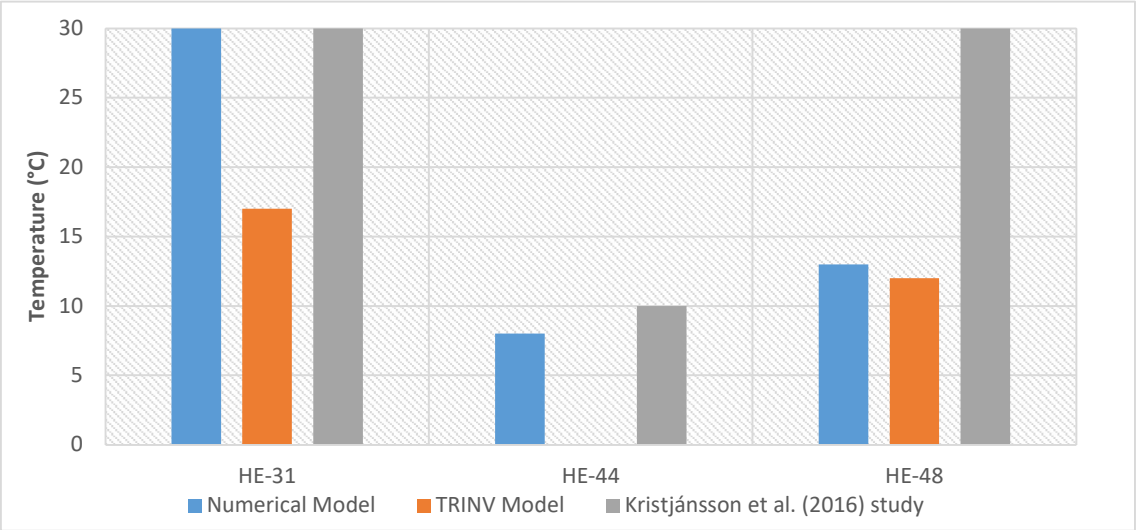

Figure 6.3 Thermal breakthrough comparison between this study and Kristjánsson et al. (2016) for 40 years of reinjection period. Note: Temperature cooling prediction in this study is made using numerical and TRINV models based on HN-16 tracer reinjection while temperature prediction by Kristjánsson et al. (2016) is made using TRINV based on HN-17 tracer reinjection.

The TRINV model does not calculate downhole temperature profiles. Besides, due to limitation of data accessibility for recent (June 2022) downhole measurement of all boreholes incorporated in this study, the only downhole data accessible was for well HE-31, which is demonstrated here. Accordingly, the downhole temperature logging of well HE-31 indicates that heating of the entire rock formation is seen from surface down to 1100 m b.s.l. depth and at a depth lower than 1600 m b.s.l where the intrusive rock is situated. On the other hand, neither cooling nor heating is observed at depths of 1100, 1400 and 1600 m b.s.l. while cooling has been visible in-between these depths. At depths of 1300 and 1550 m b.s.l, approximate cooling of 8 and 15°C is recorded, respectively, in the onsite measurement while a temperature decline of 30 and 15°C is predicted (see figure 5.10.a) by the numerical model in this thesis at corresponding depths. Based on the analysis of HE-31, the long-term temperature prediction investigated due to long term reinjection in this study by the numerical model is underestimated to some level at these depths (1300 and 1550) however in the remaining depths, it is in fair correspondence with the field value. This argument demonstrates that the geological formations and stratigraphy including their hydrological parameters and both the fault structures which the carrier of the tracer in the direction of fluid flow i.e. SW-NE and the barrier in the direction of W-E are fairly aligned in the constructed tracer state model of the reservoir system.

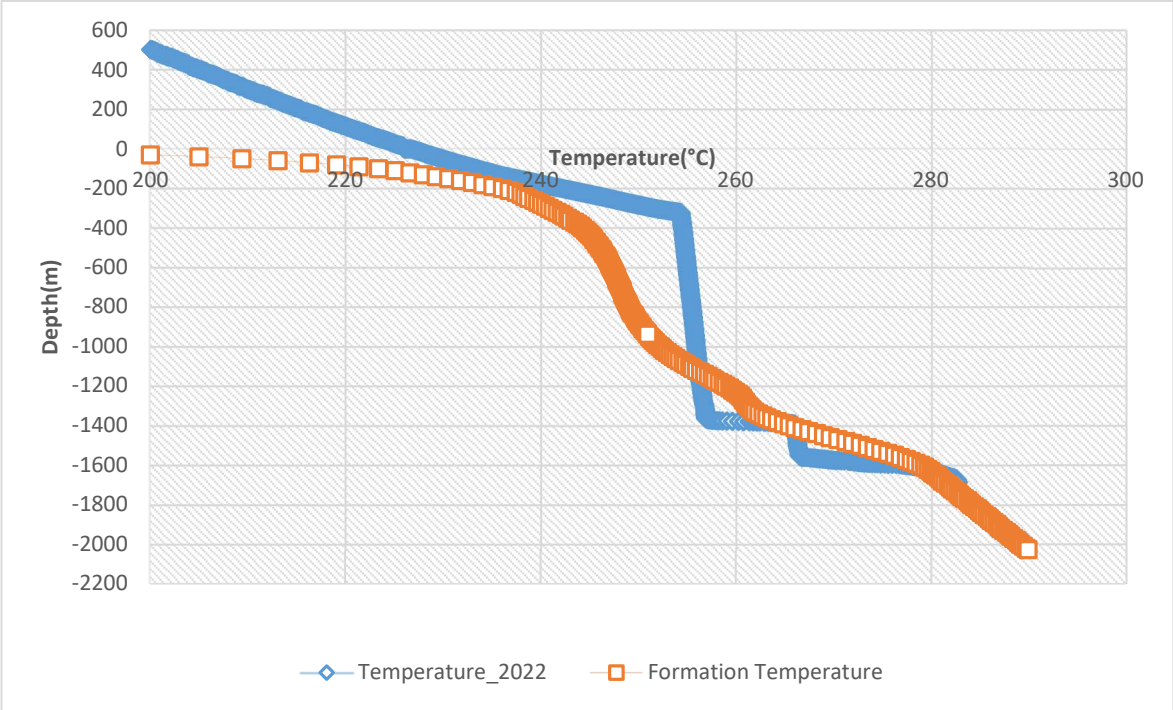

Figure 6.4 Downhole temperature conditions in well HE-31; formation temperature estimated during the warm-up period (July 2007)and a new temperature log from 2022.

6.5 Limitations of Geothermal Modelling

Physically based models or *white box models*, such as three-dimensional numerical models like the one presented in this study, involve a complex and difficult task of simulation of physical reality using numerical approximations and simplifying assumptions regarding the geologic structure of the subsurface. Although simplified, these models are generally more complex and time-consuming to calibrate than *black box models* such as the TRINV one-dimensional model. Numerical reservoir models are not always capable of modelling the inherent complexity of heat transport and fluid flow in geothermal systems, yet they are often easier to understand because they represent the subsurface in 3 dimensions and in terms of equations and rock properties for discrete geologic units that are relatively easy to understand. For the sake of obtaining a reliable outcome, the size of the model, boundary conditions, time step size, block size, thickness of the numerical grid and grid structure, should represent the geological, hydrological, and thermal nature of the matrix-fracture formation of the reservoir system as precisely as possible. The available borehole data set has also a major impact on the outcome of numerical modelling calibration. The modelling approach assuming single porosity or dual porosity also has tremendous influence on model predictions and output estimation, especially in tracer test analysis and other calculations involving chemical components and temperature conditions. Due to these constraints, numerical model results are not always very accurate, like the results presented in this study, certainly have a level of uncertainty. The very significant constraints applied in this study involves the use of tracer test data from a single reinjection well (HN-16) in the model which contributes some level of uncertainty in terms of tracer return and cooling prediction.

Integration of tracer test data collected during 2013, 2014 and 2018, involving different reinjection wells located in the Húsmúli reinjection area, in one complex three-dimensional model would be important to fill the gaps and increase the certainty of the result in the present study. Besides that, numerical models are uncertain as they try to model a very large volume, but the data used to constrain them is very limited, especially in space. That is, the model volume is perhaps hundreds of km^3, but data is only available from a few isolated points.

On the other hand, even though *black box models* such as the simple one-dimensional TRINV model, provide greater simulation accuracy, their inner working principle or how the different features interact is difficult to understand, leading to a potential risk of impacting the output through oversimplifications or incorrect assumptions. Black box models just involve a functional relationship between system inputs and outputs, which in other words is more related to curve-fitting tasks (Ljung, 2001).

7 Conclusions and Recommendation

7.1 Conclusions

Three dimensional numerical models are powerful tools when studying the nature of geothermal systems and validity of conceptual models and for utilization reservoir management, based on comprehensive monitoring, at reasonable cost and time. Geothermal numerical reservoir modelling for the greater Hengill volcanic geothermal system has been ongoing for several decades in conjunction with increasing development, supported by continuous geothermal exploration, well drilling and field monitoring.

The development of a natural state numerical modelling, using the ***Volsung*** geothermal reservoir simulator, was the foundation of this study with the output consequently utilized as initial state conditions for simulating the outcome of a tracer test conducted in 2018. The permeability of the rock formations of the reservoir system and the strength of heat sources were tuned until simulated production well downhole temperature reached an acceptable fit to measured data. Extrusive volcanics and intrusive basement are assumed to constitute the reservoir system of the model, integrated through a double porosity approach. The longitudinal and transverse permeability in addition to the amount of hot fluid mass injected into the heat-source layer of the model were the essential parameters that help to obtain steady state conditions for primary variables during the simulation which is used for tracer recovery model. Temperature inversion is seen in the depth range extending from the caprock down to the bottom of the extrusive rock. Maximum temperature of over 300°C is estimated at a depth 2000 m b.s.l., down to the entire depth of the model where intrusive basement appeares.

The tracer return curves calculated by the numerical modelling shows that a dual porosity approach produces much better fit between field and model data, and a reasonable fit is obtained for all monitoring wells except well HE-33. Better fit is attained because the volume of rock formation associated with the fault is reduced greatly as it is configured into fracture and matrix formations, through which the tracer migrates much faster than through the matrix formation. Among the reservoir parameters, permeability, porosity, and fracture ratio are the sensitive ones controlling the shape and size of the tracer return curves, simulating the field data. Increasing the porosity and fracture ratio leads to slower and smaller recovery in the model, and vice versa.

The NE trending fault structures act as flow carriers that favor the tracer transport, while the EW trending faults act as barriers for the tracer, that causes the tracer to propagate slowly towards the production wells. Wells HE-31 and HE-48 are among the two production wells that respond clearly and quickly in terms of tracer recovery, partly due to the fact that their feed zones are situated at a relatively shallow depth. This is the depth were the wells intercept the NE striking faults. In contrast, well HE-44 shows a slower and smaller recovery because its feed zones are relatively deep, despite intercepting the same faults.

Tracer simulation by the one-dimensional model (TRINV) results in a considerably better match with the 2,6-NDS field data, in terms of peak concentration, timing of the peak in all the producing wells and general shape of the tracer recovery curves. The close match of the one-dimensional tracer simulation reflects the fact that the main tracer transport mechanisms, such as advection and dispersion in the complex fracture network, are better captured by that model than the numerical one. Also, the fact that in the 1-dimensional model, only smaller flow volumes that comes from a single well is simulated. The value of dispersity for production wells ranges generally from 1 to 410 m, which shows the importance of dispersion which is not included in the numerical model. The tracer transport velocity, towards the feed zones of the production wells, is quite slow, or less than 1 m/s.

Average annual cooling due to reinjection, no greater than 1°C, is predicted in this study by both the numerical and one-dimensional model. However, the cumulative temperature decline over the entire 40-year simulation period is of course considerable as well as being somewhat greater in the numerical model. Production wells HE-31 and HE-48 are the one which are more affected by the reinjection of cold water while HE-33 is the only one which is found to be not influenced by the reinjected fluid where as HE-44 is moderately impacted by the reinjection of colder fluid in both the models. The greater reinjection flow from five reinjection wells and production fluid from six production wells in the numerical model have brought a different temperature breakthrough in the reservoir system than the one-dimensional model.

The magnitude of reinjected fluid is the essential factor in shaping the temporal temperature gradient in the numerical model while flow fraction (ratio of flow per flow channel) and the cross-sectional area of flow channels are the key parameters influencing the trend of temperature gradient over time in the one-dimensional model. Increasing the rate of cold-water reinjection facilitates cold thermal front to propagate rapidly and vice versa. On the other hand, reducing the aspect ratio of the flow channel in TRINV brings fast cooling in the reservoir system. Thermal breakthrough of cold-water reinjection obtained through TRINV model shows no cooling for the first 6 to 8 years of production for all the tracer pronounced wells while in the numerical model, the cooling started immediately since the reinjection commenced. This study shows that a 2°C decline is estimated by the three-dimensional model, while no cooling is predicted by the simple model for well HE-33 over 40 years of period (no flow channels).

To sum up, according to the results of the cooling predictions, using the two models here, the author concludes that with the current reinjection rate ongoing in the Húsmúli reinjection zone, the production wells in the Hellisheiði geothermal well field can likely be operated with slight to no danger of cooling for the next four decades. A worst case scenario indicates that either some reduction in reinjection may be needed or the production well most seriously affected (well HE-31) may need to be abandoned and a make-up well drilled.

7.2 Recommendations

The three-dimensional numerical model of the Hengill geothermal system, constructed in this study, is based on a tracer test involving only a single reinjection well (i.e. HN-16), which is believed to be insufficient to model accurately the entire fracture networks existing in the Hellisheiði system, which connect the reinjection and production aquifers. To obtain

a better image of the extensional and transform component fault structures that control the tracer transport and reinjection, it is strongly recommended to incorporate all available tracer test data, collected during all tracer tests performed since 2013 in numerical models of the Hengill area developed in the future. In addition, rather than using single transform component structure to characterize the apparent barrier hindering the tracer transport in the model, it is highly recommended to integrate further transform type faults to control the advection of tracer more accurately.

Due to the limitation of data accessibility of recent downhole logging measurements, the cooling forecast in this thesis is only constrained by a single well i.e. HE-31, hence it is recommended to further compare and calibrate the reinjection cooling with real data values of recent downhole measurement of additional wells (HE-48 and HE-44) to be more certain and get more accurate results.

The author also recommends that numerical reservoir modelling for the Hellisheiði field should be based on a more refined network of cells or blocks in the models mesh structure, if more accurate results are expected. Due to limited computer capability in performing the simulations done here, the minimum element size in the present study is 200 m^3, which is at the feed zones of production wells. But to take into account the different geological and structural features of the geothermal system, it is advisable to further refine this at least down to 25 m^3 element size.

To have very accurate overall result, all the geological formations and all the available structures such as faults and fracture networks in the Hellisheiði reservoir system must be incorporated in their correct elevation appearance rather than assuming them to be flat and horizontally uniform throughout the entire model.

Due to its capability to handle super-heated water calculations (temperature range 0 to 800 °C and pressure range 0 to 1000 bar) in addition to the convenience of performing the entire modelling using a single graphical user interface, something TOUGH2 doesn't manage, the author further recommends applying the ***Volsung*** geothermal reservoir simulation software in future numerical modelling studies, not only in the Hengill volcanic system but also in other high temperature fields in Iceland and worldwide, as an alternative modelling tool. Besides, ***Volsung*** is more flexible when the modelling needs to switch between equations of state, to switch from single porosity to dual porosity and further to different matrix layers (**MINC**) to approximate fracture flow at a reasonable numerical cost. Another impressive part of ***Volsung*** is its compatibility in accepting TOUGH2 input and initial condition files for execution purposes, and on top of that its capability to visualize TOUGH2 listing files. Not only this, but ***Volsung***'s compatibility with LEAPFROG files, such as being able to import grid geometry as well as geological and structural files, makes it more convenient for modellers and engineers engaged in geothermal modelling worldwide.

This study further strongly recommends, geothermal reservoir simulation tools to be designed in a way that they are able to incorporate dispersion and diffusion involved in tracer transport.

References

Aradóttir, E.S.P., Sonnenthal, E.L., Björnsson, G. and Jónsson, H. (2012). Multidimensional reactive transport modeling of CO2 mineral sequestration in basalts at the Hellisheidi geothermal field, Iceland. *International Journal of Greenhouse Gas Control*, vol. 9, pp. 24–40.

Arnason, K., Karlsdottir, R., Eysteinsson, H., Flovenz, O., and Gudlaugsson, S. (2000). The Resistivity Structure of high-temperature geothermal systems in Iceland. *World Geothermal Congress, 2000*, Kyushu, Japan, 6 pp.

Axelsson, G. (2012). Role and management of geothermal reinjection. Presented at "Short Course on Geothermal Development and Geothermal Wells", organized by UNU-GTP and LaGeo, in Santa Tecla, El Salvador, March 11-17, 2012.

Axelsson, G. (2013). Tracer tests in geothermal resource management. *EPJ Web of Conferences*, vol. 50 (02001), pp. 1–8.

Axelsson, G. (2020). Geothermal resources management and related issues. *University of Iceland, UnPulished Lecture Note*, 50 pp.

Axelsson, G. (2022). The Physics of Geothermal Resources. In: Letcher, Trevor M. (eds.) *Comprehensive Renewable Energy*, 2nd edition, vol. 7, Oxford, Elsevier, pp. 98–131.

Axelsson, G., Bjornsson, G., and Montalvo, F. (2005). Quantitative interpretation of tracer test data. In *Proceedings of the World Geothermal Congress 2005*, pp. 24-29.

Axelsson, G., Björnsson, G., Flóvenz, Ó.G., Kristmannsdóttir, H., and Sverrisdóttir, G. (1995): Injection experiments in low-temperature geothermal areas in Iceland. *Proceedings of the World Geothermal Congress 1995*, Florence, Italy, 3, 1991-1996.

Axelsson, G., O.G. H. and G. Sverrisdóttir (1993). Injection experiment at Laugaland in Central North Iceland (in Icelandic). Report OS-93052/JHD-13, National Energy Authority, Reykjavik, 69 pp.

Ágústsson, K., Kristjánsdóttir, S., Flóvenz, Ó.G. and Guðmundsson, Ó. (2015). Induced Seismic Activity during Drilling of Injection Wells at the Hellisheiði Power Plant, SW Iceland. *Proceedings World Geothermal Congress 2015*. Melbourne, Australia.

Árnason, K., Eysteinsson, H., and Hersir, G. (2010). Joint 1D inversion of TEM and MT data and 3D inversion of MT data in the Hengill area, SW Iceland. *Geothermics,* 39 (1), 13–34.

Baker Hughes (2023). Brine flow measurement in a geothermal power plant. Retrieved from https://www.bakerhughes.com/panametrics/success-stories/brine-flow-measurement-geothermal-power-plant

Barenblatt, G.I., Zheltov, I.P., Kochina, I.N. (1960). Basic concepts in the theory of seepage of homogeneous liquids infissured rocks. *Journal of Applied Mathematics and Mechanics,* 24 (5), 1286–1303.

Batir, J., Davatzes, N.C., and Asmundsson, R. (2012). Preliminary model of fracture and stress state in the Hellisheidi geothermal field, Hengill volcanic system, Iceland. *Proceedings*, *Thirty-Seventh Workshop on Geothermal Reservoir Engineering*. Stanford, California.

Bjornsson, A., Hersir, G., and Björnsson, G. (1986). The Hengill high-temperature area SW-Iceland: Regional Geophysical Survey. *Geothermal Resources Council,* Vol 10.

Björnsson, G., Hjartarsson, A., Bodvarsson, G., and Steingrimsson, B. (2003). Development of a 3-d geothermal reservoir model for the greater Hengill volcano in SW-Iceland. *TOUGH Symposium,* Berkeley, California, 11 pp.

Björnsson, G., Hjatarson, A., Bodvarsson, G. S., and Steingrimsson, B. (2010). The Hengill Geothermal System, Conceptual Model and Thermal Evolution. *Proceedings World Geothermal Congress*. Bali, Indonesia.

Bodvarsson, G.S. (1993). *Recalibration of the three-dimensional model of the Nesjavellir geothermal field.* Report prepared for the Reykjavik District Heating, 111 pp.

Bodvarsson, G.S. (1998). *Update of the three-dimensional model of the Nesjavellir geothermal field*. Report prepared for Reykjavik District Heating, 11 pp.

Bodvarsson, G., Bjornsson, S., Gunnarsson, A., Gunnlaugsson, E., Sigurdsson, O., Stefansson, V., and Steigrimsson, B. (1990). The Nesjavellir Geothermal Field, Iceland. Part 2: Evaluation of the generating capacity of the system. Reykjavik, Iceland: *Geotherm. Sci. and Tech.*, Vol. 2 (3).

Bouhifd, M.A., Besson, P., Courtial, P., Gérardin, C., Navrotsky, A., and Richtet, P. (2007). Thermochemistry and melting properties of basalt. *Contributions to Mineralogy and Petrology*, vol. 153 (6), pp. 689–698.

Clauser, C., and Huenges, E. (1995). Thermal Conductivity of Rocks and Minerals. In: Ahrens, T.J. (eds) *Rock Physics and Phase Relations: A Handbook of Physical Constants. AGU reference shelf 3*. Washington: American Geophysical Union, pp. 105–126.

Croucher, A. (2021). *PyTOUGH:* a Python scripting library for automatic TOUGH2 simulations. Auckland, New Zealand.

D'Amore, F. and Arnórsson, S. (2000). Geothermometry. In Arnórsson, S. (Ed.): *Isotopic and Chemical Techniques in Geothermal Exploration, Development and Use.* IAEA, Vienna, 152-199.

Diaz, A.R., Kaya, E., and Zarrouk, S.J. (2016). Reinjection in geothermal fields. A worldwide review update. *Renewable and Sustainable Energy Reviews,* 53, 105-162.

Finsterle, S. (2007). iTOUGH2 User's Guide. Lawrence Berkeley National Laboratory, report LBNL-40040, Berkeley, California.

Franz, P., and Clearwater, J. (2021). Volsung User Manual; Version 1.16.2. 150 pp.

Franz, P., Clearwater, J., and Burnell, J. (2019). Introducing the volsung geothermal simulator: benchmarking and performance. *Proceedings New Zealand Geothermal Workshop*, Auckland, New Zealand, 10 pp.

Franzson, H. (1998). The Nesjavellir high-temperature field, SW-Iceland, reservoir geology. *Proceedings 19th Annual PNOC-EDC Geothermal Conference*, Manilla, Philippines.

Franzson, H., Kristjánsson, B., Gunnarsson, G., Björnsson, G., Hjartarson, A., Steingrímsson, B., Gunnlaugsson, E., and Gíslason, G. (2005). The Hengill-Hellisheiði Geothermal Field. Development of a Conceptual Geothermal Model. *Proceedings World Geothermal Congress 2005*, Antalya, Turkey, 24-29 April 2005.

Franzson, H., Gunnlaugsson, E., Árnason, K., Sæmundsson, K., Steingrímsson, B., and S. Harðarson, B. (2010). The Hengill Geothermal System, Conceptual Model and Thermal Evolution. *Proceedings World Geothermal Congress*. Bali, Indonesia.

Goloshubin, G. (2006). Dual Porosity Biot-Barenblatt Model: *68th EAGE Conference and Exhibition incorporating* SPE EUROPEC. doi:10.3997/2214 4609.201402289

Gunnarsdóttir, S., and Poux, B. (2016). 3D Modelling of Hellisheiði Geothermal Field using Leapfrog: Data, Workflow and Preliminary Models. Reykjavik, Iceland: Orka náttúrunnar.

Gunnarsson, G., and Mortensen, A. (2016). Dealing with intense production density: Challenges in understanding and operating the Hellisheiði Geothermal Field, SW-Iceland. *41st Workshop on Geothermal Reservoir Engineering*. Stanford, California.

Gunnarsson, G. (2011). Mastering reinjection in the Hellisheiði Field, SW-Iceland: A story of successes and failures. *Proceedings, 36th Workshop on Geothermal Reservoir Engineering.* Stanford, California.

Gunnarsson, G. (2020). Numerical calculations. *Unpublished lecture note presented at the University of Iceland*.

Gunnarsson, G., and Aradóttir, E. (2014). The Deep Roots of Geothermal Systems in Volcanic Areas: *Boundary Conditions and Heat Sources in Reservoir Modeling*. 17 pp.

Gunnarsson, G., and Mortensen, A. (2016). Dealing with intense production density: Challenges in understanding and operating the Hellisheiði Geothermal Field, SW-Iceland. *PROCEEDINGS, 41st Workshop on Geothermal Reservoir Engineering*. Stanford, California.

Gunnarsson, G., Arnaldsson, A., and Oddsdóttir, A. (2010). Model Simulations of the Geothermal Fields in the Hengill Area, South-Western Iceland. *World Geothermal Congress*, Bali, Indonesia, 8 pp.

Gunnarsson, I., Aradóttir, E., Oelkers, E., Clark, D., Arnarson, M., Sigfússon, B., and Gíslason, S. (2018). The rapid and cost-effective capture and subsurface mineral storage of the rapid and cost-effective capture and subsurface mineral storage of. *International Journal of Greenhouse Gas Control,* 79, 10 pp.

Gunnarsdóttir, S.H., and Poux, B. (2016). 3D Modelling of Hellisheiði geothermal field using Leapfrog: Data, workflow and preliminary models. Report ÍSOR-2016/039, 25 pp.

Hardarson, B., Einarsson, G., Kristjánsson, B., Gunnarsson, G., Helgadóttir, H., Franzson, H., and Gunnlaugsson, E. (2010). Geothermal Reinjection at the Hengill Triple Junction, SW Iceland. *World Geothermal Congress 2010*, Bali, Indonesia, 7 pp.

Heffer, K., (2002) Geomechanical Influences in Water Injection Projects: An Overview. *Oil & Gas Science and Technology,* Vol. 57, No. 5, pp. 415-422.

Hersir, G., and Árnason, K. (2009). Resistivity of rocks. *Presented at Short Course IV on Exploration for Geothermal Resources, organized by UNU-GTP, KenGen and GDC, at Lake Naivasha, Kenya,* 9 pp.

Hersir, G., Árnason, K., and Steingrímsson, B. (2009). Exploration and development of the Hengill geothermal field. *Presented at "Short Course on Surface Exploration for Geothermal Resources",organized by UNU-GTP and LaGeo, in Ahuachapan and Santa Tecla, El Salvador,* 12 pp.

Hjörleifsdóttir, V., Snæbjörnsdóttir, Ó., Gunnarsson, G., and Kristjánsson, B., (2021). Induced Earthquakes in the Hellisheiði Geothermal Field, Iceland. *Proceedings World Geothermal Congress 2020+1*, Reykjavik, Iceland, April - October 2021.

Horne, R.N. and Rodriguez, F. (1983). Dispersion in tracer flow in fractured geothermal systems. *Geophy. Res. Lett.*, 10, 289-292.

Javandel, I., Doughty, C., and Tsang, C.F. (1984). *Groundwater Transport. Handbook of Mathematical Models.* Water Resources Monograph Series, 10, American. Geophys. Union, 228 pp.

Jung, Y., Finsterle, S., Doughty, C., and Heng, G. (2018). TOUGH3 User's Guide. *Earth Sciences Division, Lawrence Berkeley National Laboratory.* Berkeley, California, USA.

Kamila, Z., Kaya, E., and Zarrouk S.J. (2021). Reinjection in geothermal fields: An updated worldwide review 2020. *Geothermics,* 89.

Karson, J. A., Farrell, J. A., Chutas, L. A., Nanfito, A. F., Proett, J. A., Runnals, K. T., and Sæmundsson, K. (2018). Rift-Parallel Strike-Slip Faulting Near the Iceland Plate Boundary Zone: Implications for Propagating Rifts. *Tectonics, 37,* 4567–4594.

Khodayar, M. (2013). *Fracture analysis from aerial imageries and correlation with triggered earthquakes by injection at Húsmúli, Hengill, South Iceland.* Report Iceland GeoSurvey, ÍSOR-2013/008, 26 p, 3 Maps.

Khodayar, M., Axelsson, G., and Steingrímsson, B. (2015). Potential Structural Flow Paths for Tracers and Source Faults of Earthquakes at Húsmúli, Hengill, South Iceland. Reykjavik, Iceland: ON Power (Orka náttúrunnar).

Kitamura, K., Takahashi, M., Mizoguchi, K., Masuda, K., Ito, H., and Song, S.R. (2010). Effects of pressure on pore characteristics and permeability of porous rocks as estimated from seismic wave velocities in cores from TCDP Hole-A. *Geophysics Journal International.,* 182**,** 1148–1160.

Kristjánsson, B., Axelsson, G., Gunnarsson, G., Gunnarsson, I., and Óskarsson, F. (2016). Comprehensive Tracer Testing in the Hellisheiði Geothermal Field in SW-Iceland. *PROCEEDINGS, 41st Workshop on Geothermal Reservoir Engineering*. Stanford, California.

Kristmannsdóttir H. (1979). Alteration of basaltic rocks by hydrothermal activity at 100-300 °C. *Developments in Sedimentology* 27, 359-367.

Kristmannsdóttir, H. and Tómasson, J. (1978). Zeolite zones in geothermal areas in Iceland. Natural Zeolites: Occurrence, Properties, Use. Pergamon Press, Elmsford, New York.

Lin, W. (2002). Permanent strain of thermal expansion and thermally induced microcracking in Inada granite. *J. Geophys. Res.,* 107(B10), 2215 pp.

Ljung, L. (2001). "Black-box models from input-output measurements," *IMTC 2001. Proceedings of the 18th IEEE Instrumentation and Measurement Technology Conference. Rediscovering Measurement in the Age of Informatics (Cat. No.01CH 37188)*, *Vol. 1*, pp. 138-146.

Mahzari, P., Stanton-Yonge, A., Sanchez-Roa, C., Sald, G., Mitchell, T., and Snaebjornsdottir, ÓJones, A. (2021). Characterizing fluid flow paths in the Hellisheiði geothermal field using detailed fault mapping and stress-dependent permeability. *Geothermics,* 94, 14 pp.

Mortensen, A. (2017). Hengill Geothermal System : Nesjavellir and Hellisheiði High Temperature Fields. *United Nations University Geothermal Training Program, Unpublished Lecture Notes*, 84 pp.

Mortensen, A., and Axelsson, G. (2013). Developing a Conceptual Model of Geothermal System. *Presented at "Short Course on Conceptual Modelling of Geothermal Systems" organized by UNU-GTP and LaGeo,* Santa Tecla, El Salvador, 10 pp.

Nyambayar, T.-A. (2006). Resistivity survey in the Hengill area, SW-Iceland. *United Nations University Geothermal Training Programme Report*, 30 pp.

Mutonga, M. (2007). The isotopic and chemical characteristics of geothermal fluids in Hengill area, SW-Iceland: Hellisheidi, Hveragerdi and Nesjavellir fields. *UNU-GTP Report No 15*, Reykjavik, Iceland, 38 pp.

Óskarsson, F. and Ármannsson, H. (2015). Geochemical methods in geothermal surface exploration. *Presented at Short Course X on Exploration for Geothermal Resources,*

organized by UNU-GTP, GDC and KenGen, at Lake Bogoria and Lake Naivasha, Kenya, Nov. 9-Dec. 1, 2015, 12 pp.

O'Sullivan, M. (2015). Geothermal reservoir simulation: the state-of-practice and emerging trends. *New Zealand Geothermal Workshop.* Auckland, New Zealand, 9 pp.

O'Sullivan, M., Croucher, A., O'Sullivan, J., Yeh, A., Burnell, J., and Kissling, W. (2019). A parallel open-source geothermal flow simulator. *Computers & Geosciences*.

Pruess, K., Oldenburg, C.M., and Moridis, G.J. (1999). *TOUGH2 User's Guide Version 2.* Earth Sciences Division, Lawrence Berkeley National Laboratory. Berkeley, California, USA. Report LBNL-43134.

Pruess, K., Curt , O., and George , M. (2012). *TOUGH2 user's guide, version 2.* Lawrence Berkeley National Laboratory, University of California, California.

Ratouis, T., Snæbjörnsdóttir, S., Gunnarsson, G., Ingvi, G., Kristjánsson, B., and Aradóttir, E. (2019). Modelling the Complex Structural Features Controlling Fluid Flow at the CarbFix2 Reinjection Site, Hellisheiði Geothermal Power Plant, SW-Iceland. *44th Workshop on Geothermal Reservoir Engineering*, Stanford, California.

Ratouis, T., Snæbjornsdottir, S., Voigt, M., Sigfússon, B., Gunnarsson, G., Aradottir, E.S., and Hjorleifsdottir, V. (2022). Carbfix 2: A transport model of long-term CO2 and H2S injection into basaltic rocks at Hellisheiði, SW-Iceland. *International Journal of Greenhouse Gas Control,* 114.

Rose, P., Benoit, D., Lee, S., Tandia, B., and Kilbourn, P. (2000). Testing the naphthalene sulfonates as geothermal tracers at dixie valley, ohaaki, and awibengkok. *Proceedings, Twenty-Fifth Workshop on Geothermal Reservoir Engineering*, Stanford University, Stanford, California, 7 pp.

Scott, W., Gunnarsson, I., Arnórsson, S., and Stefansson, A. (2014). Gas chemistry, boiling and phase segregation in a geothermal system, Hellisheidi, Iceland. *Geochimica et Cosmochimica Acta*, January 2014, doi: 10.1016/j.gca.2013.09.027

Scott, W., and Driesner, T. (2018). Permeability Changes Resulting from Quartz Precipitation and Dissolution around Upper Crustal Intrusions. *Geofluids Journal*, Volume 2018, Article ID 6957306, 19 pp. https://doi.org/10.1155/2018/6957306

Seequent. (2020). Leapfrog Geothermal (Seequent): Leapfrog Geothermal - 3D Geological Modelling Tool: http://www.leapfrog3d.com/products/leapfrog-geothermal

Snæbjörnsdóttir, S.Ó., Tómasdóttir, S., Sigfússon, B., Aradóttir, E.A., Gunnarsson, G., Niemi A., Basirat, F., Dessirier, B., Gislason, S.R., Oelkers, E.H., and Franzson, H.(2018).The geology and hydrology of the CarbFix2 site, SW-Iceland. *Energy Procedia*, Volume 146, 146-157.

Sæmundsson K. (1967). Vulkanismus und Tektonik des Hengill – Gebietes in Sudwest-Island. Acta Nat. Isl. 2, 109 pp.

Sæmundsson K. (1992). Geology of the Thingvallavatn area. Oikos 64, 40–68.

Sæmundsson, K., Jóhanneson, H., Hjartarson, Á., and Kristinsson, S. (2010). *Geological Map of Southwest Iceland, 1:100000.* Reykjavik, Iceland: Iceland GeoSurvey (ISOR).

Steingrimsson, B., Bodvarsson, G.S., Cuellar, G., and Escobar, C. (1989). Changes in thermodynamic conditions of the Ahuachapan reservoir due to production and injection. Proceedings, *14th Workshop on Geothermal Reservoir Engineering*. Stanford, California, SGP-TR-122.

Stefánsson, V. (1997). Geothermal Reinjection Experience. *Geothermics,* 26 (1), 99-139.

Tómasdóttir, S. (2018). Flow paths in the Húsmúli reinjection zone, Iceland. *MSc thesis*, Uppsala University.

Warren, J.E., and Root, P.J. (1963). The behavior of naturally fractured reservoirs. *Society of Petroleum Engineers Journal,* 3 (3), 245–255.

Witherspoon, and Bodvarsson. (1989). Geothermal Reservoir Engineering. Berkeley, CA: Earth Sciences Divesion, Lawrence Berkeley Labratory, University of California.

Yeh, A., Croucher, A., and O'Sullivan, J. (2013). TIM – yet another graphical tool for TOUGH2. *35th New Zealand Geothermal Workshop,* Rotorua, New Zealand, 5 pp.

Zhao, D., Kanamori, H. and Negishi, H. (1996). Tomography of the Source Area of the 1995 Kobe Earthquake: Evidence for Fluids at the Hypocentre? Science, 274, 1891-1894. http://dx.doi.org/10.1126/science.274.5294.1891

Appendix 1

Information on percentage of flow contribution of the feedzones. The well names annotated by HE and HN denotes production and reinjection wells respectively. Feedzones are labeled by arabic numbers (1, 2 and 3).

Well-Name	Feedzone-Name	Measured Depth(m)	Percentage of flow contribution
	1	1196	0,32
	2	1396	0,36
HE-05	3	1618	0,32
	1	1802	0,333
	2	2270	0,333
HE-31	3	2496	0,333
	1	1006	0,2
	2	1250	0,6
HE-33	3	1570	0,2
	1	2211	0,704
HE-44	2	2420	0,296
	1	1098	0,4
	2	1602	0,25
HE-46	3	2366	0,35
	1	1130	0,33
	2	1650	0,34
HE-48	3	2148	0,33
	1	1905	0,2
	2	2355	0,4
HN-09	3	2555	0,4
	1	680	0,4
HN-12	2	1918	0,6
	1	1400	0,38
HN-14	2	1923	0,62
	1	712	0.125
	2	990	0.25
	3	1380	0.25
	4	1919	0,125
HN-16	5	2170	0,25
	1	1321	0,33
	2	1700	0,33
HN-17	3	2100	0,33

Appendix 2

Predicted temperature decline of wells HE-31, HE-44 and HE-48 using three flow channels (TRINV).

HE-31

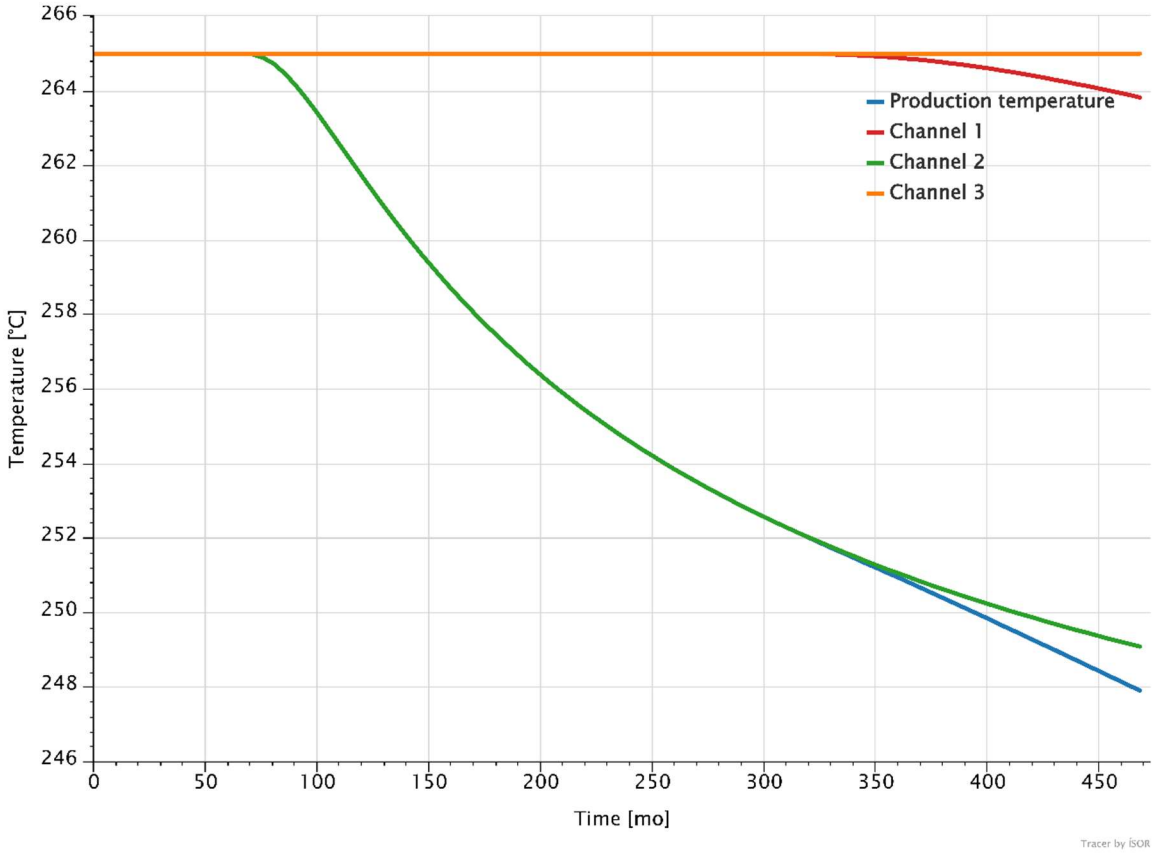

HE-44

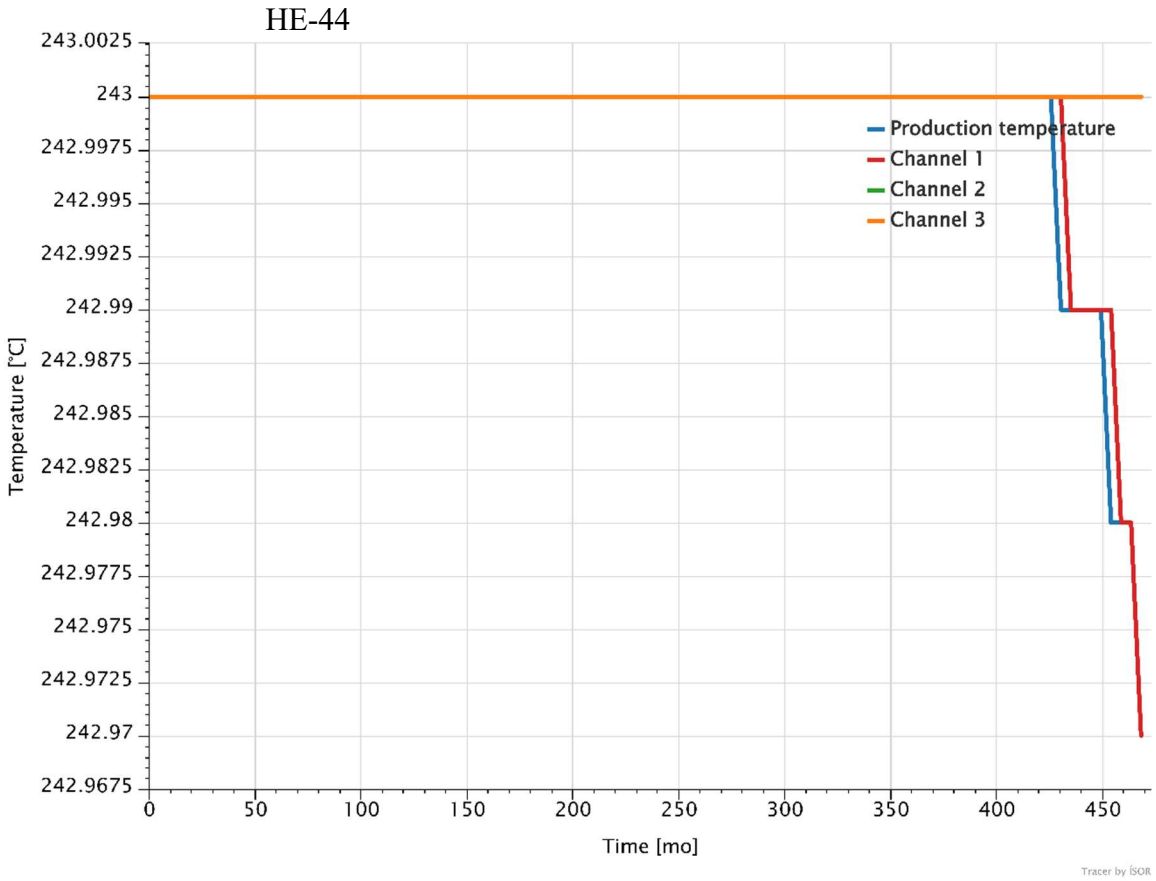

HE-48

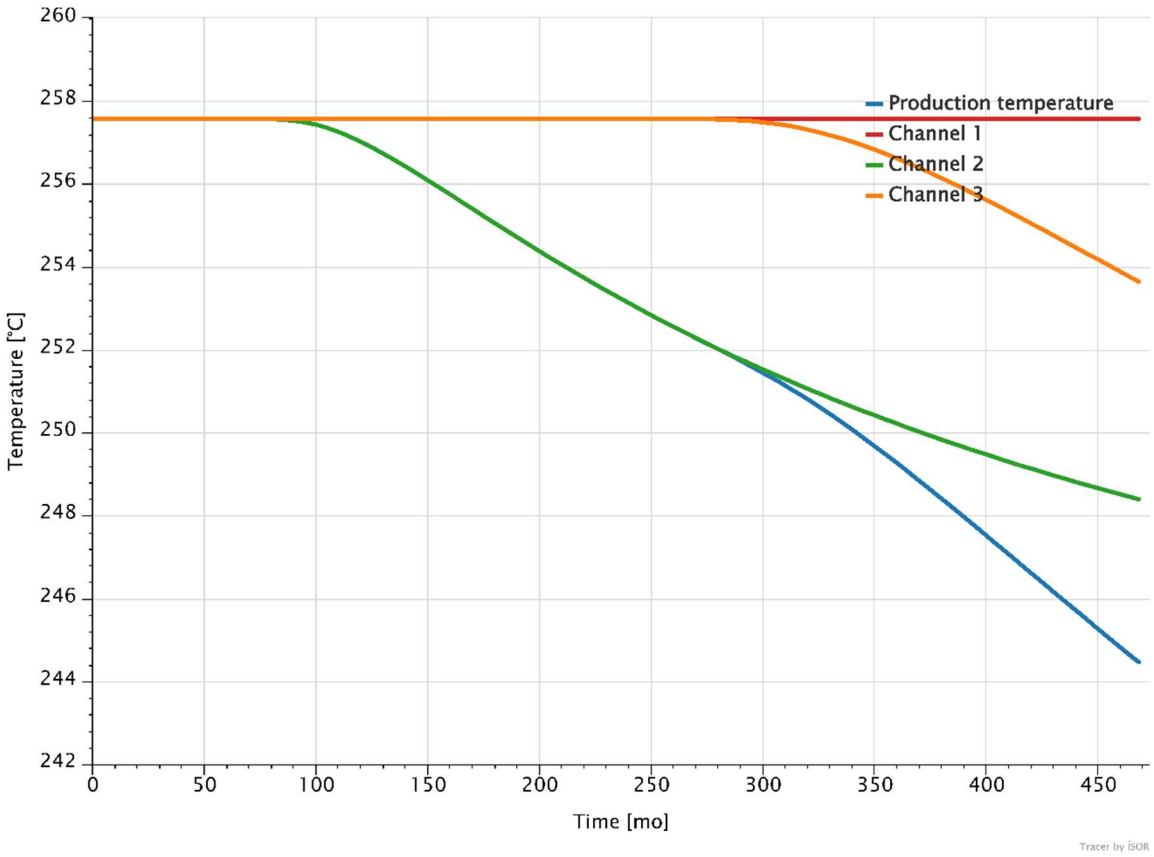
Production temperature
Channel 1
Channel 2
Channel 3
Temperature [°C]
260
258
256
254
252
250
248
246
244
242
0
50
100
150
200
250
300
350
400
450
Time [mo]
Tracer by ÍSOR

Appendix 3

Stratigraphic arrangement of the numerical model

a) Top Layer

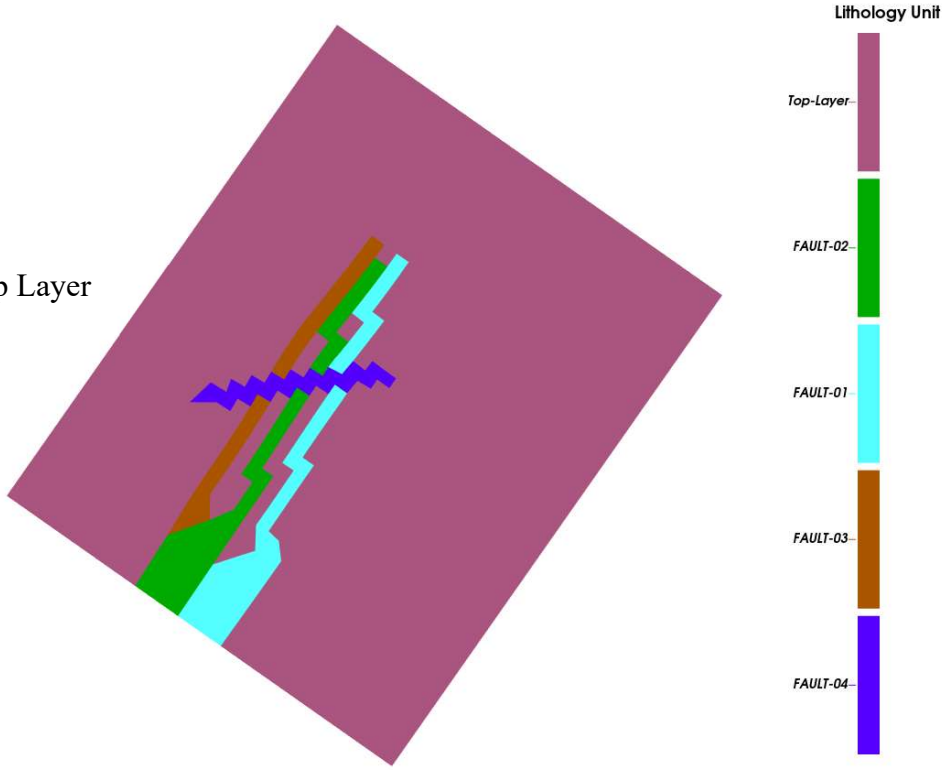

b) Cold Ground Water System Layer (100 m a.s.l)

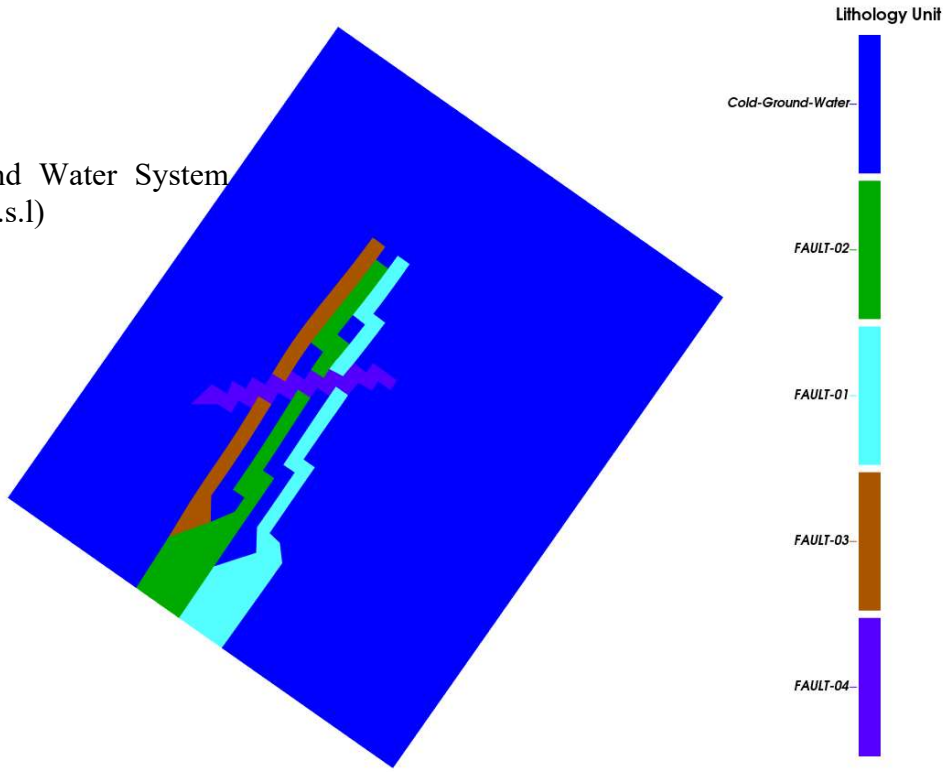

c) Cap Rock Layer (100 m b.s.l)

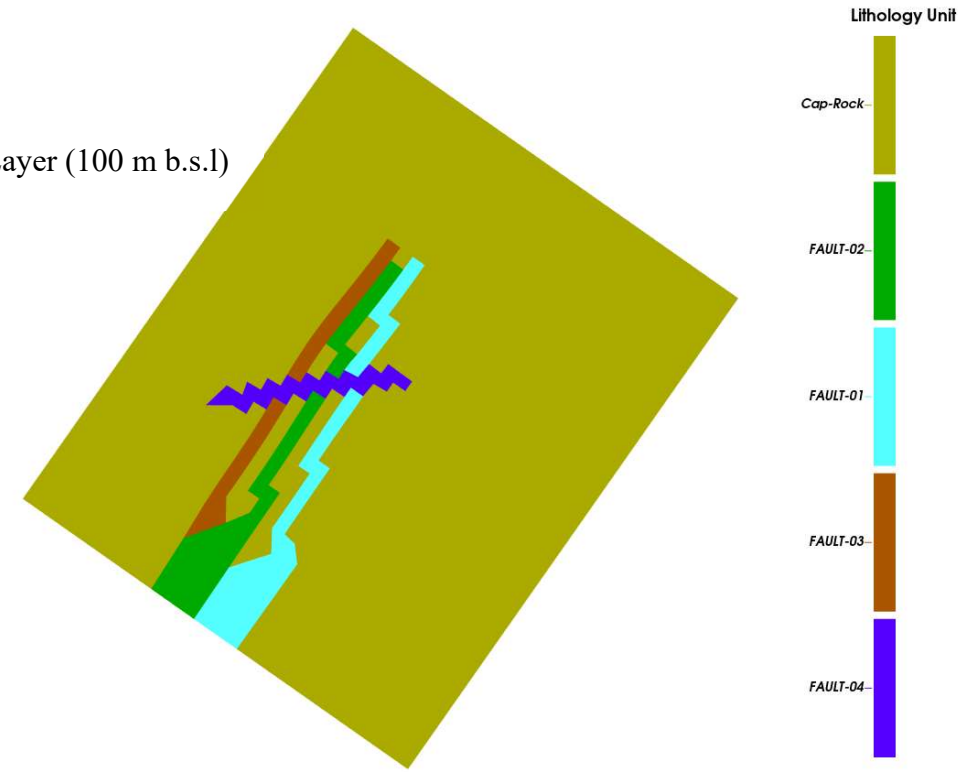

d) Extrusive Volcanics Layer (200 m b.s.l)

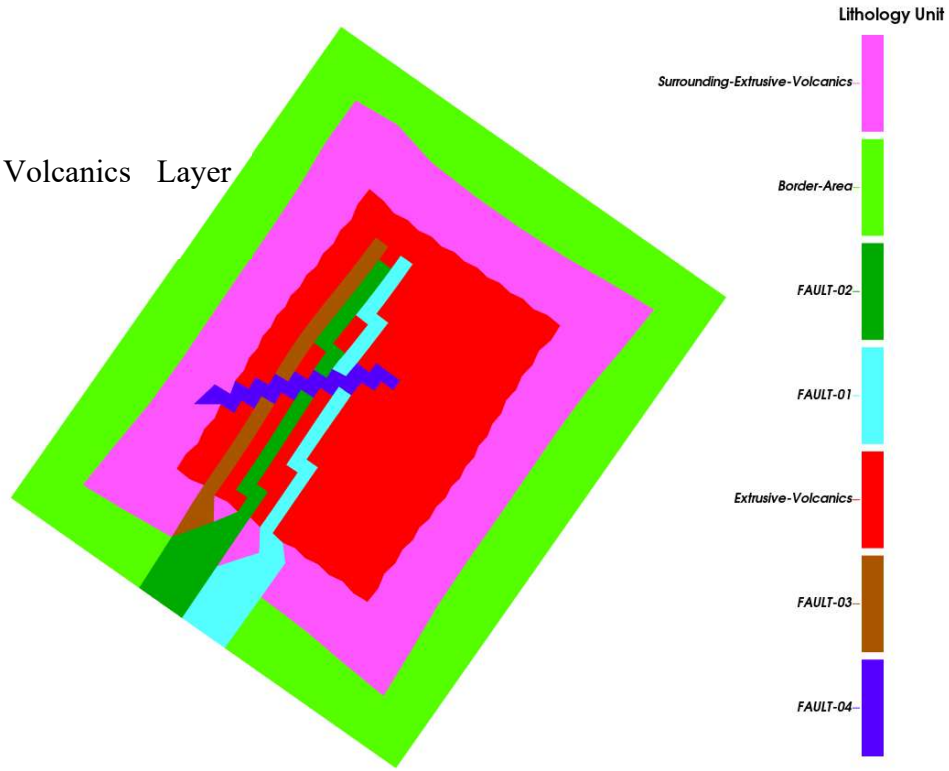

e) Intrusive Basement Layer (1400 m b.s.l).

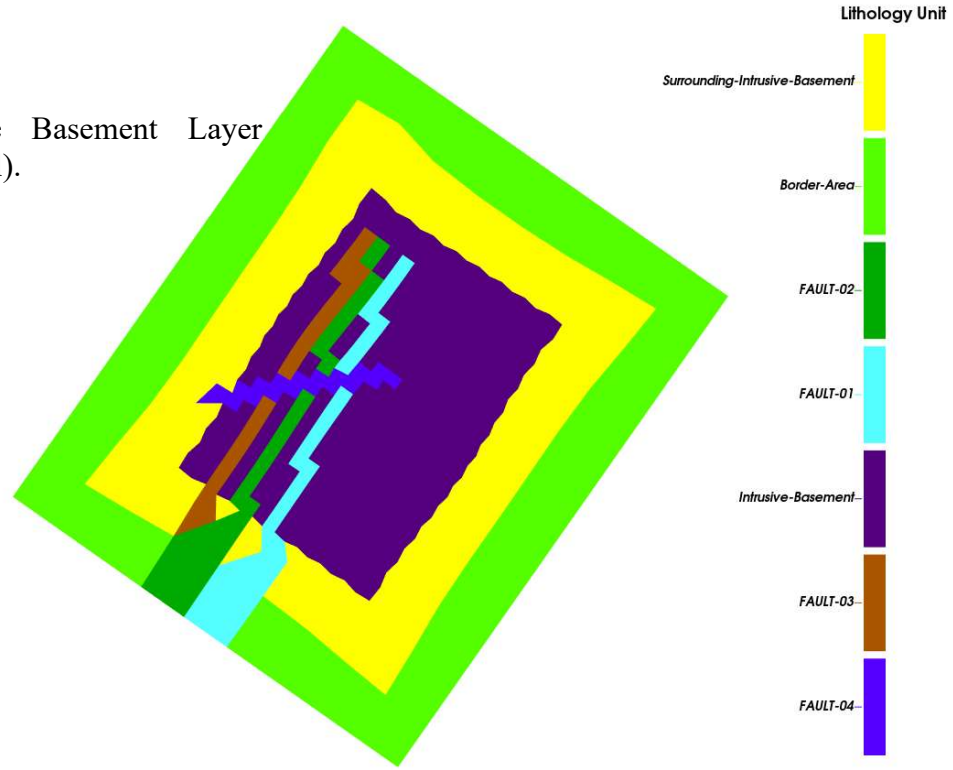

f) Bottom Layer (2500 m b.s.l)

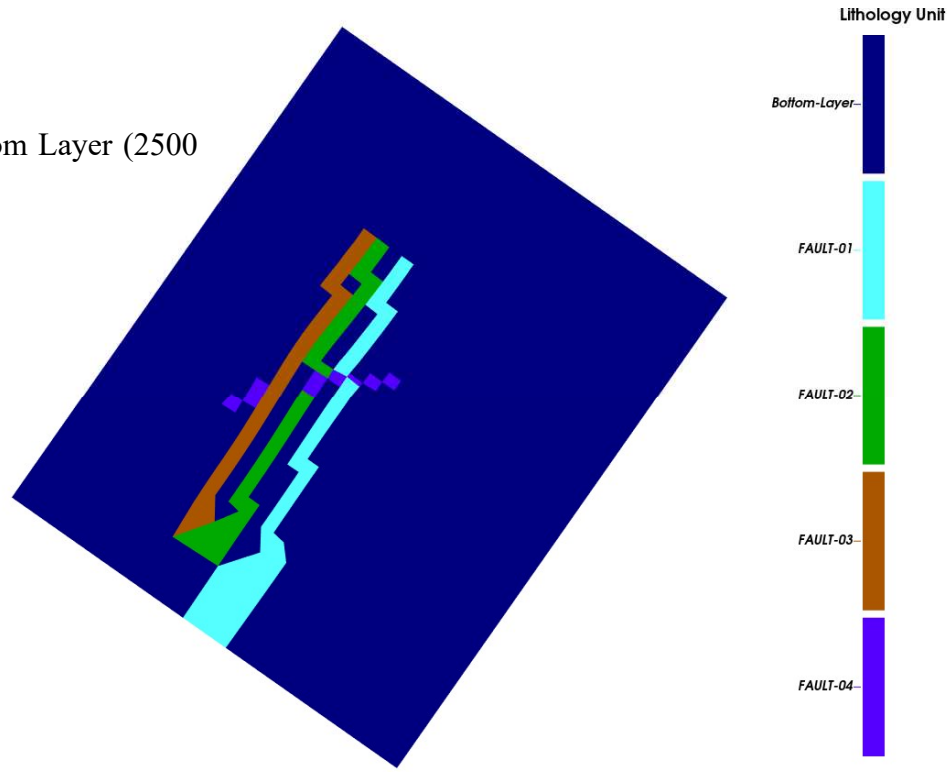

Appendix 4

Borehole data (Flow rate of production and reinjection wells, Wellhead Pressure of production wells and Enthalpy of reinjected fluid) for simulation of tracer transport in the numerical model.

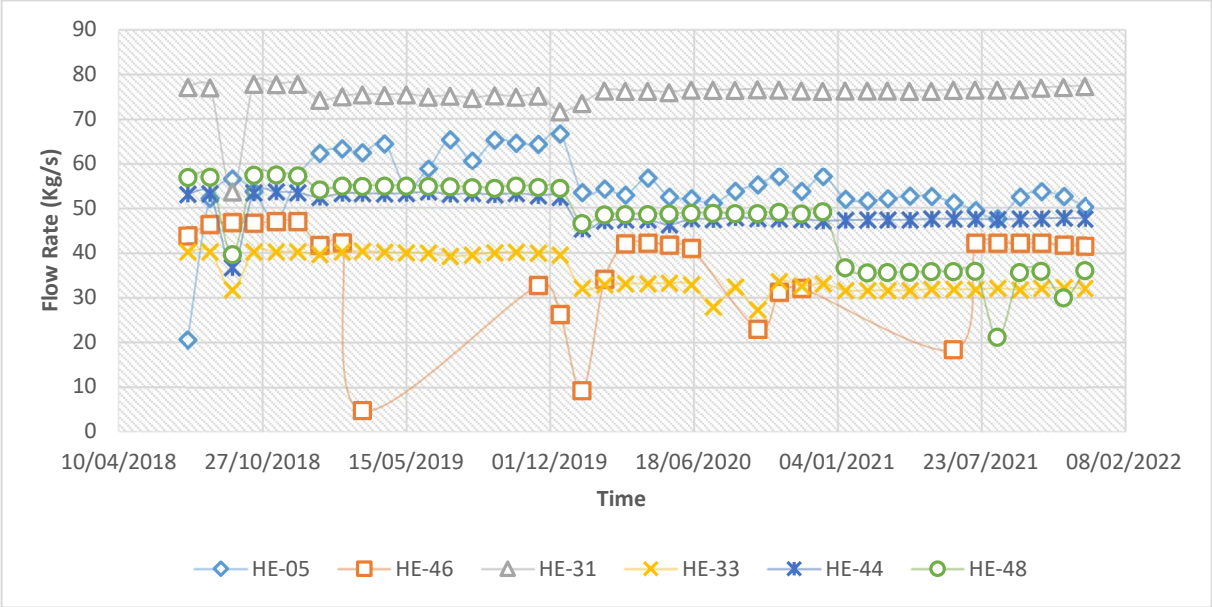

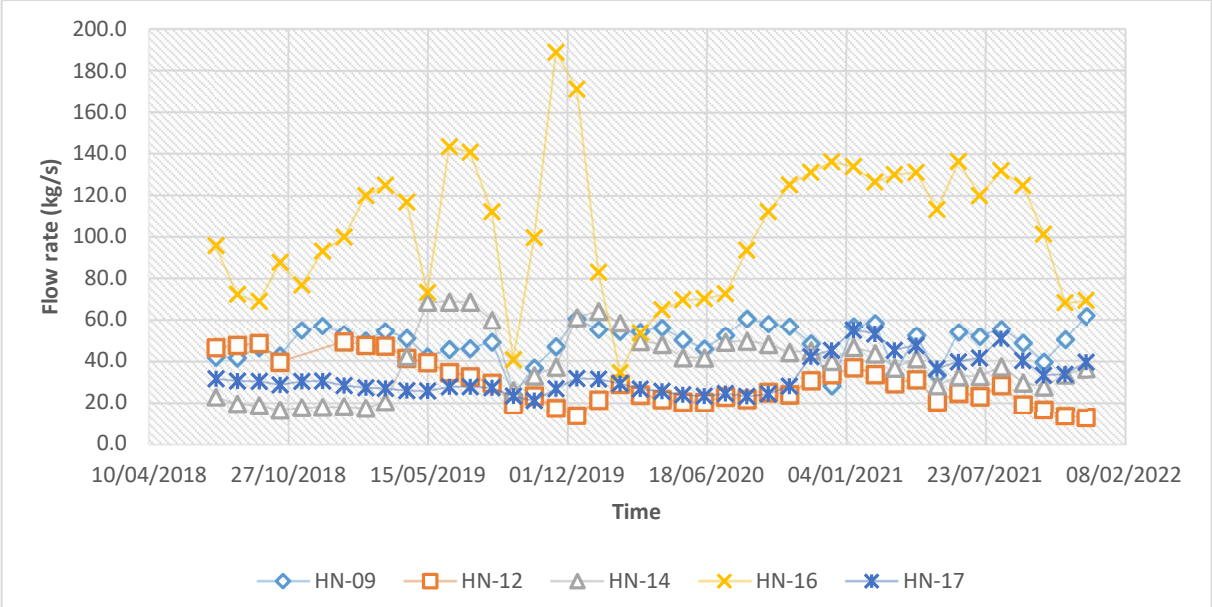

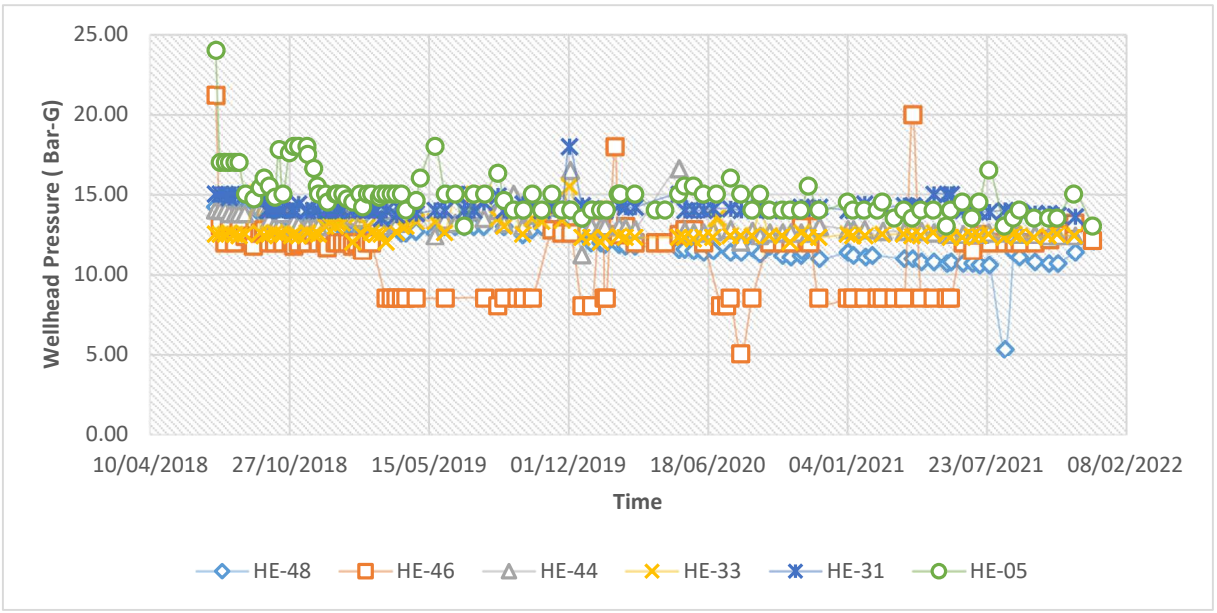
25.00
20.00
15.00
10.00
5.00
0.00
Wellhead Pressure (Bar-G)
10/04/2018
27/10/2018
15/05/2019
01/12/2019
18/06/2020
04/01/2021
23/07/2021
08/02/2022
Time
HE-48
HE-46
HE-44
HE-33
HE-31
HE-05

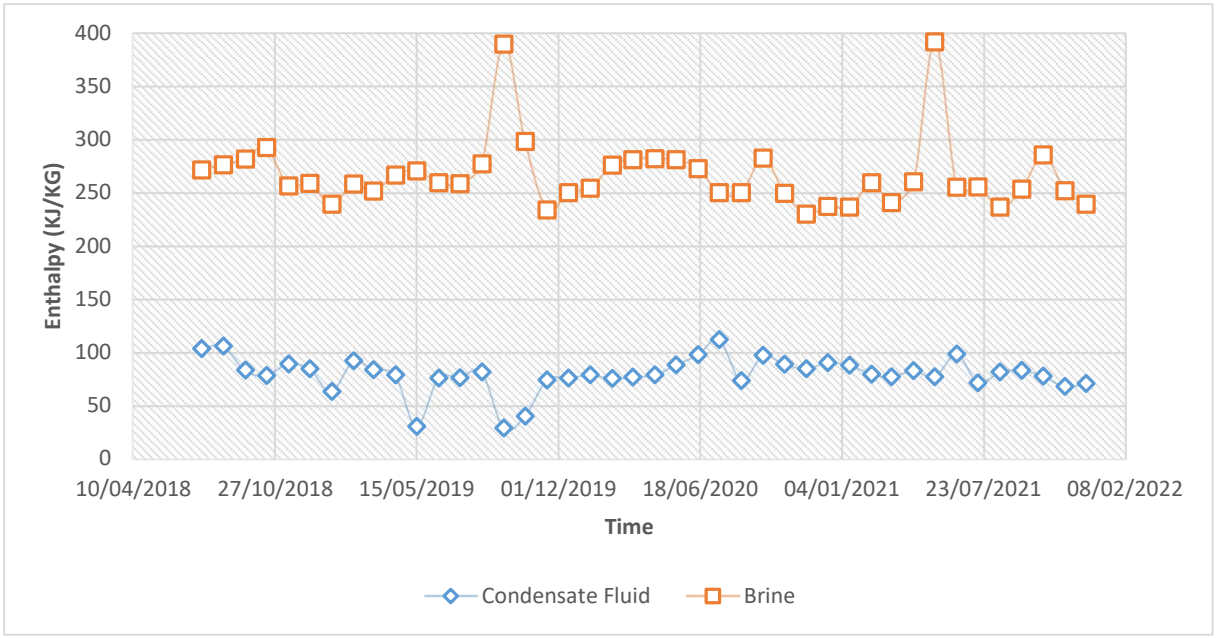
400
350
300
250
200
150
100
50
0
Enthalpy (KJ/KG)
10/04/2018
27/10/2018
15/05/2019
01/12/2019
18/06/2020
04/01/2021
23/07/2021
08/02/2022
Time
Condensate Fluid
Brine